AN ABSTRACT OF THE THESIS OF

Brandon Patrick Haugh for the degree of Master of Science in Nuclear Engineering presented on May 28, 2002.

Title: Multi Application Small Light Water Reactor Containment Analysis and Design

Abstract Approval: Redacted for privacy

Jose N. Reyes, Jr.

This thesis presents the assessment of the Multi Application Small Light Water Reactor (MASLWR) containment design during steady-state and transient conditions. The MASLWR project is a joint effort between Idaho National Environmental and Engineering Laboratory (INEEL), NEXANT Bechtel, and Oregon State University. The project is funded under a Nuclear Energy Research Initiative (NERI) grant from the Department of Energy (DOE).

The GOTHIC code was used to simulate the full scale prototype and the Oregon State University MASLWR test facility. Detailed models of the full scale prototype and OSU test facility were generated in GOTHIC. GOTHIC condensation heat transfer models produced heat transfer coefficients that vary by an order of magnitude. This had a significant impact on the pressurization rate and peak pressure achieved within containment. A comparison of the GOTHIC calculation results for the full scale prototype and the test facility model shows reasonable agreement with respect to containment pressure trends and safety system mass flow rates.

Multi Application Small Light Water Reactor Containment Analysis and Design

by
Brandon Patrick Haugh

A THESIS

Submitted to

Oregon State University

in partial fulfillment of
the requirements for the
degree of

Master of Science

Presented May 28, 2002
Commencement June 2003

Master of Science thesis of Brandon Patrick Haugh presented on May 28, 2002.

APPROVED:

Redacted for privacy

Major Professor, representing Nuclear Engineering

Redacted for privacy

Head of the Department of Nuclear Engineering

Redacted for privacy

Dean of Graduate School

I understand that my thesis will become part of the permanent collection of Oregon State University libraries. My signature below authorizes release of my thesis to any reader upon request.

Redacted for privacy

Brandon Patrick Haugh, Author

TABLE OF CONTENTS

TABLE OF CONTENTS (Continued)

TABLE OF CONTENTS (Continued)

LIST OF FIGURES

LIST OF FIGURES (Continued)

LIST OF FIGURES (Continued)

LIST OF TABLES

LIST OF TABLES (Continued)

LIST OF TABLES (Continued)

Multi Application Small Light Water Reactor Containment Analysis and Design

1 INTRODUCTION

This thesis presents an analysis of the behavior of the Multi Application Small Light Water Reactor (MASLWR) containment vessel during steady-state operation and simulated accident transients. The analysis will be performed on the full-scale prototype and a scaled test facility constructed at Oregon State University using the GOTHIC computer code. The MASLWR containment operates at high pressures exceeding 300 psia. High pressure containments like the design used in MASLWR have not been analyzed in the past. The containments used in current light water reactors are designed not to exceed 65 psia. The MASLWR takes advantage of the high pressure containment to reduce coolant inventory losses during a loss of coolant accident (LOCA). The important phenomenon of interest during a LOCA is the condensation that occurs on the containment wall, because it is the primary mechanism of energy removal and pressure reduction during the LOCA. To better understand this phenomenon a literature review was performed to assess condensation heat transfer modeling on vertical walls in the presence of noncondensible gases, and in direct contact condensation of steam bubbles in subcooled liquid.

The specific objectives for analysis of the MASLWR containment are:

- To determine the bounding pressure for the MASLWR containment.
- To examine the effect that the different condensation heat transfer models in the GOTHIC computer code have on the peak MASLWR containment pressure.
- To compare, using GOTHIC calculations, the scaled OSU experiment thermal hydraulic behavior with the full scale prototype thermal hydraulic behavior.

The MASLWR project is a joint effort between the Idaho National Environmental and Engineering Laboratory (INEEL), NEXANT Bechtel, and Oregon State University. The project is funded under a Nuclear Energy Research Initiative (NERI) grant from the Department of Energy (DOE).

The MASLWR is being considered for a Generation IV reactor classification. Generation IV is a new generation of nuclear energy systems that will be available to the commercial power generation market by 2030 or before. The goal of the Generation IV program is to provide sustainable clean energy for the world market. These systems should also minimize waste, reduce the future burden for waste storage and assure that the fuel is proliferation resistant to reduce possible diversion of weapons material. They must excel in safety and reliability, with a low probability of reactor core damage. The need for offsite emergency response should be eliminated. Generation IV systems should have a competitive financial risk with other energy sources, and have a distinct cost advantage.

The MASLWR design meets all of the Generation IV goals. To meet the sustainable goals of a changing global energy market the design was kept to a low power. This would help decrease costs and provide flexibility to commercial energy providers by allowing them to choose the number of systems to fulfill their local energy requirements. This design also incorporates extended refueling schedules with a goal of five to ten years between refueling. Proliferation resistant fuel is also being considered; specifically a thorium uranium mix is being considered which greatly decreases the production of plutonium, making it an unattractive source for weapons material. To help meet the economic goals, the reactor will be driven entirely by natural circulation. To further decrease costs, the design is modular and the entire containment and reactor will fit on a single rail car. This allows the system to be constructed at a factory. For safety and reliability the use of natural circulation is key. There are no pumps to break down and no other moving parts within the reactor vessel to wear. An integral part of the safety system is the containment itself. The containment is a pressure vessel, which is submerged in a containment pool at the reactor site.

The design itself is very simple. A schematic cross section of the MASLWR design is shown in Figure 1.1.

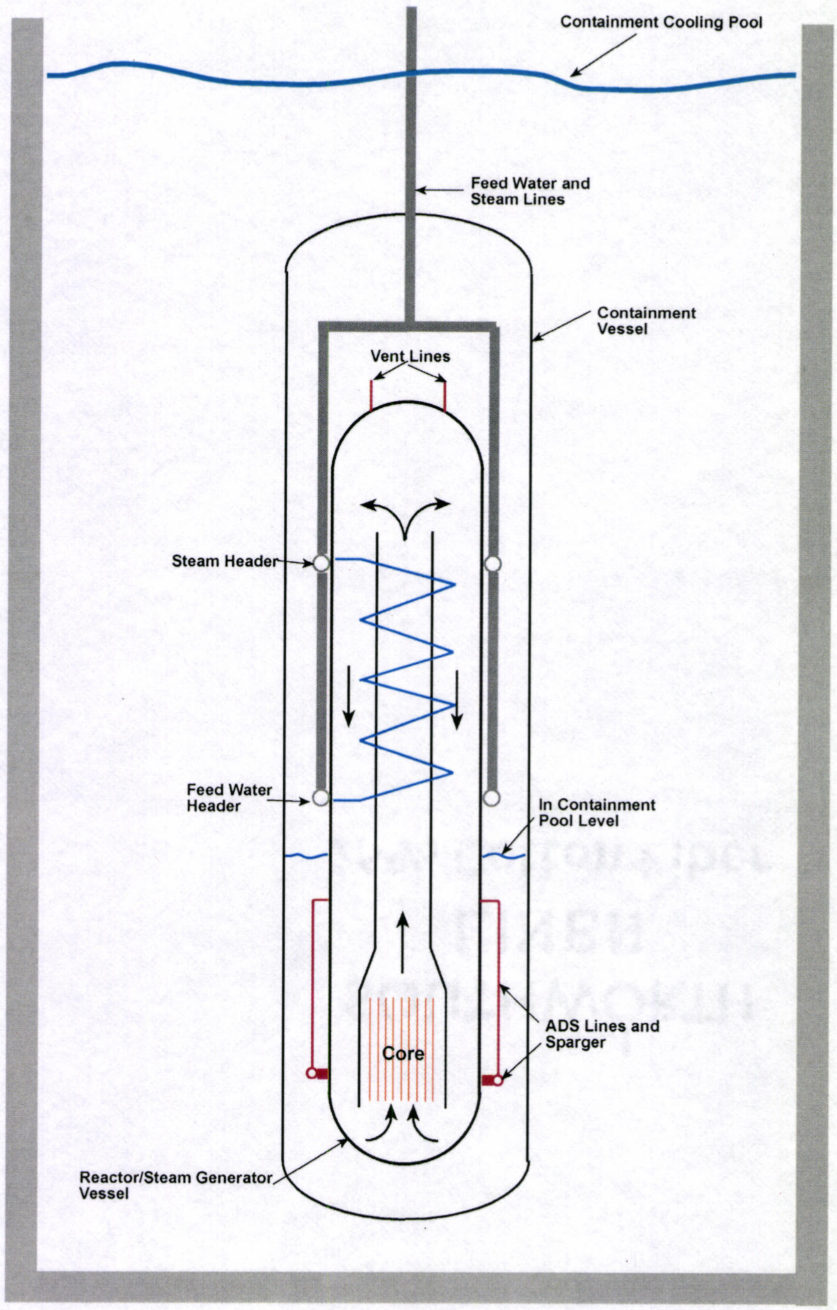

Figure 1.1: MASLWR Schematic

As shown in Figure 1.1, the primary fluid is within a single vessel with no typical cold or hot legs. The core is located at the bottom of the RX/SG vessel inside of a shroud. On top of this is the riser section where hot water leaving the core circulates upwards to the top of the vessel where it spills out. On the outside of this riser is the Steam Generator (SG) located within the downcomer annulus. This helical SG has equal length tubes that coil around the riser. The secondary fluid passes on the inside of these tubes with the goal of obtaining some superheat at the exit. A three dimensional drawing of the SG tube configuration is shown in Figure 1.2. The primary fluid cooled by the SG circulates to the bottom of the downcomer annulus where it enters the RX core.

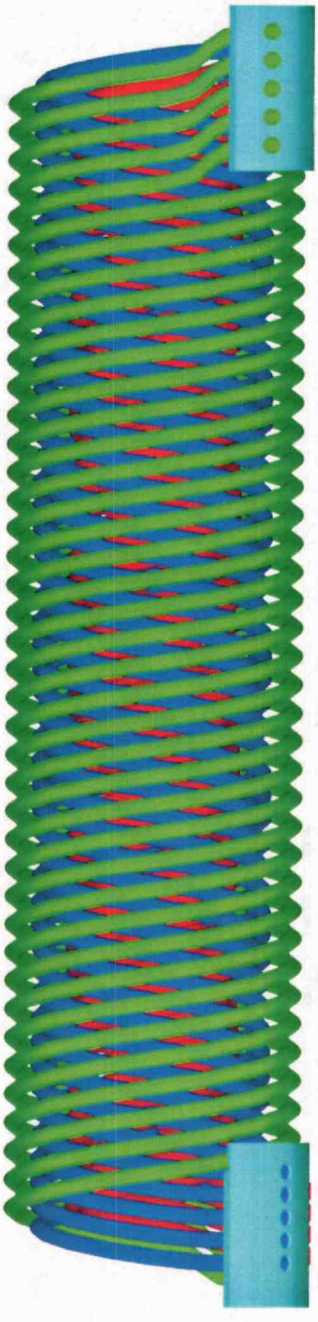

Figure 1.2: 3D Helical Steam Generator Tubes

Surrounding the RX/SG vessel is the containment vessel. The containment vessel is also a pressure vessel, which is different from most current designs. It also acts as the ultimate heat sink during accident scenarios, since it is submerged in a large pool of water.

2 LITERATURE REVIEW

Condensation heat transfer must be modeled correctly to obtain accurate predictions of containment pressures in MASLWR. Therefore, the literature review presented here includes descriptions of GOTHIC condensation models. It also will address the relevant research in the areas of direct contact condensation heat and wall condensation heat transfer modeling.

2.1 Description of GOTHIC

GOTHIC is an acronym, which stands for Generation of Thermal-Hydraulic Information for Containments. GOTHIC is a general-purpose thermal-hydraulics computer program for design, licensing, safety and operating analysis of nuclear power plant containments and other confinement buildings. Applications of GOTHIC include evaluation of containment and sub-compartments response to a variety of line breaks and equipment failures. The code is developed by Electric Power Research Institute (EPRI) and is maintained by Numerical Applications Inc. The full GOTHIC package includes three codes: GOTHIC_P, the pre and post processing graphical user interface, GOTHIC_S, the solver, and GOTHIC_G the graphics package.

GOTHIC_P is a graphical and menu driven preprocessor and post processor used to set up GOTHIC models, and interpret solution results. During preprocessing a model is built and used to write an input file for the solver GOTHIC_S. When preprocessing, the user draws a schematic picture of the model being built. From this schematic, cell connections, scale and other input parameters are interpreted. This input is organized in tables with appropriate units and headings. Either metric or English units may be used in the model construction. During postprocessing GOTHIC_P is used to select appropriate system variables and plot them to display. The variables can also be written to a formatted text file accessible using a third party program Tecplot.

GOTHIC_S is an advanced program that solves the conservation equations for mass, momentum, and energy for multi-component, multi-phase flows. The phase balance equations are coupled by mechanistic models for interface mass, energy and momentum transfer that cover the entire flow regime. The interface models allow for the possibility of thermal nonequilibrium between phases and unequal phase velocities. It also includes full treatment of the momentum transport terms in multi-dimensional models, with options for turbulent shear and turbulent mass and energy diffusion. The conservation equations are solved for three primary fields, Steam/Gas mixture, Continuous Liquid, and Liquid Droplets. There are also two possible secondary fields, Mist, and Ice.

2.1.1 Model Development

To run a problem in GOTHIC an appropriate model for the problem must be generated. Model generation is performed with GOTHIC_P. There are many steps in generating a model depending on the complexity. First of all the computational volume needs to be created. The volume or volumes can be either a single node lumped volume or may be 1, 2, or 3 dimensional with an orthogonal mesh. In the volume, parameters are specified for turbulence models, hydrogen burn models, molecular diffusion, etc. The volumes communicate hydraulically through flow paths. Flow paths can be pipes, ducts, doorways, or hallways. The volumes communicate thermally through conductors. The conductors can represent walls of adjacent volumes, or structures within a volume. There is also additional equipment that can be used. These components consist of spray nozzles, heat exchangers, heaters/coolers, pumps, fans, hydrogen recombiners, igniters, valves, and pressure relief valves. Once all of the appropriate components for a model are in place and the necessary input values for these components are inputted, initial conditions for the problem and the solution techniques to be used are then specified.

2.1.2 Governing Equations

GOTHIC solves a set of conservation equations for mass, energy and momentum. They are presented in integral form, because this is closely related to the finite volume numerical method used to solve them. The equations are written for a fixed volume V, bounded by an area A. The volume V may be interpreted as the entire computational volume, but in practice it is actually the volume of a computational cell.

2.1.2.1 Mass Conservation

Mass conservation equations are solved for five phases; liquid, steam, mist, ice, and drops, and for each noncondensing gas. The steam/gas mixture will now be referred to as the vapor phase, and may exist as bubbles or a continuous region. Liquids may be in the form of pools, films, or slugs. The general form of the mass balance is given by

$$\underbrace{\frac{\partial}{\partial t}\int_V \Theta \alpha_\phi \rho_{\phi\varsigma} dV}_{storage} = \underbrace{-\int_A \Psi \alpha_\phi \rho_{\phi\varsigma} \vec{u} \cdot \vec{n} dA}_{convection} + \underbrace{\int_{A_f} \Psi \alpha_\phi \rho_\phi D_\phi^c \vec{\nabla}\left(\frac{\rho_{\phi\varsigma}}{\rho_\phi}\right) \cdot \vec{n} dA}_{diffusion}$$

$$+ \underbrace{\int_{A_w} s_{\phi\varsigma}^c dA}_{boundary\ source} + \underbrace{\int_{A_{I_\phi}} S_{\phi\varsigma}^c dA_{I_\phi}}_{interface\ source} + \underbrace{E_{\phi\varsigma}^c}_{equipment\ source} + \underbrace{C_{\phi\varsigma}^c}_{combustion\ source} \qquad 2.1$$

where the subscript ϕ refers to the phase and takes on the values v (vapor), l (liquid), d (drops) and i (ice). An assumption that the mist takes up no volume in the vapor phase is used so that α_v is used for α_ϕ in the mist mass balance. The subscript ς refers to a component of the vapor, ($\varsigma = s$ for the steam component, $\varsigma = n$ for a single component of the noncondensing gas mixture, and $\varsigma = g$ for the noncondensing gas mixture). Since the vapor phase is the only phase with multiple components, the component subscripts can be ignored for other phases. Θ is the volume porosity and Ψ is the area porosity factor. The porosity factors vary from 0 to 1 with 1 being a completely unobstructed volume or area. α is the volume fraction, ρ is the density, $\vec{u}$ is the velocity, $\vec{n}$ is outward normal to the surface dA, A_f is that portion of the total surface area in contact with the adjacent fluid volumes, D^c is the mass diffusion coefficient (including turbulence effects only), s^c is the mass source per unit area generated at, or passing through, bounding wall A_w, S^c is the mass source per unit area coming from the interfacial area A_I, E^c is the mass source from engineered safety equipment and C^c is the mass source from hydrogen combustion. For liquid, drop, mist and ice phases, there is no contribution to the mass balance due to mass diffusion. There are also no convection terms included in the mass balance for ice.

2.1.2.2 Energy Conservation

Energy conservation equations are solved for three phases; drops, liquid, and vapor/mist, and for solid thermal conductors. The fluid energy equation is solved for enthalpy, so the equation is written in terms of enthalpy rather than internal energy. The fluid energy equation is as follows:

$$\frac{\partial}{\partial t}\int_V \Theta\alpha_\phi\left(\rho_\phi(h+ke)_\phi - P\right)dV = -\int_A \Psi\alpha_\phi\rho_\phi(h+ke)_\phi\vec{u}_\phi\cdot\vec{n}dA$$

storage *convection and flow work*

$$+\int_{A_f}\Psi\alpha_\phi\rho_\phi c_{p\phi}D_\phi^e\vec{\nabla}T_\phi\cdot\vec{n}dA + \sum_\varsigma\int_{A_f}\Psi\alpha_\phi D_\phi^c\rho_\phi\vec{\nabla}\left(\frac{\rho_{\phi\varsigma}}{\rho_\phi}\right)h_{\phi\varsigma}\cdot\vec{n}dA \qquad 2.2$$

thermal diffusion *mass diffusion*

$$+\int_{A_w}s_\phi^e dA + \int_{A_{I_\phi}}S_\phi^e dA_{I_\phi} + E_\phi^e + C_\phi^e$$

boundary source *interface source* *equipment source* *combustion source*

where h is enthalpy, ke is kinetic energy, P is static pressure, D^e is the thermal diffusion coefficient, s^e is the energy source per unit wall area, S^e is the energy source per unit interfacial area, E^e is the equipment energy source and C^e is the energy source from hydrogen combustion. Kinetic energy is included or neglected by user selection, and all other energy forms not explicitly represented above are neglected, such as viscous dissipation. The kinetic energy is defined as $ke_\phi = \frac{u_\phi^2}{2}$. All components of the vapor are assumed to be at the same temperature. The enthalpy in the vapor energy is the mixture energy of the steam, noncondensing gas mixture and the mist. The energy transported with the mass through mass diffusion is included only for the vapor. The ice energy equation is eliminated by assuming that the ice remains at its initial temperature until melted.

The energy equation for the solid conductors is

$$\int_{V_{cn}}\rho_{cn}c_{p,cn}\frac{\partial T_{cn}}{\partial t}dV_{cn} = \int_{A_i}D_{cn}^e\vec{\nabla}T_{cn}\cdot\vec{n}dA + \int_{A_b}s_{cn}^e dA \qquad 2.3$$

storage *diffusion* *boundary source*

where the subscript cn refers to a particular conductor, V_{cn} is the volume of the conductor or portion of a conductor, A_i is the surface area of V_{cn} internal to the conductor, D_{cn}^e is the diffusion coefficient (conductivity) and A_b is the external bounding surface area of the conductor which may be in contact with one or more fluid phases.

2.1.2.3 Momentum Conservation

Momentum conservation equations are solved for three phases; liquid, vapor, and drops. The general integral form of the conservation equation is

$$\underbrace{\frac{\partial}{\partial t}\int_V \Theta\alpha_\phi\rho_\phi\vec{u}_\phi dV}_{storage} = \underbrace{-\int_A \Psi\alpha_\phi\rho_\phi\vec{u}_\phi(\vec{u}_\phi\cdot\vec{n})dA}_{convection} + \underbrace{\int_{A_f} \Psi\alpha_\phi\underline{\sigma}_\phi\cdot\vec{n}dA}_{surface\ stress} + \underbrace{\int_V \Theta\vec{g}\alpha_\phi\rho_\phi dV}_{body\ force}$$

$$+ \underbrace{\int_{A_w} \vec{s}_\phi^m\, dA}_{boundary\ source} + \underbrace{\int_{A_I} \vec{S}_\phi^m dA_{I_\phi}}_{interface\ source} + \underbrace{\vec{E}_\phi^m}_{equipment\ source} \qquad 2.5$$

where the tensor $\underline{\sigma}_\phi$ includes the static pressure and viscous Reynolds stress terms. $\vec{g}$ is the gravitational acceleration, $\vec{s}^m$ is the momentum source per unit wall area, $\vec{S}^m$ is the momentum source per unit interfacial area and $\vec{E}^m$ is the momentum source from equipment. All components of the vapor are assumed to be at the same velocity. The density in the vapor momentum equation includes all of the component densities at their partial pressures, as well as the mist per unit vapor volume.

2.1.3 Equations of State

2.1.3.1 Vapor

The Dalton model is used for the steam/gas mixture. It is assumed that each component of the vapor phase exists at the volume and temperature of the mixture.

The total pressure (P_v) is equal to the sum of the component partial pressures shown here

$$P_v = \sum_{\varsigma} P_{v\varsigma} \qquad 2.6$$

where $P_{v\zeta}$ is a partial pressure of a vapor component. A correction may need to be applied to the vapor pressure if in the same computational cell there exists a pool surface. The pressure variable lives at the center of the cell and if the pool surface is above this the liquid pressure head needs to be subtracted from the vapor pressure. The steam density and temperature are obtained from the steam/water table correlations using enthalpy and pressure properties. All vapor phase components are assumed to be at the same temperature, with the density of each component calculated by

$$\rho_{v\varsigma} = \frac{P_{v\varsigma}}{R_{v\varsigma} T_{v\varsigma}} \qquad 2.7$$

where $R_{v\zeta}$ is the gas constant for gas component ζ. Changes in the gas enthalpy are given by

$$dh_{v\varsigma} = c_{p_{v\varsigma}} dT_{v\varsigma} \qquad 2.8$$

The total vapor phase density is then just the sum of the component densities, and the vapor phase enthalpy is given by

$$h_v = \frac{1}{\rho_v} \sum_{\varsigma} h_{v\varsigma} \rho_{v\varsigma} \qquad 2.9$$

2.1.3.2 Liquid and Drops

For the liquid and drops the static pressure is assumed to be the total pressure. The temperature and density of the liquid and drops is obtained from the steam tables based on enthalpy and pressure.

2.1.3.3 Mist

GOTHIC uses the mist macroscopic density (ρ_{mt}), which is mist density per unit volume. The thermodynamic density is need to calculate this and is determined from steam tables based on vapor phase pressure and saturation temperature at the steam partial pressure. The enthalpy (h_{mt}) is also evaluated by these properties.

2.1.4 Source Terms

Source terms are included in the governing equations. These sources can consist of energy, mass, and momentum sources coming from boundary conditions, or interaction of the fluids with the bounding conductors.

2.1.4.1 Mass Source

Surface mass source terms include sources and sinks due to phase change at a non-fluid surface. E.g. condensation heat transfer on a conductor is a sink for steam and a source for liquid. The boundary source terms for the mass balances are

$$\int_{A_w} s_v^c dA = \sum_w \Gamma_{w_v} \qquad 2.10$$

$$\int_{A_w} s_l^c dA = \sum_w \Gamma_{w_l} \qquad 2.11$$

$$\int_{A_w} s_d^c dA = 0 \qquad 2.12$$

where Γ_w is the phase change resulting directly from heat transfer to the wall and the sum is over all conductors connected to the volume.

2.1.4.2 Energy Source

Energy sources include convection, and radiation heat transfer from walls. It also includes the energy associated with phase change during condensation and evaporation at the conductor wall. One assumption is there is no heat transfer between the drop phase and the walls. The boundary energy source terms are given by

$$\int_{A_w} s_v^e dA = \sum_w Q_{w_v} \tag{2.13}$$

$$\int_{A_w} s_l^e dA = \sum_w Q_{w_l} \tag{2.14}$$

$$\int_{A_w} s_d^e dA = 0 \tag{2.15}$$

where Q_w includes the sensible heat flux from the wall to the fluid and also the energy due to phase change (Γ_w).

For the solid conductors, the surface heat flux is either specified or it is calculated from known conductor and fluid temperatures and heat transfer coefficients. The boundary source term for the conductor energy equation, including the sensible heat flux and latent heat associated with phase change is

$$\int_{A_w} s_{cn}^e dA = -Q_w \tag{2.16}$$

where Q_w, is the wall heat calculated from the specified wall boundary conditions.

The heat transferred to the wall takes the form of

$$Q_{w_v} = \Gamma_w^{cond} h_v + Q_{conv_v} + Q_{rad} \tag{2.17}$$

for the vapor phase, and

$$Q_{w_l} = -\Gamma_w^{cond} h_f + Q_{conv_l} \tag{2.18}$$

for the liquid phase.

The convective component is given by correlations for forced and natural convection. The heat transfer is given by

$$Q_{conv_v} = A_{cn} H_{conv_v} \Delta T_{conv_v} \tag{2.19}$$

for the vapor phase, and

$$Q_{conv_l} = A_{cn} H_{conv_l} (T_w - T_l) \tag{2.20}$$

where A_{cn} is the conductor surface area within a cell, H_{conv_v} and H_{conv_l} are the vapor and liquid convective heat transfer coefficients. For the vapor convective heat transfer ΔT_{conv_v} can be selected from

$$\Delta T_{conv_v} = \begin{bmatrix} Max(T_w, T_{sat}) - T_v \\ T_w - T_v \\ T_w - T_{sat} \\ T_w - T_i \end{bmatrix} \tag{2.21}$$

where T_w is the wall temperature, T_v is the vapor temperature, T_{sat} is the saturation temperature at the steam partial pressure, and T_i is input by the user. The convective heat transfer coefficients are broken up into natural and forced convection. For the case we are considering the natural convection option was used for a vertical surface. The natural convection heat transfer coefficient for a flat vertical surface is

$$H_{nc} = \frac{k}{l} Max\left(0.59 Ra^{0.25}, 0.13 Ra^{1/3}\right) \tag{2.22}$$

where Ra is the Rayleigh number (the product of the Prandtl number and Grashof number). The forms of the Prandtl number and Grashof number are

$$Pr = \frac{c_p \mu}{k} \tag{2.23}$$

$$Gr = \frac{g|\rho_w - \rho|\rho l^3}{\mu^2} \tag{2.24}$$

where ρ_w is the density given at the wall conditions.

The radiant component transfers heat between the steam and the conductor surface. The radiant heat flux is given by

$$Q_{rad} = A_{cn} \sigma_B \frac{\left(1 + \varepsilon_w^r\right)}{2} \left(\alpha_{vw}^r T_w^4 - T_v^4\right) \tag{2.25}$$

where σ_B is the Stefan-Boltzmann constant, ε_w^r is the surface emissivity equal to 0.65 for dry walls and 0.96 for wet walls. The gas emissivity is given by

$$\varepsilon_v^r = 0.680\left(1 - e^{-1.22\sqrt{\chi_p}}\right) \tag{2.26}$$

where χ_p is

$$\chi_p = P_{vs} l_{eff} \frac{300}{T_v}\left(P_{vg} + bP_{vs}\right) \tag{2.27}$$

and b is the self-broadening coefficient

$$b = 5\left(\frac{300}{T_v}\right)^{0.5} + 0.5 \tag{2.28}$$

The vapor temperature T_v is given in Kelvin. The pressures are in atmospheres, and $l_{eff} = 0.9D_h$ is the effective beam length in meters. The gas absorptivity is

$$\alpha_{vw}^r = \varepsilon_v^r\left(\frac{T_v}{T_w}\right)^{0.5} \tag{2.29}$$

The last mode of heat transfer is associated with condensation. GOTHIC offers several options for the calculation of condensation heat transfer to the walls, but only those used in this work are presented here. These models are those of Uchida and Gido/Koestel. The condensation heat transfer is given by

$$Q_{cond} = H_{cond} A_{cn} \Delta T_{cond} \tag{2.30}$$

The temperature difference used ΔT_{cond} is one of these options

$$\Delta T_{cond} = \begin{bmatrix} T_w - Min(T_v, T_{sat}) \\ T_w - T_v \\ T_w - T_{sat} \\ T_w - T_i \end{bmatrix} \tag{2.31}$$

The condensation heat transfer coefficient for the Uchida option is given by

$$H_{Uchida} = 79.33\left(\frac{\rho_{vs}}{\rho_{vg}}\right)^{0.8} \frac{Btu}{hr - ft^2 - F} \tag{2.32}$$

the upper bound of this correlation is 278 and the lower bound is 2 *Btu/hr-ft*^{2}*-F*. This correlation does not take into account the effect of local velocity on the heat and mass transfer rates. The Gido/Koestel correlation has some dependency on the velocity and room height for natural convection effects. GOTHIC uses the maximum of the natural and forced convection correlations. They are

$$H_{GK}^{NC} = 5.25\left[\left(\frac{u_f}{u_w}\right)^2 \frac{1}{Sc_t}\frac{u_w}{u_\delta} C^* \frac{\left(\rho_{vs}-\rho_{vs_i}\right)}{\rho_l}\right]^{\frac{12}{7}} \frac{\rho_l h_{fg}}{T_{sat}-T_w}\left[\frac{\rho_l g^4 l^5}{\mu_l}\right]^{\frac{1}{7}} \tag{2.33}$$

and

$$H_{GK}^{FC} = \frac{\left(\frac{u_f}{u_v}\right)^2 \frac{u_v}{Sc_t} C^* h_{fg}\left(\rho_{vs}-\rho_{vs_i}\right)}{\left(1-\frac{u_w}{u_v}\right)\left(T_{sat}-T_w\right)} \tag{2.34}$$

where u_f/u_w is the ratio of the interface friction velocity to the wave crest velocity (assigned a value of 1/7.0). Sc_t is the turbulent Schmidt number (assigned a value of 0.5). u_w/u_δ is the ratio of wave crest velocity to the condensate interface velocity (assigned a value of 1). ρ_{vs_i} is the interface steam density, and l is the height of the room. u_f/u_v is the ratio of the interface friction velocity to the bulk gas velocity (assigned a value of 0.05). u_v is the bulk vapor velocity from junctions into the cell and other connected cells. u_w/u_v is the ratio of the wave crest velocity to the bulk gas velocity (assigned a value of 0.425). C^* is a correction factor for high condensation rates given by

$$C^* = \frac{\ln\left(1+\lambda^*\right)}{\lambda^*} \tag{2.35}$$

the parameter λ^* is

$$\lambda^* = \frac{P_{sat}\left(T_w\right)-P_{vs}}{P-P_{sat}\left(T_w\right)} \tag{2.36}$$

From the total condensation heat transfer rate, the wall condensation rate can be computed from

$$\Gamma_w^{cond} = \frac{Q_{cond}}{h_{vs}-h_f\left(P_{vs}\right)} \tag{2.37}$$

where h_{vs} is the steam enthalpy and P_{vs} is the steam partial pressure.

2.1.4.3 Momentum Source

The boundary momentum source includes friction and form drag due to walls, orifices, and obstructions. The boundary source terms for the momentum equations are

$$\int_{A_w} s_\phi^m dA = D_\phi \tag{2.38}$$

The drag for an obstruction or orifice is given by

$$D_\phi^o = A\alpha_\phi \frac{K}{2}\rho_\phi u_\phi |u_\phi| \tag{2.39}$$

where K is a user defined loss coefficient, A is the free area of the flow connection and u_ϕ is the velocity component normal to A. The drag is calculated for the liquid, vapor, and drop phases.

Friction drag for the walls is calculated for the vapor and liquid phases only and is given by

$$D_\phi^f = \lambda_{f_\phi} A \frac{f(\mathrm{Re}_\phi)l}{2D_h} \rho_\phi u_\phi |u_\phi| \tag{2.40}$$

where l is the length of the wall and λ_f represents ramp functions that put all of the drag on the liquid phase until the flow is in the single phase vapor regime.

2.1.5 Interface Source Terms

The interface source terms are calculated by performing mass, momentum , and energy balances for the interfaces. There are seven interface conditions considered in GOTHIC; liquid/vapor, drops/vapor, ice/vapor, ice/liquid, drops/liquid, mist/vapor and mist/(drop or liquid). The interchange at these interfaces includes heat transfer associated with a change in phase and mechanical interactions that result in interfacial mass and momentum transfer.

The choices of interfacial heat transfer coefficients, drag coefficients, and areas depend highly on the geometry of the multi-phase flow. To help in deciding what geometry is present flow regime maps have been established for vertical and horizontal flow to predict the flow regime based on void fractions within a cell or junction. The vertical flow regimes are shown in Figure 2.1. For each of the flow regimes different correlations and models are used for bubble size, interfacial area, heat and mass transfer.

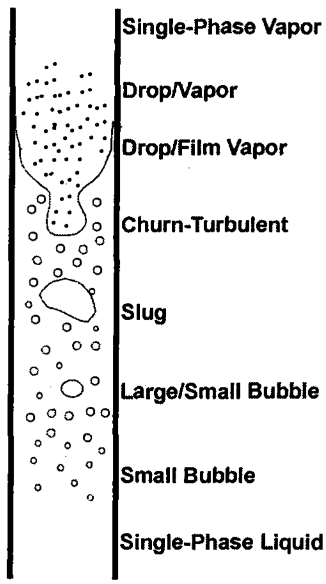

Figure 2.1: Vertical Flow Regimes

This flow regime map is only used for cells with walls that have a temperature less than the critical heat flux temperature. For models and correlation selection GOTHIC has condensed this map by combining the slug flow and Large/Small Bubble regimes.

2.1.5.1 Small Bubble Regime

If the vapor volume fraction (α_v) within a cell is less than 0.2 the small bubble regime is assumed with spherical or distorted bubbles. The average radius for the bubbles is given by a critical Weber number criterion

$$r_{sb} = Min\left(\frac{0.5We_b^c\sigma}{\rho_l u_{vl}^2}, 0.5D_h, 0.02ft\right) \tag{2.41}$$

where We_b^c is the critical Weber number, assigned a value of 10, σ is the surface tension, D_h is the hydraulic diameter of the cell, and u_{vl} is the vapor/liquid relative velocity (u_v-u_l). The condition for radius corresponds to the Weber number limited bubble radius with a velocity of 1ft/s. The second is that the small bubble diameter not exceed the hydraulic diameter of the cell. The last condition is that the assumed minimum size for the small bubble radius is 0.02 ft. Some small bubbles will exist throughout the flow regimes until film conditions are achieved. In these regimes the same equation is used for the small bubble radius. The bubble rise velocity is calculated by

$$u_{br} = \frac{\sqrt{2}\left(\frac{\sigma g \Delta\rho}{\rho_l^2}\right)^{0.25}}{1-\alpha_v} \tag{2.42}$$

where σ is the liquid surface tension and $\Delta\rho = \rho_l - \rho_v$. The interfacial area for the small bubbles is calculated by

$$A_{vl} = \frac{3V_v}{r_b} \tag{2.43}$$

$$A_{vd} = \begin{pmatrix} 0.0 \; for \; heat \; and \; mass \; transfer \\ A_d''' \; for \; momentum \; transfer \end{pmatrix} \tag{2.44}$$

where A_{vl} is the vapor/liquid interfacial area, and A_{vd} is the vapor/drop interfacial area. An assumption of no heat and mass transfer between these phases is used. A_d''' is the drop interfacial area concentration. The interfacial drag force per unit volume is calculated by

$$\tau'''_{vl} = -0.375 C_{D_b} \frac{\alpha_v \rho_l}{r_b} |u_{vl}| u_{vl} \qquad 2.45$$

where C_{D_b} is the bubble drag coefficient for small bubbles given by

$$C_{D_{sb}} = (1-\alpha_v)^2 Max\left[\begin{array}{c} Max\left(\frac{24}{\text{Re}_b}\left(1+0.1\text{Re}_b^{0.75}\right), 0.45\right) \\ Min\left(\frac{\sqrt{2}}{3}\left(\frac{\mu_l}{(\rho_l\sigma_l)^{0.5}\left(\frac{\sigma_l}{g(\rho_l-\rho_v)}\right)^{0.25}}\right)\text{Re}_b, 2.67\right) \end{array}\right] \qquad 2.46$$

here Re_b is the bubble Reynolds number given in Table 2.5.

2.1.5.2 Large/Small Bubble Regime

When void fraction in a flow increases, bubbles will begin to coalesce into larger bubbles. It is assumed that this regime begins as the vapor volume fraction increases beyond 0.2 (refered to as the small bubble limit, α_{sbl}). For a cell with a vapor volume fraction greater than α_{sbl}, the liquid is assumed to contain small dispersed bubbles at a vapor volume fraction of α_{sbl}, while the remainder of the vapor forms a large bubble. As the vapor volume fraction grows the large bubble reaches a critical radius and then another large bubble will form. With these assumptions for a cell of volume V, the large bubble radius is given by

$$r_{lb} = \left(\frac{3V}{4\pi}\left(\alpha_v - \alpha_{sbl}\frac{(1-\alpha_v)}{(1-\alpha_{sbl})}\right)\right)^{\frac{1}{3}} \qquad 2.47$$

where the maximum diameter is assumed to be 6 inches or the hydraulic diameter of the cell. The interfacial area is calculated using the same equations as the small bubble regime. The interfacial drag force per unit volume is the same as for small bubbles, but with a different drag coefficient that is weighted between the small and large bubbles. The large bubble drag coefficient is given by

$$C_{D_{lb}} = (1-\alpha_v)^2 Max\left[\frac{24}{\mathrm{Re}_b}\left(1+0.1\mathrm{Re}_b^{0.75}\right), 0.45\right] \quad 2.48$$

For the mixed bubbles the drag coefficient is

$$C_{D_{s,lb}} = 0.5\rho_l\left(\frac{N_{sb}C_{D_{sb}}}{g_{sb}^2}+\frac{N_{lb}C_{D_{lb}}}{g_{lb}^2}\right)|u_{vl}| \quad 2.49$$

where

$$N_{sb} = \alpha_{sb,\lim}\frac{3V}{4r_{sb}} \quad 2.50$$

$$N_{lb} = (\alpha_v - \alpha_{sb.\lim})\frac{3V}{4r_{lb}} \quad 2.51$$

with $\alpha_{sb,\lim} = 0.2$, and

$$g_{sb} = \frac{\alpha_{sb,\lim} + \dfrac{\alpha_v - \alpha_{sb.\lim}}{y_b}}{\alpha_v} \quad 2.52$$

$$g_{lb} = \frac{\alpha_{sb,\lim} y_b + (\alpha_v - \alpha_{sb,\lim})}{\alpha_v} \quad 2.53$$

$$y_b = \sqrt{\frac{\alpha_{sb,\lim}}{(\alpha_v - \alpha_{sb,\lim})}\frac{N_{lb}}{N_{sb}}\frac{C_{D_{lb}}}{C_{D_{sb}}}} \quad 2.54$$

2.1.5.3 Churn-Turbulent and Film Regimes

As the vapor volume fraction continues to increase the large bubbles will begin to coalesce and the flow will progress to a churn-turbulent regime followed by a film flow regime. The transition to churn-turbulent flow is assumed to begin as the vapor volume fraction exceeds 0.5. This regime is assumed to exist until a stable liquid film is established. When this occurs depends on the flow channel size and vapor velocity. The minimum stable film thickness is given by

$$\delta_{crit} = \frac{0.5\sigma}{\rho_v u_{vl}^2} \tag{2.55}$$

This film thickness can also be related to the stable film vapor volume fraction if a cylindrical channel of diameter equal to the hydraulic diameter is assumed:

$$\alpha_{v_{crit}} = 1 - \frac{4\delta_{crit}}{D_h} \tag{2.56}$$

The lower limit on the vapor volume fraction for the film flow regime, $\alpha_{f_{limit}}$, is assumed to be the larger of $\alpha_{v_{crit}}$ and 0.8. In calculating interfacial area, drag coefficient, and heat transfer coefficient a weighting is used between the large bubble and film regimes. The weighting factors are given by

$$\lambda_{film} = \left(\frac{\alpha_v - 0.5}{1 - \alpha_{v_{crit}} - \alpha_d - 0.5} \right)^2 \tag{2.57}$$

$$\lambda_{bubble} = \left(\frac{1 - \alpha_{v_{crit}} - \alpha_d - \alpha_v}{1 - \alpha_{v_{crit}} - \alpha_d - 0.5} \right)^2 \tag{2.58}$$

where α_d is the drop volume fraction. For the film regime the interfacial area is given by

$$A_{vl} = \sqrt{1 - \alpha_d}\, P_w \frac{V}{A} \tag{2.59}$$

$$A_{vd} = A_d''' V \tag{2.60}$$

where A is the cell cross-sectional area, and P_w is the wetted perimeter. The drag per unit volume for a film is expressed as

$$\tau_{vl}''' = 4 \frac{f_I}{D_h} \sqrt{\alpha_v}\, \rho_v |u_{vl}| u_{vl} \tag{2.61}$$

where the same drag is imposed on the vapor but in the opposite direction. For stable films the friction factor, f_I, is given by

$$f_I = 0.0025(1 + 75\alpha_l) \tag{2.62}$$

In the film regime, drops are present and the drag per unit volume is analogous to the small bubble drag eith the vapor properties replaced by drop properties.

2.1.5.4 Liquid/Vapor, Drop/Vapor Heat and Mass Transfer

Heat and mass are transferred at the phase interfaces by vaporization and condensation. The convected heat from the vapor and vapor to the interface are, respectively:

$$Q_{vl}^{c} = H_{vl} A_{vl} (T_v - T_{Il}) \qquad 2.63$$

$$Q_{ll}^{c} = H_{ll} A_{vl} (T_l - T_{Il}) \qquad 2.64$$

Here T_{Il} is the interface temperature to be calculated, H_{vl} and H_{ll} are the convective heat transfer coefficients on the vapor and liquid sides of the interface and A_{vl} is the interface area. An energy balance at the interface gives

$$\Gamma_l \Delta h_{sl} = Q_{vl}^{c} + Q_{ll}^{c} \qquad 2.65$$

where Γ_l is the rate of phase change and Δh_{sl} is the heat associated with the change of phase and is given by

$$\Delta h_{sl} = h_{vs} - h_l \qquad 2.66$$

where h_{vs} is the enthalpy of the steam in the vapor phase and h_l is the enthalpy of the liquid. The rate of phase change Γ_l is given by

$$\Gamma_l = H_{ml} M_s A_{vl} \frac{\phi_{Ils} - \phi_{vs}}{1 - \phi_{Ils}} \qquad 2.67$$

where H_{ml} is the mass transfer coefficient, M_s is the molecular weight of steam, ϕ_{Ils} is the steam mole fraction at the interface and ϕ_{vs} is the steam mole fraction in the bulk vapor. ϕ_{Ils} is a partial pressure ratio

$$\phi_{Ils} = \frac{P_{sat}(T_{Il})}{P} \qquad 2.68$$

where $P_{sat}(T_{Il})$ is the steam partial pressure at the interface and P is the total pressure. The temperature at the interface can be computed using equations 2.63-2.68. With T_{Il} known, the phase heat sources can be calculated and are

$$Q_{vl} = H_{vl} A_{vl} (T_{Il} - T_v) + \Gamma_l h_{vs} \qquad 2.69$$

$$Q_{vl} = H_{ll} A_{vl} (T_{Il} - T_l) + \Gamma_l h_l \qquad 2.70$$

The equations for the vapor/drop phase interface are analogous.

The heat transfer coefficients are obtained from the Nusselt number where

$$H = Nu\frac{k}{d} \qquad 2.71$$

where k is the fluid conductivity and d is a characteristic length. The mass transfer is obtained by analogy with the heat transfer coefficient giving a mass transfer Nusselt number

$$Nu_m = H_m \frac{d}{\Phi_v D_{sg}} \qquad 2.72$$

where H_m is the mass transfer coefficient, Φ_v is the molar concentration of the vapor phase, D_{sg} is the binary diffusion coefficient for steam in the noncondensing gas mixture. The Nusselt number correlations are given in Table 2.1-2.4 for bubbles, films, drops, and pool surfaces.

Table 2.1: Bubble Interfacial Heat and Mass Transfer Correlations

Coefficient	Correlation
$Nu_{vl}(d_b)$	$2.0 + 0.74 Re_{bv}^{0.5} Pr_v^{1/3}$
$Nu_{ll}(d_b)$	$2.0 + 0.74 Re_{bl}^{0.5} Pr_v^{1/3}$
$Nu_{ml}(d_b)$	$2.0 + 0.74 Re_{bl}^{0.5} Pr_v^{1/3}$

Table 2.2: Film Interfacial Heat and Mass Transfer Coefficients

Coefficient	Correlation
$Nu_{vl}(D_h)$	$Max\begin{pmatrix} 0.13(Gr_v Pr_v)^{1/3} \\ f_I Re_v Pr_v^{1/3} \end{pmatrix}\Theta_T$
$Nu_{ll}(D_h)$	$Max\begin{pmatrix} \frac{f_I \rho_v}{\rho_l} Re_l Pr_l^{1/3} \\ 8Pr_l^{1/3} \\ \frac{2D_h}{\delta_{film}} \end{pmatrix}$
$Nu_{ml}(D_h)$	$Max\begin{pmatrix} 0.13(Gr_v Sc_v)^{1/3} \\ f_I Re_v Sc_v^{1/3} \end{pmatrix}\Theta_M$

Table 2.3: Drop Interfacial Heat and Mass Transfer Coefficients

Coefficient	Correlation
$Nu_{vd}(d_d)$	$2.0 + 0.74 Re_d^{0.5} Pr_v^{1/3}$
$Nu_{dd}(d_d)$	$\left(Nu_l^6 + Nu_t^6\right)^{1/6}$ $Nu_l = 2.0 + 0.53 Ra^{0.25}$ $Nu_t = 0.098 Ra^{0.345}$
$Nu_{md}(d_d)$	$2.0 + 0.74 Re_d^{0.5} Sc_v^{1/3}$

Table 2.4: Pool Interfacial Heat and Mass Transfer Coefficients

Coefficient	Correlation
$Nu_{vl}(D_h)$	$Max\begin{pmatrix} 0.036Re_v^{0.8}Pr_v^{1/3} \\ 0.21(Gr_vPr_v)^{1/3} \\ \frac{D_h}{L} \end{pmatrix}\Theta_T$
$Nu_{ll}(D_h)$	$Max\begin{pmatrix} \frac{2D_h}{PoolDepth} \\ 0.13(Gr_lPr_l)^{1/3} \end{pmatrix}$
$Nu_{ml}(D_h)$	$Max\begin{pmatrix} 0.036Re_v^{0.8}Sc_v^{1/3} \\ 0.21(Gr_vSc_v)^{1/3} \\ \frac{D_h}{L} \end{pmatrix}\Theta_M$

In the film correlations Θ_T and Θ_M are factors used in the case of high mass transfer to take into account diffusion induced convection. The factors are

$$\Theta_T = \frac{\varphi_T}{e^{\varphi_t} - 1} \qquad 2.73$$

$$\Theta_M = \frac{\varphi_M}{e^{\varphi_M} - 1} \qquad 2.74$$

$$\varphi_t = \frac{\Gamma_l'' c_{p_x}}{H_{vl}} \qquad 2.75$$

$$\varphi_m = \frac{\Gamma_l''}{H_{ml}} \qquad 2.76$$

Table 2.5: Parameters for Interfacial Transfer

Parameter	Definition	Description
Gr_l	$\dfrac{d^3 \rho_l g \Delta\rho_l}{\mu_l^2}$	Liquid Grashof Number
Gr_v	$\dfrac{d^3 \rho_v g \Delta\rho_v}{\mu_v^2}$	Vapor Grashof Number
Pr_v	$\dfrac{c_{p_v} \mu_v}{k_v}$	Vapor Prandtl Number
Pr_l	$\dfrac{c_{p_l} \mu_l}{k_l}$	Liquid Prandtl Number
Re_{bl}	$\dfrac{2r_b \rho_l \lvert u_{vl} \rvert}{\mu_{mb}}$	Bubble Reynolds Number for Liquid
Re_{bv}	$\dfrac{2r_b \rho_v \lvert u_{vl} \rvert}{\mu_v}$	Bubble Reynolds Number for Vapor
Re_d	$\dfrac{2r_d \rho_v \lvert u_{vd} \rvert}{\mu_{mb}}$	Drop Reynolds Number
Re_f	$\dfrac{D_h \rho_l \lvert u_l \rvert}{\mu_l}$	Liquid Reynolds Number for Annular Flow
Re_v	$\dfrac{D_h \rho_v \lvert u_{vl} \rvert}{\mu_v}$	Vapor Reynolds Number for Annular Flow
Sc_v	$\dfrac{\mu_v}{\rho_v D_{sg}}$	Vapor Schmidt Number
μ_{mb}	$\mu_l (1-\alpha_v)^{-2.5\frac{\mu_v+0.4\mu_l}{\mu_v+\mu_l}}$	Mixture Viscosity for Bubbly Flow
μ_{md}	$\mu_v (\alpha_v)^{-2.5\frac{\mu_l+0.4\mu_v}{\mu_v+\mu_l}}$	Mixture Viscosity for Drops

Other mechanisms for interface transfer are included in GOTHIC, such as drop entrainment and deposition and jet breakup models. Details of these models are omitted in this thesis, as they are not of interest in the current study. This information can be found in reference [1].

2.1.6 Finite Volume Equations

The equations presented earlier cannot, in general be, solved analytically. For this reason GOTHIC uses numerical techniques to solve the balance and transport equations. The solution requires that the balance equations be discretized. In GOTHIC, a rectangular mesh is used. The scalar mass and energy balances are solved on the grid lines, while the momentum balances are solved on the shifted grid show in Figure 2.2. The Cell of Interest is Cell C. The solid lines enclose the subvolumes in which the scalar mass and energy balances are solved. The dashed lines denote the shifted cell in which the momentum balances are solved. The finite volume equations used in GOTHIC use a porous medium representation of the balance equations. This is done to represent obstructions within the rectangular cells by varying the volume and surface porosities.

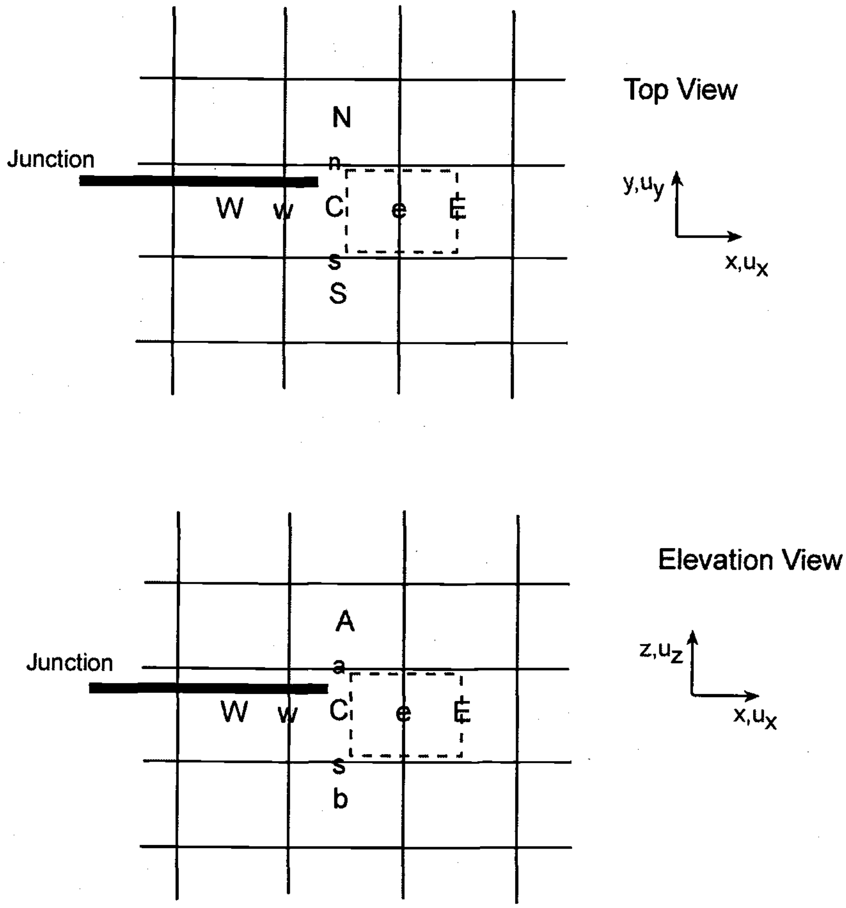

Figure 2.2: GOTHIC Computational Grid

The equations are then modified to account for the porosity by a Heaviside function defined by

$$H(x) = \begin{pmatrix} 1 \textit{ if } x \textit{ is in the fluid} \\ 0 \textit{ if } x \textit{ is in an obstacle} \end{pmatrix} \qquad 2.76$$

2.1.6.1 Mass Balance

The finite volume equation for mass balance is

$$\int_V \left(\frac{\partial}{\partial t} H\alpha\rho + \vec{\nabla} \cdot \vec{u} H\alpha\rho - \vec{\nabla} \cdot \left(H c_m \alpha\rho \vec{\nabla} \bar{\chi} \right) + H S_m \right) dV \qquad 2.77$$

where α is the phase volume fraction, $\vec{u}$ is the fluid velocity, c_m is the diffusion coefficient, χ is the mole concentration, and S is a source term. If the time derivative is taken outside the integral and the divergence theorem is applied, the volume integral can be converted to a surface integral:

$$\frac{\partial}{\partial t} \int_V H\alpha\rho dV = -\int_A H\alpha\rho \vec{u} \cdot \vec{n} dA + \int_A H\alpha\rho c_m \vec{\nabla} \bar{\chi} \cdot \vec{n} dA + \int_V H S_m dV \qquad 2.78$$

Assuming that α, ρ and S are constant within V, the surface integrals can be replaced by discrete summations over the grid given by

$$V\Theta \frac{\partial \alpha\rho}{\partial t} = - \sum_{i \in \{nsewab\{j\}\}} \langle H\alpha\rho u \rangle_i A_i + \sum_{i \in \{nsewab\{j\}\}} \langle H\alpha\rho c_m \nabla \chi \rangle_i A_i + V\Theta S_m \qquad 2.79$$

where the $\langle\ \rangle$ represent a surface-averaged value, with the summations over the cell surfaces (north, south, east, west, above, below) and the set of junctions *{j}* connected to the cell.

2.1.6.2 Energy Balance

Energy is treated in the same manner as mass. The resulting form after some manipulation is

$$V\Theta \frac{\partial \left(\alpha\rho \left(e + \frac{u_C^2}{2} \right) \right)}{\partial t} = - \sum_{i \in \{nsewab\{j\}\}} \left\langle H\alpha\rho \left(h + \frac{u^2}{2} \right) u \right\rangle_i A_i$$

$$+ \sum_{i \in \{nsewab\{j\}\}} \langle H\alpha c_t \nabla T \rangle_i A_i + \sum_{i \in \{nsewab\{j\}\}} \sum_{\varsigma} \langle H\alpha\rho c_m (\nabla \chi_\varsigma) h_\varsigma \rangle_i A_i + V\Theta S_e \qquad 2.80$$

where e is the internal energy and the subscript ς refers to one component of the mixture. The double sum represents energy transported by mass diffusion.

2.1.6.3 Momentum Balance

The momentum balance equation is solved on the shifted cell. The shifted cell for the east cell face is shown as a dashed box in Figure 2.2. The corresponding formulation of the momentum balance for this dashed cell is

$$\frac{\partial}{\partial t}\int_{V_e} H\alpha\rho u_x dV = -\int_{A_e} H\alpha\rho u_x \vec{u}\cdot\vec{n}dA + \int_{A_e} H\alpha(\bar{\tau}\cdot\vec{e}_x)\cdot\vec{n}dA$$
$$+\int_{V_e} H\alpha(\nabla P)_x dV + \int_{V_e} H\alpha\rho g_x dV + \int_{V_e} HS_{u_x} dV \qquad 2.81$$

where V_e and A_e are the volume and surface area of the shifted momentum control volume. $\bar{\tau}$ is the stress tensor given in index notation by

$$\tau_{ij} = (\mu+\mu^T)(u_{i,j}+u_{j,i}) - \frac{2}{3}\delta_{ij}(\mu u_{k,k}+\rho\kappa) \qquad 2.82$$

where μ is the molecular viscosity, μ^T is the turbulent eddy viscosity and κ is the turbulent kinetic energy. The integrals can be replaced by volume (in brackets []), or surface average quantities to yield

$$\begin{aligned}\frac{\partial[\alpha\rho u_x H]_e}{\partial t} &= \langle H\alpha\rho u_x u_x\rangle_C A_C - \langle H\alpha\rho u_x u_x\rangle_E A_E + \langle H\alpha\rho u_x u_y\rangle_{es} A_{es} \\ &-\langle H\alpha\rho u_x u_{yz}\rangle_{en} A_{en} + \langle H\alpha\rho u_x u_z\rangle_{eb} A_{eb} - \langle H\alpha\rho u_x u_z\rangle_{ea} A_{ea} \\ &+\sum_{j\in\{j\}}\langle\alpha\rho u_x u_j\rangle_j A_j + \langle H\alpha(\bar{\tau}\cdot\vec{e}_x)_x\rangle_C A_C - \langle H\alpha(\bar{\tau}\cdot\vec{e}_x)_x\rangle_E A_E \\ &+\langle H\alpha(\bar{\tau}\cdot\vec{e}_x)_y\rangle_{es} A_{es} - \langle H\alpha(\bar{\tau}\cdot\vec{e}_x)_y\rangle_{en} A_{en} + \langle H\alpha(\bar{\tau}\cdot\vec{e}_x)_z\rangle_{eb} A_{eb} \\ &-\langle H\alpha(\bar{\tau}\cdot\vec{e}_x)_z\rangle_{ea} A_{ea} + [V\Theta\alpha(\nabla P)_x] + [VH\alpha\rho g_x] + \frac{V_C\Theta_C + V_E\Theta_E}{2} S_{u_x}\end{aligned} \qquad 2.83$$

2.2 Direct Contact Condensation

The phenomenon of direct contact condensation occurs when either steam or a mixture of steam and noncondensible gases comes into contact with subcooled water. This can occur at any vapor/liquid interface. The main topic of interest here deals with bubbles being injected into a subcooled water pool. The number of papers on this subject is rather limited. This section of the literature review will address the previous work in this area.

The direct contact condensation of bubbles in subcooled liquid has been classified by a regime map proposed by Chan et al. [2]. The different regimes represent the condensation process dominated by different physical phenomena at subsonic vent conditions. The experiment used to determine this regime map was steam injection into a single downward vertical vent with a 0.051m diameter. The experiment was performed at atmospheric pressure with steam mass fluxes ranging from 1 kg/m^2-s to 175 kg/m^2-s, with pool temperatures ranging from 20-100 °C. The regime map proposed is shown in Figure 2.3. The coordinates of the map are pool temperature on the vertical axis, which characterizes the condensation, and steam mass flux on the horizontal axis, which characterizes the driving mechanism. The boundary of the regimes are approximate and system dependent.

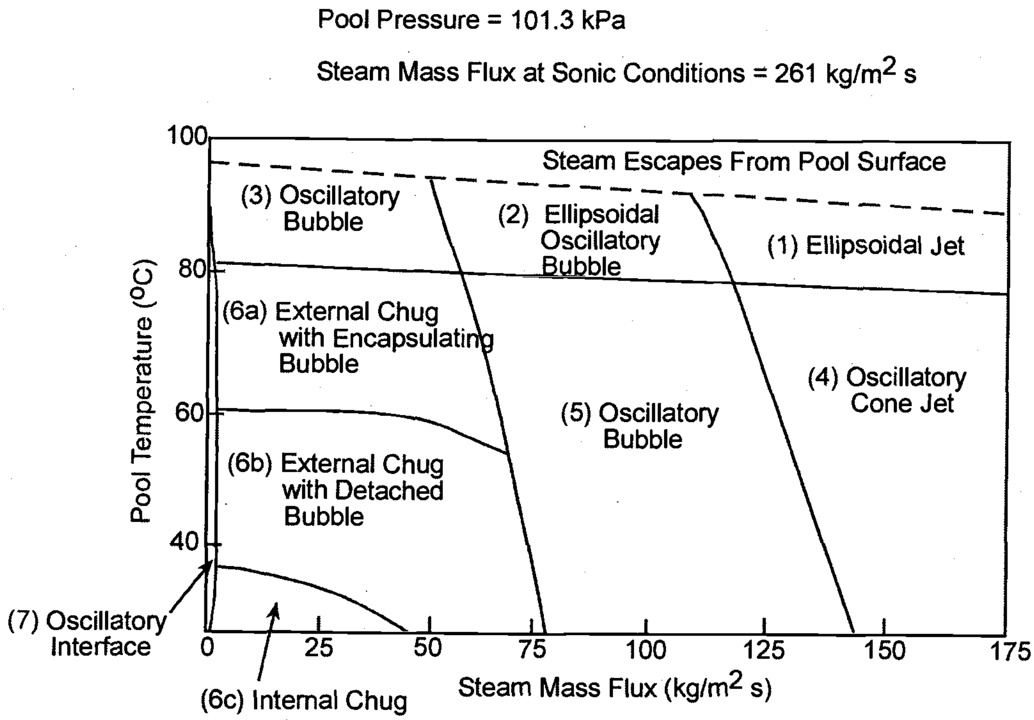

Figure 2.3: Chan et al. Condensation Regime Map

These regimes represent the dynamics of the direct condensation, but not the heat transfer. It is likely that the heat transfer mechanisms are different for some of the regimes.

Bankoff [3] considered many aspects of condensation phenomena related to light water reactor safety. The simple schematic of a BWR suppression pool is shown in Figure 2.4. In a BWR suppression steam flows down through vertical vent pipes into subcooled liquid. Kowalchuk et al. [4] used a transient conduction solution with the definition of the eddy diffusivity for heat:

$$\alpha_T = \beta \bar{u}_b D \tag{2.84}$$

where β is an empirical coefficient, on the order of 10^{-2}, $\bar{u}_b$ is the time-averaged mean flow speed in one oscillation cycle, and D is the pipe diameter. Kowalchuk et al. [4] broke the condensation into two regions. The first treats the condensation that occurs while the bubble is within the pipe, and the second treats the condensation after the bubble exits the pipe. The heat flux into the water while the interface is within the pipe is given by

$$q = \rho_L c_L \sqrt{\frac{\beta \bar{u}_b D}{t_o + t}} \left(T_{sat} - T_L\right) \tag{2.85}$$

where the time t is measured from the instant of entry into the pipe, and t_o is an artificial delay time, which is

$$t_o = \alpha_T \left(\frac{\rho_L c_L \left(T_{sat} - T_L\right)}{q_o} \right)^2 \tag{2.86}$$

where q_o is the heat flux just before the interface enters the pipe. The form of the heat flux when the bubble exits the pipe, assuming the thermal boundary layer scales as the pipe diameter, is

$$q = St_c \rho_L c_L \bar{u}_b \left(T_{sat} - T_L\right) \tag{2.87}$$

where St_c is an empirical constant which can be identified as a "condensation Stanton number", which is on the order of 10^{-1}. When the two modes of heat transfer are combined the total heat flux to the liquid is given by

$$q = \frac{St_c \rho_L c_L \bar{u}_b \left(T_{sat} - T_L\right)}{\left(1 + \frac{\delta \pi St_c^2}{\beta} \frac{\bar{v}t}{D}\right)^2} \tag{2.88}$$

where δ=0 for an interface outside of the pipe, and δ=1 for an interface within the pipe.

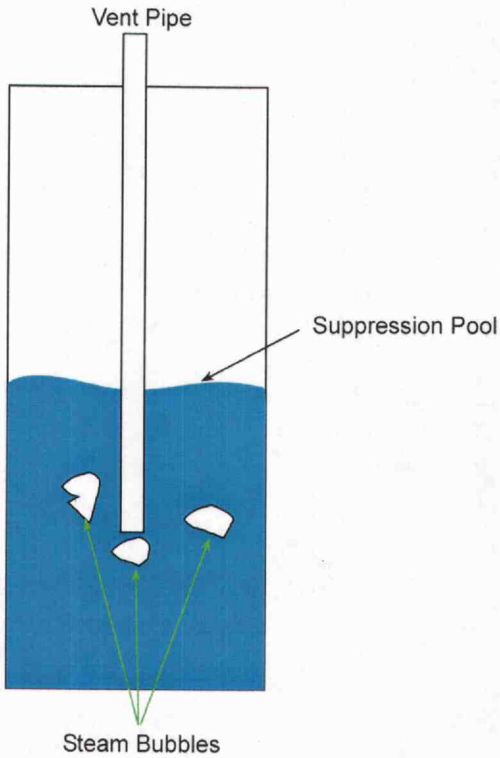

Figure 2.4: BWR Suppression Pool Schematic

A different model proposed by Sursock [5] assumes that inside the vent, the interface is quiescent and condensation ceases. When the interface reaches the exit of the vent the heat transfer coefficient is assumed to be proportional to the liquid subcooling. An interface energy balance requires at every instance

$$q = R\rho_G h_{fg} = \frac{\alpha_t \rho_L c_L \Delta T_{sub}}{(\alpha_t t_c)^{\frac{1}{2}}} \qquad 2.89$$

where α_t is the turbulent diffusivity, t_c is a characteristic time for eddy transport in the liquid, R is the bubble radius, and ΔT_{sub} is the degree of subcooling of the liquid. This equation is then integrated from $t = 0$ to $t = t_c$ to obtain an average heat transfer coefficient given as

$$\Delta R\rho_G h_{fg} = \rho_L c_L \Delta T_{sub} (\alpha_t t_c)^{\frac{1}{2}} \qquad 2.90$$

where $\Delta R = R(t_c) - R(0)$. If ΔR is constant for a given system then $h_L \propto \Delta T_{sub}$.

Simpson et al. [6] examined the rate of collapse of steam bubbles in subcooled water. The experiments consisted of the injection of saturated steam upward into a subcooled pool. The conditions for the various tests are given in Table 2.6. The experimental apparatus was deaerated before all experiments so the effects of non-condensable gases are not considered.

Table 2.6 : Simpson Test Conditions

Test Parameter	Test Values
Orifice Diameter	1mm, 2mm
System Pressure	1 bar, 2 bar
Steam Flow Rate	0.5, 1.0, 1.5 gal/min
Water Subcooling	At 1bar: 5 K – 29.7 K At 2 bar: 9.3 K – 36.6 K

The analysis involved a total of 114 bubbles. During the time of collapse, the bubble volume, surface area, and position were obtained from high-speed films. This data was used to derive an empirical correlation for bubble rise velocity, given by

$$U = 2.148\left(\frac{P_o}{P}\right)^{\frac{1}{2}}\left(1 + 6.52\times10^{-3} Ja_o\right)\left(\frac{\sigma}{R\rho_w} + \frac{\rho_w - \rho_s}{\rho_w} gR^{\frac{1}{2}}\right) \qquad 2.91$$

where P is the pressure, P_o is a reference pressure equal to 1 bar, Ja_o is the Jakob number given as

$$Ja = \frac{c_p\left(T_s - T_{sat}\right)}{h_{fg}} \qquad 2.92$$

where T_s-T_{sat} is the subcooling of the liquid pool, c_p is the specific heat of the liquid and h_{fg} is the latent heat. This correlation predicted the experimental data within

2%. The experimental data was also used to correlate the height to collapse, Z_c. This correlation takes the form

$$\frac{Z_c}{R_o}=\frac{2.26\left(1+6.52\times10^{-3}Ja_o\right)\left[\frac{\left(\frac{\sigma}{R_o\rho_w}+\frac{\rho_w-\rho_s}{\rho_w}gR_o\right)^{\frac{1}{2}}}{\alpha}R_o\right]}{\left(\frac{P}{P_o}\right)^{\frac{1}{2}}Ja_oPe_o^{\frac{1}{2}}} \qquad 2.93$$

2.3 Wall Condensation Heat Transfer

The phenomenon of condensation heat transfer on walls is difficult to predict. Many researchers have developed heat transfer coefficients at the wall. Work began on the subject many years ago with Nusselt [7] in 1916, who derived a similarity solution for the temperature distribution and film thickness for an isothermal vertical flat plate laminar film condensation. The work was continued by Koh [8] and Rohsenow [9] whom formulated the average Nusselt number as:

$$\overline{Nu}=\frac{\overline{h}x}{k}=0.943Ra^{*\frac{1}{4}} \qquad 2.94$$

where

$$Ra^*=\frac{g(\rho_l-\rho)Pr^*x^3}{\rho_l v_l^2} \qquad 2.95$$

and

$$Pr^*=\frac{\mu\left[\frac{3C_p}{4}+\frac{h_{fg}}{(T_s-T_w)}\right]}{k} \qquad 2.96$$

This correlation didn't take into account the motion of the vapor, variable properties, or the presence of non-condensable gases.

The work of Minkowycz and Sparrow [10] examined the same problem while including variable properties and non-condensable gasses. They also considered the buoyancy forces and transport phenomena that occur in the presence of thermal and concentration gradients. Their results showed that the decrease in heat transfer was due to the diffusion resistance of the vapor mixture at the interface temperature. This is explained by the physics of the problem. The vapor to be condensed must be carried to the interface by convective processes. This convection also carries non-condensable gases to the interface as well. The reasonable assumption is made that the interface is impermeable to the non-condensable gasses, which means that the gas must be removed at the same rate at which it arrives. This removal is accomplished by the diffusion of the gas back into the bulk fluid. The diffusion occurs because of a concentration gradient from the interface to the bulk fluid. The resulting build up at the surface to drive the diffusion decreases the vapor partial pressure at the surface. This reduction in pressure reduces the saturation temperature at which the condensation is taking place, which lowers the driving temperature difference for heat transfer. The calculated reduction of heat transfer was 50 percent for an air mass fraction of 0.5 percent. The heat transfer decreased linearly for increased mass fractions. The effect of superheat in the vapor tended to increase heat transfer for large temperature gradients. This did not overcome the decrease from the presence of the air.

The experimental work of Uchida et al. [11] is used in many computer codes today to predict condensation heat transfer coefficients on vertical walls. The experiment was conducted at Hitachi Ltd. The condensing surface was a 140mm wide and 300mm tall flat plate. Different non-condensable gases of air, nitrogen, and argon were used. The heat transfer coefficients as a function of the weight ratio of the steam to non-condensable gas (ω_N/ω_S) were measured. The data shows that the effect on heat transfer was independent of the gas type, but dependent on the gas to vapor ratio (ω_N/ω_S).

The work of Gido, and Koestel [12] presents considerations for large-scale containments. Uchida [11] experimented on a small vertical surface where the film condensate level was laminar. In large-scale tests, the transition from laminar to turbulent condensate layers takes place at a distance of 1-2m down the wall. The turbulence of the liquid film promotes the formation of waves at the surface. These waves increase the heat transfer by causing turbulent mixing of the air/vapor mixture at the interface. Based on these observations an average heat transfer coefficient was derived. A formulation was derived for both natural and forced convection situations. The resulting average heat transfer coefficients are:

$$\bar{h}_{NC} = \frac{\rho_l h_{fg}}{T_\infty - T_K} 5.25 \frac{1}{\left(\frac{\nu_l}{g^4 H^5}\right)^{\frac{1}{7}}} \left[\left(\frac{V_*}{u_K}\right)^2 \frac{1}{Sc_t} \frac{u_k}{u_\delta} \frac{\beta_s}{\beta} \frac{\rho_{v\infty} - \rho_{vk}}{\rho_l}\right]^{\frac{12}{7}} \qquad 2.97$$

and

$$\bar{h}_{FC} = \frac{\left(\frac{V_*}{u_g}\right)^2 \frac{u_g}{Sc_t} \frac{\beta_s}{\beta} h_{fg} (\rho_{v\infty} - \rho_{vK})}{\left(1 - \frac{(\rho u)_K}{(\rho u)_\infty}\right)(T_\infty - T_K)} \qquad 2.98$$

where V_* is the shear stress velocity, u_g is the vapor velocity u_K is the wave crest velocity and the subscript K is represents the interface between the liquid and vapor. The subscript ∞ denotes the value in the bulk vapor far from the wall. The turbulent Schmidt number (Sc_t) is given by the ratio of momentum diffusivity to mass diffusivity. The ratio of β/β_s is the ratio of mass transfer coefficients for a permeable and semipermeable membrane representing the liquid/vapor interface, and is given by:

$$\frac{\beta_s}{\beta} = \frac{\ln(1 + \lambda^*)}{\lambda^*} \qquad 2.99$$

where

$$\lambda^* = \frac{P_K - P_{v\infty}}{P - P_K} \qquad 2.100$$

These correlations were compared with large-scale tests done by Battelle-Frankfurt [13], and at the CVTR [14] test facility. The correlations predicted the measured values of the heat transfer coefficients well as can been seen graphically in their report. There was no measure of error provided by Gido and Koestel [12]. The Uchida data was the fit to a corresponding derivation for a laminar vapor boundary layer and was found to predict that data well. The conclusion of the authors is that the small scale experiment of Uchida [11] provides data for laminar vapor boundary layers, but cannot be scaled for use in large containments due to the presence of turbulent boundary layers on a large portion of the surface.

Corradini [15] also derived heat transfer coefficients for forced and natural convection condensation heat transfer. His approach was similar to that of Gido and Koestel [12] except he did not consider the effects of turbulence. The final result was formulations for Nusselt and Sherwood numbers for both natural and forced convection. The forced convection correlations are:

$$Nu_{FC} \equiv \frac{h_{conv}L}{k_g} = 0.037 Re_L^{0.8} Pr^{\frac{1}{3}} \qquad 2.101$$

and

$$Sh_{FC} = \frac{g}{v_g} = 0.037 Re_L^{-0.2} Sc^{-\frac{2}{3}} \qquad 2.102$$

where L is the length of the vertical surface, k_g is the gas conductivity, h_{conv} is the convective heat transfer coefficient, and g is the mass transfer coefficient. The Reynold's number used is defined as:

$$Re_L \equiv \frac{\rho_g v_g L}{\mu_g} \qquad 2.103$$

The corresponding correlations for natural convection are given as:

$$Nu_{NC} \equiv \frac{h_{conv}L}{k_g} = 0.0295 Gr_L^{\frac{2}{5}} Pr^{\frac{7}{15}} \left(1 + 0.494 Pr^{\frac{2}{3}}\right)^{-\frac{2}{5}} \qquad 2.104$$

and

$$Sh_{NC} = \frac{g}{\Gamma_L} = 0.0188 Re_L^{-\frac{1}{4}} Sc^{-\frac{2}{3}} \qquad 2.105$$

where

$$Re_L \equiv \frac{\rho_g \Gamma_L \delta_L}{\mu_g} \qquad 2.106$$

and

$$\Gamma_L = 1.185\left(\frac{\nu}{L}\right) Gr_L^{\frac{1}{2}}\left(1 + 0.494 Pr^{\frac{2}{3}}\right)^{-\frac{1}{2}} \qquad 2.107$$

$$\delta_L = 0.565 L Gr_L^{-0.1} Pr^{-\frac{8}{15}}\left(1 + 0.494 Pr^{\frac{2}{3}}\right)^{-0.1} \qquad 2.108$$

Here Γ_L is a characteristic velocity for turbulent natural convection, and δ_L is the boundary layer thickness.

The effect of high mass transfer needs to be taken into account for these processes since the condensation process thins the boundary layers. The correction applied by Corradini is taken from Bird [16] and is given by:

$$C_0 = \frac{\ln(R+1)}{R} \qquad 2.109$$

where

$$R \equiv \frac{Y_I - Y_B}{1 - Y_I} \qquad 2.110$$

and Y_I and Y_B are the mole fraction of steam at the interface, and in the bulk fluid. The corrected heat and mass transfer coefficients g^* and h^*_{conv} are:

$$g^* = C_o g \qquad 2.111$$

and

$$h^*_{conv} = C_o h_{conv} \qquad 2.112$$

These solutions were compared with the experimental data of Uchida [11]. The experimental data was correlated as a function of the mass ratio of air to steam and is given by:

$$h_{tot} = 379\left(\frac{m_g}{m_v}\right)^{-0.707} \qquad 2.113$$

where h_{tot} is the sum of the convective and condensation heat transfer coefficients. This is a very similar correlation to the one used in GOTHIC to represent the Uchida[11] data. Corradini found that his data predicted the Uchida data pretty well. In the Corradini model, the gas velocity in the bulk fluid is required. In the Uchida experiments no velocities were measured so Corradini used a value of 2 m/s to estimate it. This velocity seemed to give the best fit to the data.

This idea was simplified by Peterson et al. [17] with the introduction of a condensation thermal conductivity (k_c) given by:

$$k_c = \frac{1}{\phi T_{avg}}\left(\frac{h_{fg}^2 P_o M_v^2 D_o}{R^2 T_o^2}\right) \qquad 2.114$$

where h_{fg} is the heat of vaporization and P_o is a reference pressure at reference temperature T_o. The diffusion coefficient D_o is evaluated at the reference point. The value of T_{avg}, and ϕ are given by:

$$T_{avg} = \frac{(T_i(sat) - T_b(sat))}{2} \qquad 2.115$$

and

$$\phi = \frac{x_{g,avg}}{x_{v,avg}} = \frac{\ln\left[\frac{(1 - x_{gb})}{1 - x_{gi}}\right]}{\ln\left[\frac{x_{gb}}{x_{gi}}\right]} \qquad 2.116$$

where x_g is the vapor concentration and the subscripts i and b represent the interface and bulk conditions respectively. With the thermal conductivity defined, the use of ordinary heat transfer correlations for turbulent natural convection are used on a vertical flat plate. The Nusselt number is given by:

$$Nu_{Lt} = \frac{q_t'' \dfrac{L}{(T_{b,sat} - T_{i,sat})}}{k_c + \dfrac{C_s}{C_c}\left(\dfrac{Pr}{Sc}\right)^{0.33} k_s} = C_c Ra_{Lc}^{0.33} = C_c (Gr_{Lc} Sc)^{0.33} \qquad 2.117$$

where q_t'' is the total heat flux, k_s is the sensible heat conductivity, L is the length of the plate, C_s and C_c are empirical coefficients whose values are 0.7 and 0.10 respectively. The data was compared with Uchida [11], and Kataoka et al. [18]. The results were within a standard deviation of 7 percent for the Kataoka data and within 23% for the Uchida data.

3 MASLWR DESIGN AND SCALING

The Multi Application Small Light Water Reactor (MASLWR) is a new reactor concept developed by OSU, INEEL, and NEXANT Bechtel. This chapter will focus on the current design configuration, the scaling used to create a test facility and the final design of the scaled test facility.

3.1 Full Scale Design

The current design configuration for MASLWR is an advanced natural circulation driven Pressurized Water Reactor (PWR). The schematic in Figure 1.1 shows the basic components and flow path of the primary fluid as well as the layout of the containment and containment cooling pool. A more detailed picture of the MASWLR Power module, which consists of the RX/SG vessel, Containment, Containment Cooling Pool, turbine, generator, condenser, and feedwater pump, is shown in Figure 3.1. Additional detailed design drawings provided by NEXANT Bechtel are shown in Figure 3.2.

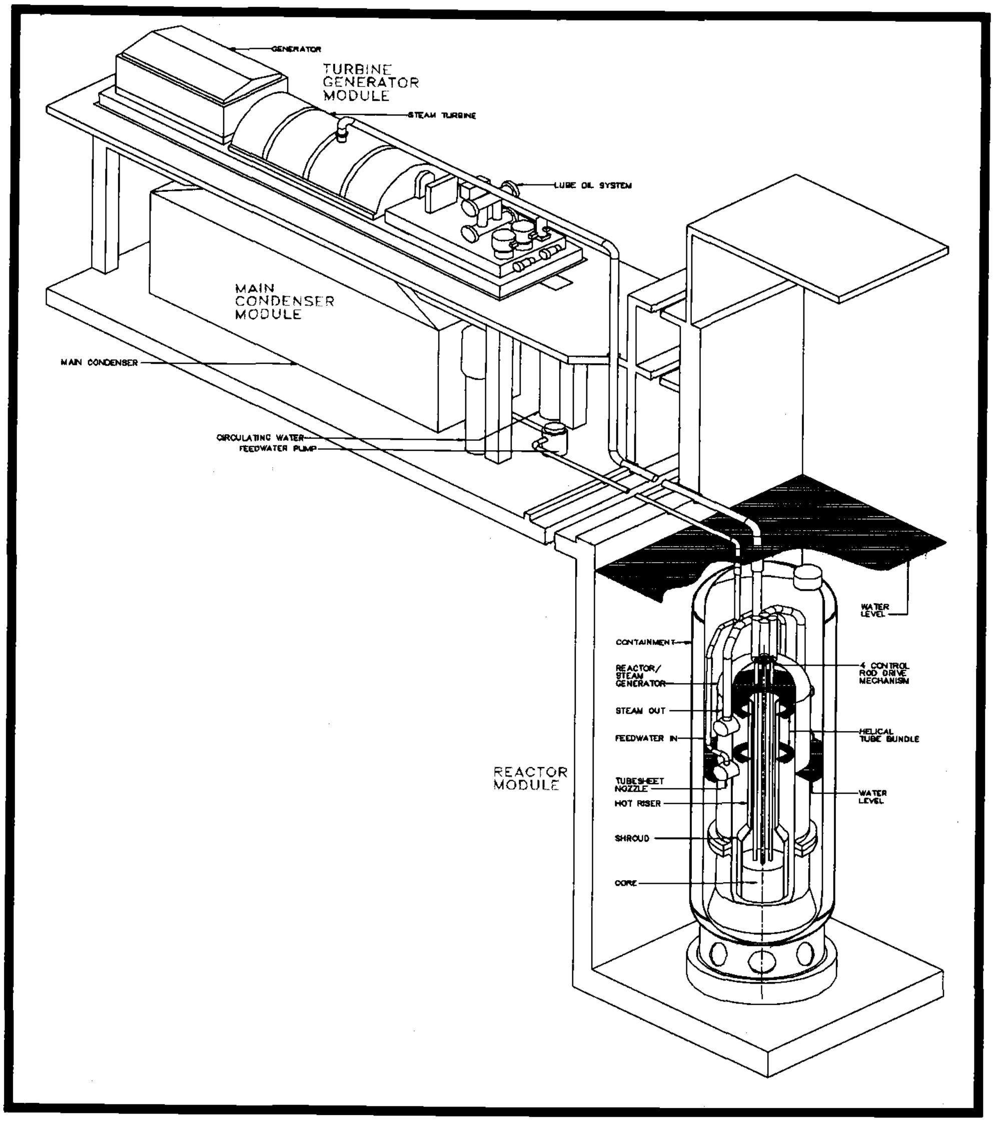

Figure 3.1: MASLWR Power Module

This section focuses on the operating conditions of MASLWR along with detailed dimensions and volumes. This description will focus on the data needed to construct and analyze the containment.

3.1.1 Operating Conditions

The operation of MASLWR can be broken down into three modes startup, steady-state natural circulation, and off normal (on transients). Startup mode occurs when the reactor is first installed or has been shut down for several days. This mode consists of a slow heat up to establish natural circulation conditions. The procedure for the startup will be developed during the first phase of testing at OSU. The difficulty of startup arises from the fact that there are no pumps in the system, so fluid in the core needs to be heated up to induce the buoyancy difference required for natural circulation flow. The heat added during this period also needs to be removed, but not completely since the plant needs to come up to full pressures and temperatures. This is vastly different than a typical pumped PWR system where initially the running of the pumps inputs an adequate amount of heat to bring the system temperature up. Also a typical PWR has a pressurizer that is used to bring the plant to pressure during warmup and also controls the pressure during steady state operation. In MASLWR there are neither pumps nor a pressurizer. As a result, the only way to control pressure and temperature is by controlling the amount of heat removed and input into the system. This is further complicated by neutronic feedback. Neutronic feedback is caused by temperature excursions. With a decrease in temperature, there is an increase in power due to Doppler narrowing of the resonances for neutron absorption in the uranium fuel. The converse is true when a temperature increase is experienced. Once the steady-state operating parameters given in Table 3.1 are established, the next mode is achieved.

Table 3.1: MASLWR Steady-State Operating Conditions

System Parameter	Value
Reactor Power	150 MWt
Primary Pressure	7.6 MPa, 1102 psia
Core Inlet Temperature	491.9 K, 425.75 °F
Core Outlet Temperature	544.3 K, 520.07 °F
Primary Mass Flow Rate	597 kg/s, 1316.16 lbm/s
Steam Outlet Temperature	481.4 K, 406.85 °F
Feedwater Mass Flow Rate	56.1 kg/s, 123.7 lbm/s

The steady-state mode is the normal operating condition. Once steady-state is achieved the plant will operate in that state for the entire fuel cycle of the plant. There are possibilities for this mode to be interrupted by transients.

The transients that occur in MASLWR can be caused by many actions. Some of these actions include feed water trips, turbine trips, inadvertent opening of safety valves, and component failures. Some of these transients are rather minor and do not require response of the plant safety systems. The focus of this thesis is to examine the response of the containment to transients that include the use of the safety systems. The safety system operation consists of two primary phases. The first is the blowdown phase where the RX/SG vessel is depressurizing into the containment. This is followed by a long term cooling phase where decay heat is removed from the core by pool boiling. The steam created from the boiling exits through the vent valves, condenses on the containment walls, and circulates back through the Automatic Depressurization System lines to the core. The test matrix considered for this analysis will be presented in Chapter 4. The component and system dimensions and operations needed for the analysis follow.

3.1.2 Reactor/Steam Generator

The components within the RX/SG vessel are the core, primary fluid, and steam generator. The RX/SG vessel is constructed from stainless steel (SS), and for the purposes of this analysis is assumed to be covered with 0.1016 m (4 inches) of Calcium Silicate (Cal-Sil) insulation. The data presented in Table 3.2 for surface areas and volumes includes the insulation.

Table 3.2: RX/SG Dimensions with 4" of Insulation

Parameter	Value
RX/SG Height	13.73 m
RX/SG Elevation Above Containment Base	0.1524 m
RX/SG External Radius	1.5776 m
RX/SG Wall Thickness	0.152 m (SS), 0.1016 m (Cal-Sil)
RX/SG Vessel Volume (external)	99.12 m^3
RX/SG Vessel Volume (fluid)	49.75 m^3
RX/SG Vessel Surface Area (external)	136.07 m^2
RX/SG Vessel Surface Area (internal)	109.98 m^2

The volume, surface area, and wall thickness characterize the RX/SG vessel. In addition, the penetrations to the vessel need to be characterized. The RX/SG Vessel has two safety systems that connect to the vessel for transient response. The first system is the steam vent valves. There are two valves located on top of the vessel at an elevation of 13.5 m from the base of containment, shown in Figure 3.2. Each valve is a 4-inch gate valve that is air operated. Within the lines connected to the valves are 3-inch orifice plates to restrict the flow from the vents. The purpose of this system is to provide a low resistance path for steam to leave during decay power removal following a plant depressurization event. The second system is the submerged Automatic Depressurization System (ADS). This system is used as the primary depressurization mechanism during an accident. There are two valves submerged ADS lines on opposite sides of RX/SG vessel they have 4-inch gate valves the same type as the steam vents. The submerged ADS lines are connected to the RX/SG vessel at an elevation of 5 m from the base of containment (see Figure 3.2).

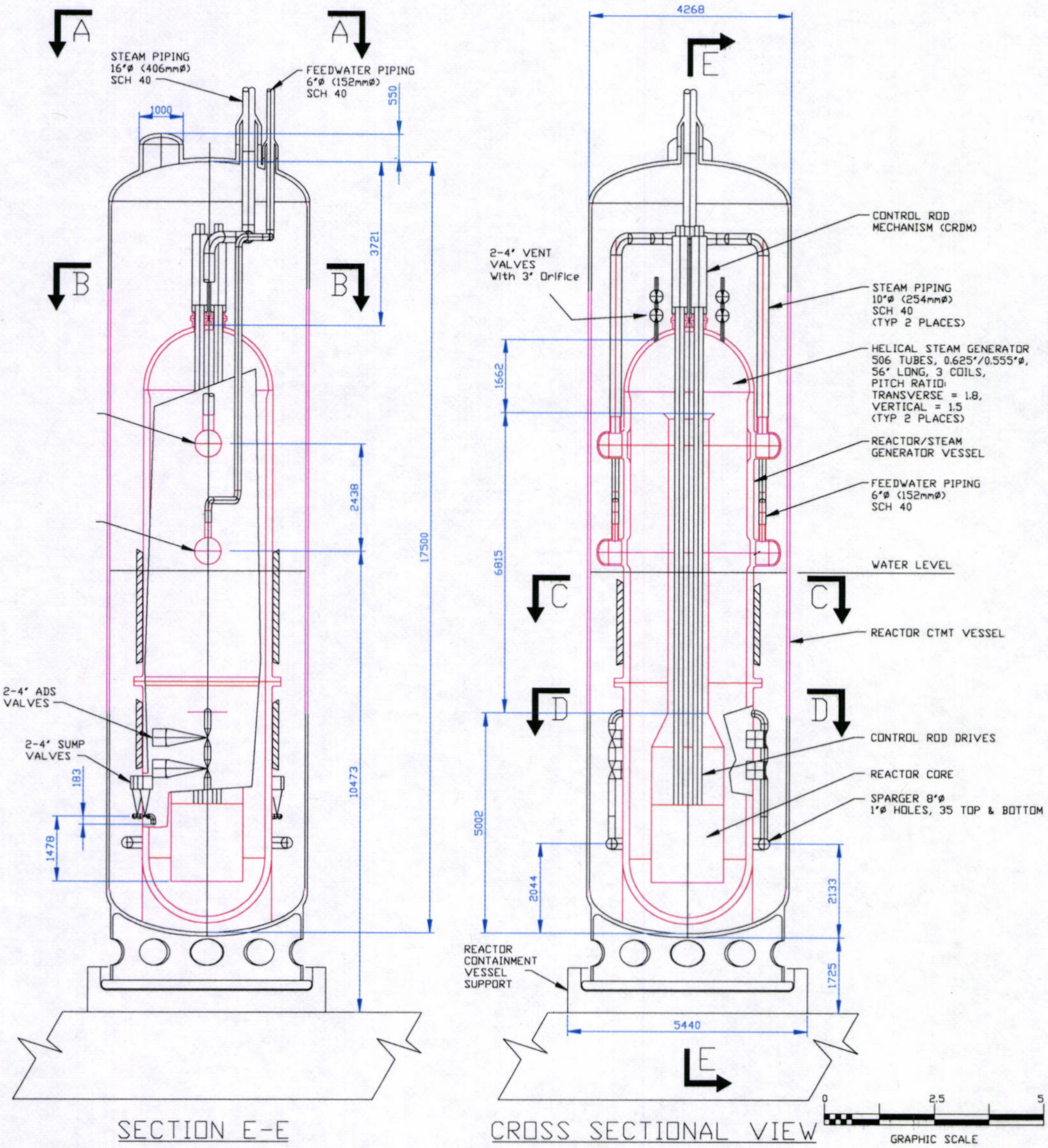

Figure 3.2: MASLWR SK-2500 Drawing (Section)[20]

The two ADS lines connect to a sparger ring located at an elevation of 2.044 m above the base of the containment. The sparger shown in Figure 3.2 is submerged in the pool within the containment. The flow areas and losses for the valves fully open and orifices are presented in Table 3.3. The data for the valves is generic data obtained from Crane [19]. The dimensions of the sparger are located in Table 3.4.

Table 3.3: RX/SG Valve and Orifice Data

Component	Flow Area	Loss Coefficient (K)
4-inch Gate Valve	0.0079 m^2	0.136
3-inch Orifice	0.00456 m^2	2.525

Table 3.4: Sparger Dimensions

Sparger Parameter	Value
Pipe Diameter	0.2032 m, 8 inch
Sparger Ring Diameter	3.353 m, 11 ft
Hole Diameter	0.0254 m, 1 inch
Number of Holes	35 top, 35 bottom

3.1.3 Containment

The containment vessel contains the RX/SG vessel and an in-containment sump pool. The function of the containment is three-fold. The first role is to mitigate accident scenarios by allowing the RX/SG vessel to blow down into the containment. This allows the RX/SG vessel to depressurize, so borated water from the containment sump can be circulated through the core for cooling and reactivity control. The second role is to prevent the release of radioactive materials during an accident by maintaining an airtight with the exterior atmosphere. The final role of the containment is to act as the ultimate heat sink. This means to allow all the heat created by the core during and after an accident to be removed through the containment walls and into the containment cooling pool. The dimensions needed for the analysis are given in Table 3.5.

Table 3.5: Containment Dimensions

Parameter	Value
Containment Height (internal)	17.5 m
Containment Radius (internal)	2.095 m
Containment Wall Thickness (cylinder)	0.381 m, 1.5 inch
Containment Wall Thickness (heads)	0.0635 m, 2.5 inch
Containment Fluid Volume	133.37 m^3
In Containment Pool Height	6.9 m
Containment Water Volume	42.07 m^3
Containment Air Volume	91.3 m^3
Containment Surface Area (internal)	242.23 m^2
Containment Design Pressure	275 psia (1.896 MPa)

3.1.4 <u>Containment Cooling Pool</u>

The containment cooling pool removes the heat from the outside of the containment walls. The containment vessel is submerged in this pool. The pool is cooled by recirculation through cooling towers on the reactor sight. Since the containment is submerged, the water acts as an additional barrier to radioactive material release. The dimensions of the containment cooling pool are given in Table 3.6.

Table 3.6: Containment Cooling Pool Dimensions

Parameter	Value
Containment Cooling Pool Length	10 m
Containment Cooling Pool Width	5 m
Containment Cooling Pool Depth	21 m
Containment Cooling Pool Liquid Vol.	808.27 m^3

3.2 MASLWR Scaling

The scaling methodology for the MASLWR design consists of a top down and bottom up analysis. This allows the proper scaling of all of the expected phenomena. It is appropriate to mention that rarely is scaling able to preserve all the phenomena. The result is that there are usually some distortions in the scaled facility. The goal is to minimize these distortions and to pick them so the overall system behavior is not changed. The system scaling performed by Reyes & King is presented in the MASLWR scaling report [20]. The key scaling ratios used in the design of the test facility are presented in Table 3.7. One key point to mention is that property similitude was chosen to scale the facility. Property similitude means that all the fluid properties in the model are identical to those in the full-scale prototype. This is achieved by running the scaled model at the same temperatures and pressures as the prototype. The containment was scaled separately and is presented next.

Table 3.7: MASLWR System Scaling Ratios

Scaling Ratio	Value
Length Scaling Ratio (l_R)	0.32263, 1/3.1
Diameter Scaling Ratio (D_R)	0.110312, 1/9.1
Cross-Sectional Area Scaling Ratio (a_R)	0.012169, 1/82.2
Volume Scaling Ratio (V_R)	0.003926, 1/254.7
Power Scaling Ratio (q_R)	0.003938, 1/253.92
Velocity Scaling Ratio ($u_{R,sp}$)	0.3228, 1/3.1
Time Scaling Ratio ($\tau_{R,sp}$)	0.9994, about 1

Dr. John King performed the containment pressurization scaling analysis for the long term cooling phase of MASLWR. The focus of the scaling was primarily on the condensation occurring on the inside of the containment walls.

The problem considered is a steady-state control volume that consists of the air space above the in-containment pool and bounded by the inner wall of the containment and the outer wall of the RX/SG vessel. The temperature response of the containment wall and containment cooling pool will also be considered. The exterior of the RX/SG vessel will be considered adiabatic since it is adequately insulated. The three phases of the analysis consist of developing the governing equations for the pressurization of a binary mixture to obtain a pressurization rate equation. Next a top-down scaling analysis is performed for the air-vapor volume, containment wall, and containment cooling pool. This allows for the development of scaling criteria for the sizing of the containment volume, heat transfer area, and containment wall thickness. The last step is a bottom-up analysis to describe the local transport process of heat transfer to the containment wall in the presence of non-condensable gases.

The analysis showed that special considerations are necessary to preserve condensation rates on the containment wall. The appropriate scaling ratios for the containment include all the system scaling ratios with the addition of those presented in Table 3.8.

Table 3.8: Containment Scaling Ratios

Scaling Ratio	Value
Active Heat Transfer Wall Thickness Scaling Ratio (x_R)	1
Active Heat Transfer Surface Area Scaling Ratio (A_R)	0.003926, 1/254.7

3.3 OSU Test Facility

Based on the scaling ratios presented in section 3.2, a test facility at Oregon State University (OSU) is being constructed. This test facility includes the RX/SG vessel and containment structures. In the test facility, the heat will be generated with electric heater rods. The facility will operate at the same temperatures and pressures as the prototype. The operating conditions, such as mass flow rate of the primary fluid and steam, are yet to be determined. These numbers will be measured during testing at OSU.

3.3.1 OSU Reactor/Steam Generator Vessel

Using the appropriate scaling a RX/SG vessel was constructed by Harris Thermal and delivered to OSU. The scaled RX/SG vessel rendering is shown in Figure 3.3. The steam generated by the facility will be vented directly to atmosphere. In the model, the containment will not surround the RX/SG vessel, but will be placed next to it. The appropriate safety system piping will be run to its corresponding location within the containment. Figure 3.3 shows that the OSU RX/SG also includes a pressurizer section at the top of the RX/SG. The pressurizer is separated from the main primary loop by a plate that has 11 equally spaced 0.5 inch holes on the outer edge. The pressurizer allows OSU to achieve appropriate pressure control until all the control algorithms are debugged. The key dimensions for the RX/SG vessel are given in Table 3.9.

Table 3.9: OSU RX/SG Dimensions

RX/SG Dimension	Value
Height (internal)	4.51 m
Diameter (internal)	0.2921 m, 11.5 inch
Wall Thickness	0.03175 m, 1.25 inch
Primary Fluid Volume	0.2612 m^3
Power	591 kW

The safety systems are the same as in the prototype. There are two submerged ADS valves that connect to a single vessel penetration at a height of 1.34 m above the base of the RX/SG Vessel. There are also two steam vent valves located on the top of the vessel at a height of 4.3 m above the base of the RX/SG. This vent valve elevation will be larger than the appropriate scaled value from the prototype due to the presence of the pressurizer. All of the valves are the same type presented in Table 3.10. Instrumentation for the test facility includes flow measurement, differential pressure, level, and temperature. All of these measurements, except flow, are taken at multiple locations around the flow loop. The flow measurement is taken within the hot leg riser using a Vcone™ flow meter.

Table 3.10: OSU Valve Data

Valve	Flow Area	Loss Coefficient (K)
Swagelock ½ inch	0.00013 m2	38.8

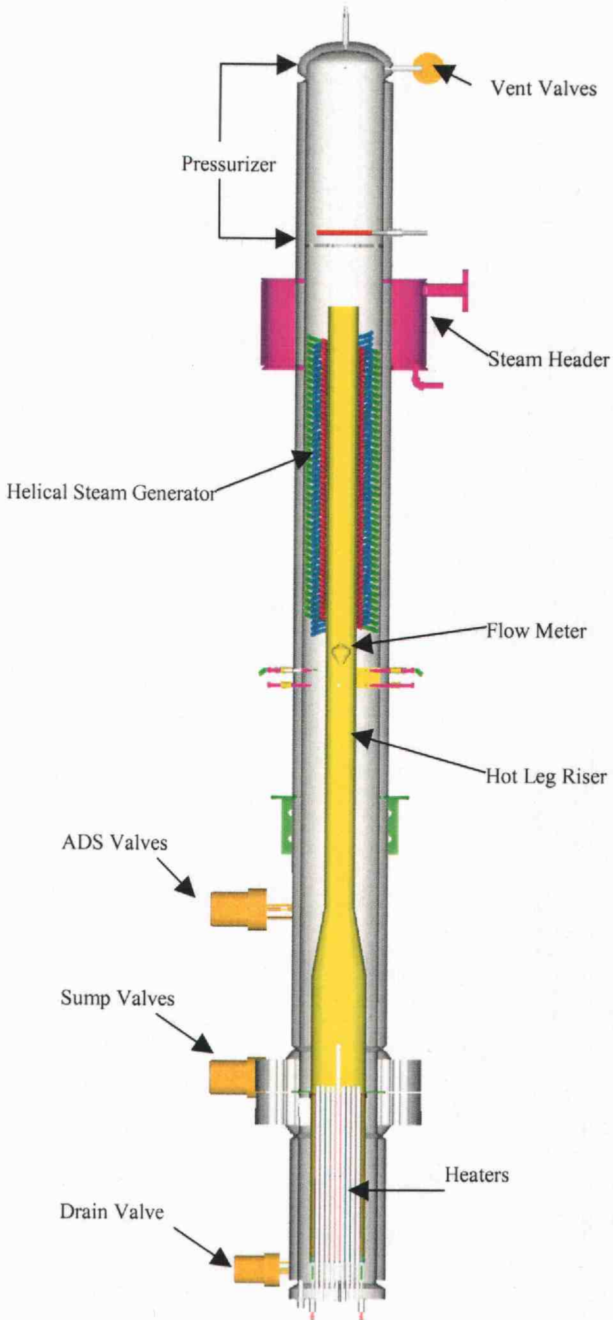

Figure 3.3: OSU MASLWR RX/SG Vessel

3.3.2 OSU Containment

Harris Thermal is also building the containment for the OSU experiments. This design was achieved in an iterative manner trying to preserve all the appropriate scaling ratios while making it affordable to construct.

The design consists of two tanks. One tank is the containment vessel, and the other is the containment cooling pool. A heat transfer plate (shown in Figure 3.4) connects the two tanks. The goal is to have all the heat transfer that occurs in the containment to be through this heat transfer wall. Heating and insulating the outer walls of the upper containment above the water line will achieve this. The appropriate volume to surface area ratios and cross-sectional areas of the containment were achieved by changing the diameter of the tank. The small diameter section is the lower part of the containment. In the prototype this section would represent the annular region between the RX/SG vessel and containment. Above the RX/SG vessel level, the tank diameter increases because there is no longer an annular region. This also preserves the appropriate filling and draining rates of the containment. Some of the important dimensions of the containment and containment cooling pool structures are given in Table 3.11 and Table 3.12 respectively. The instrumentation for the containment vessel will include level measurements, temperature, and pressure.

Table 3.11: OSU Containment Dimensions

Containment Dimension	Value
Height (internal)	5.65 m
Lower Section Radius	0.2032 m, 8 inch
Lower Section Height	4.482 m
Upper Section Radius	0.4064 m, 16 inch
Upper Section Height	1.17m
Liquid Height	2.23 m
Liquid Volume	0.1652 m^3
Total Volume	0.5236 m^3
Heat Transfer Plate Thickness	0.0381m, 1.5 inch
Heat Transfer Plate Width	0.17m, 6.69 inch

Table 3.12: OSU Containment Cooling Pool Dimensions

Containment Cooling Pool Dimension	Value
Height (liquid)	6.77 m
Volume	3.17 m^3

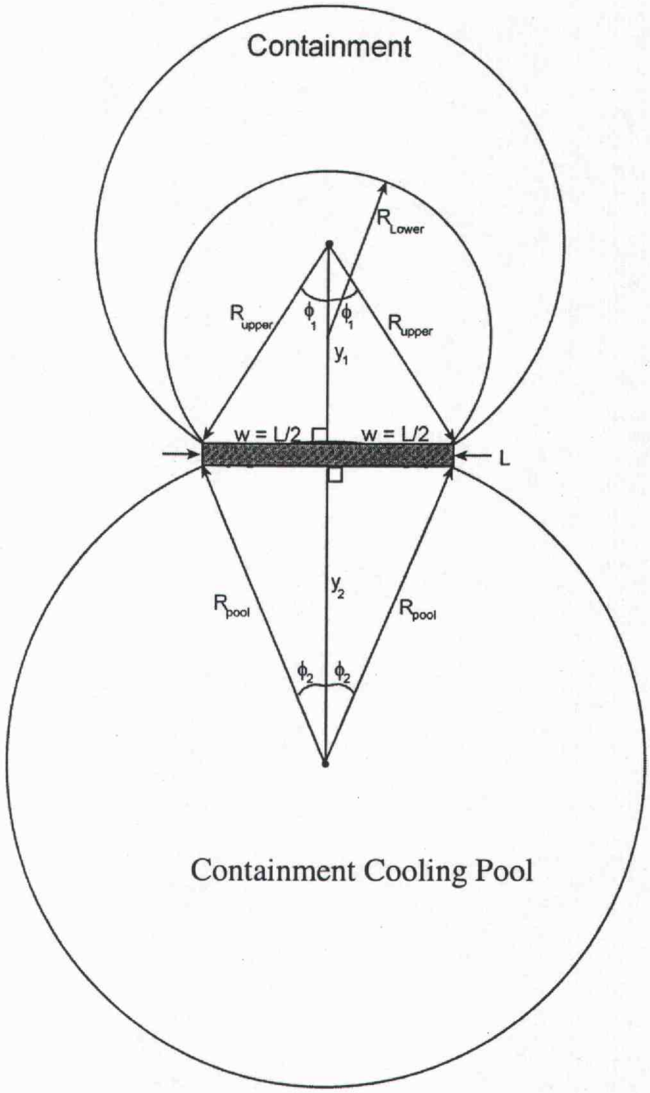

Figure 3.4: OSU Containment and Containment Cooling Pool (Top View)

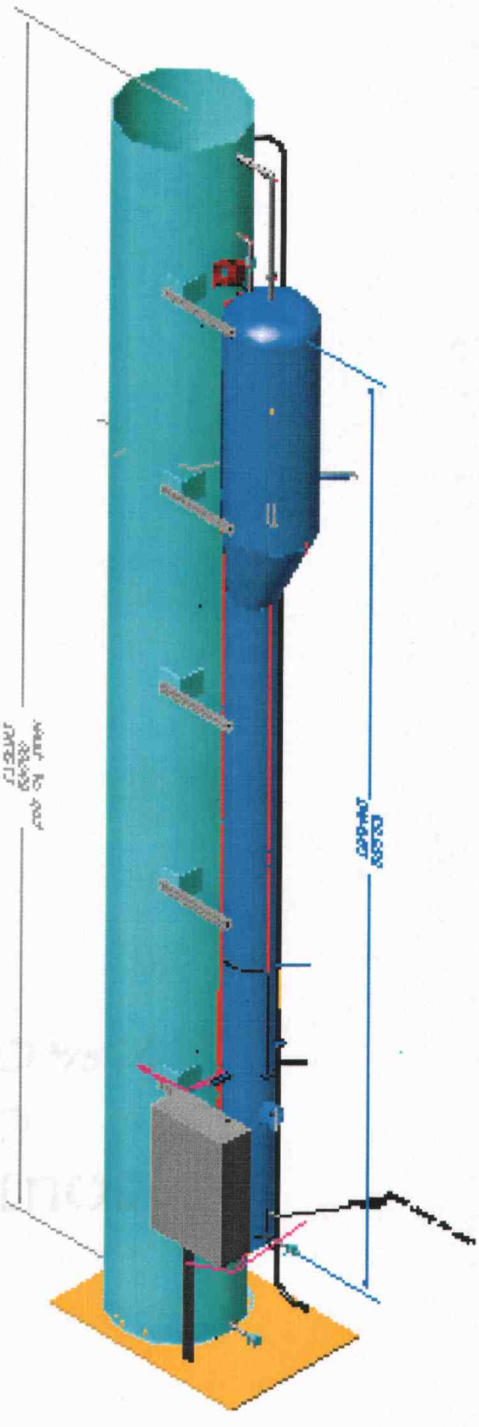

Figure 3.5: OSU Containment and Containment Cooling Pool (3-D view)

4 GOTHIC CALCULATIONS

To assess the performance of the MASLWR containment, calculations were performed using GOTHIC to predict the behavior of the containment during transients and to predict the steady-state characteristics of the prototype. Calculations were performed on both the full scale prototype, and the scaled test facility at OSU. The test matrix considered for this analysis is presented in Table 4.1.

Table 4.1: GOTHIC Test Matirx

Test	Prototype	Model
Steady-State	X	
Inadvertent Steam Vent Valve Opening, with Sump Failure. Gido/Koestel Condensation Model	X	X
Inadvertent Steam Vent Valve Opening, with single ADS Failure, and Sump Failure. Gido/Koestel Condensation Model	X	X
Inadvertent Steam Vent Valve Opening, with Sump Failure. Uchida Condensation Model	X	X
Inadvertent Steam Vent Valve Opening, with single ADS Failure, and Sump Failure. Uchida Condensation Model	X	X

4.1 Full Scale Calculations

The full scale prototype design was used to generate a model for simulations. This model is used to generate steady-state operating conditions within the containment to be used as the initial conditions for the transient simulations. The goal of this analysis is to determine the peak pressures seen in containment and to compare the results with the OSU test facility to help determine if the scaling was done correctly.

4.1.1 <u>Steady-State</u>

To assess the nominal operating conditions within the containment, a steady-state calculation is necessary. To simulate the containment and its structures a GOTHIC model was created. Following the model development and debugging a simulation was performed. The results of this simulation will give guidance into what conditions instruments and equipment will see during normal plant operation. This data will also serve as the initial conditions for the transient cases.

4.1.1.1 Model

A single volume was created to model the fluid volume within the containment vessel. Within this volume conductors were modeled to simulate the RX/SG vessel and containment vessel walls, as well as the associated boundary conditions. Following the construction of the physical elements of the model, initial conditions were established for the structures and volumes. The final step was simulation run time and solution techniques used in the numerical calculations.

4.1.1.2 Control Volumes:

For this model only a single lumped parameter volume was used to represent the fluid volume within the containment.

The inputs required for GOTHIC to correctly describe the containment fluid volume are shown in Table 4.2.

Table 4.2: Containment Volume Input Dimensions

Parameter	Value
Height	17.5 m
Fluid Volume	133.37 m^3
Hydraulic Diameter	1.41 m
Liquid Fraction	0.3155
Liquid Vapor Interface Area	5.975 m^2

4.1.1.3 Conductors:

Conductors are added to the model to simulate the heat transfer between different media. In this case the RX/SG vessel and containment vessel walls are modeled.

4.1.1.3.1 Reactor Steam Generator Vessel:

It is assumed that a 4 inch (10.16 cm) thick insulation material will cover the outside surface of the RX/SG vessel. For this study Calcium Silicate was used. The RX/SG vessel was assumed to be stainless steel AISI 304. The RX/SG vessel was modeled as a cylinder in two sections. The first section models the area that is in contact with the vapor space within the containment. The second section models the area that is in contact with the liquid pool within the containment. The cylinder wall thickness was 25.36 cm, which includes the 10.16 cm of Calcium-Silicate insulation. The conductors were subdivided into 57 regions with appropriate gradients on exposed surfaces and material interfaces to capture the temperature gradients at these locations. The regions are shown in Figure 4.1.

Figure 4.1: RX/SG Vessel Wall Noding

The vapor and liquid sections had surface areas of 69.18 m^2, and 66.88 m^2 respectively. The boundary condition on the interior surface of the RX/SG vessel was assigned a fixed temperature of 270 °C to represent an average coolant temperature of the primary fluid in the downcomer annulus. The exterior surface was exposed to the containment atmosphere and liquid pool where a direct solution for heat transfer was used. This included the use of the Uchida correlation for condensation calculations, and vertical surface natural convection for the convective heat transfer. The bulk temperature difference used for the condensation algorithm is $T_b - T_w$, where T_b is the minimum of the calculated vapor temperature and the saturation temperature T_w is the wall temperature. The bulk temperature difference used for the convection heat transfer between the vapor and the wall is $T_g - T_f$, where T_g is the vapor temperature and T_f is the maximum of the wall surface temperature or saturation temperature.

4.1.1.3.2 Containment Vessel:

The containment vessel was assumed to be stainless steel AISI 304, with 3.81 cm (1.5 inch) thick walls. The containment vessel was modeled as a wall in two sections. The sections were the same as the RX/SG conductor sections with different surface areas and boundary conditions. The conductors were subdivided into 41 regions with appropriate gradients on exposed surfaces to capture the temperature gradients at these locations. The regions are shown in Figure 4.2.

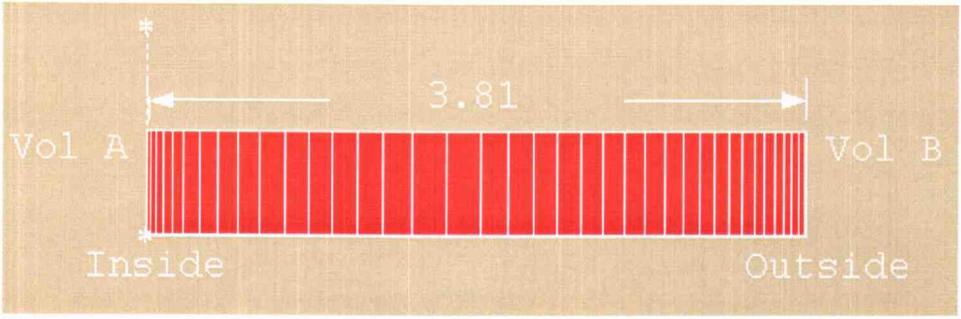

Figure 4.2: Containment Vessel Wall Noding

The interior surface of the containment was exposed to the containment atmosphere and a direct solution for heat transfer was used. The direct solution used the same parameters as the exterior of the RX/SG vessel. The exterior surface of the containment was subject to a specified temperature boundary condition of 70°F (21.1°C) to represent the water temperature in the containment cooling pool.

4.1.1.4 Initial Conditions:

To initiate the simulation, initial conditions are necessary. The containment atmosphere was initialized with air at 14.7 psia (101.353 kPa), a relative humidity of 60%, and a liquid volume fraction of 0.3155 representing the pool within the containment. The initial liquid and vapor temperatures were initialized to 70 °F (21.1 °C) in equilibrium with the containment cooling pool. The containment vessel and RX/SG vessel were also initialized at 70°F (21.1 °C).

4.1.1.5 Run Controls:

Run parameters specified for this model are shown in Table 4.3.

Table 4.3: Run Parameters

Parameter	Value
Minimum Time Step (sec)	0.001
Maximum Time Step (sec)	1.0
Transient Time (sec)	1.0E6
Graphics Interval (sec)	2000
Solution Method	Semi-Implicit
Implicit Convergence Limit	0.0001
Implicit Iteration Limit	100
Pressure Solution Method	Direct
Pressure Convergence Limit	0.0001
Pressure Iteration Limit	100
Differencing Scheme	Forward Upwind

4.1.1.6 Steady-State Results:

The calculated results for the full scale MASLWR containment are presented here. The calculation was run for 1.0E6 seconds, and steady-state was reached at approximately 100,000 seconds. The primary variables of interest are the pressure, temperature, and relative humidity. Pressure is plotted in Figure 4.3, the steady-state value is 15.43 psia (106384.7 kPa).

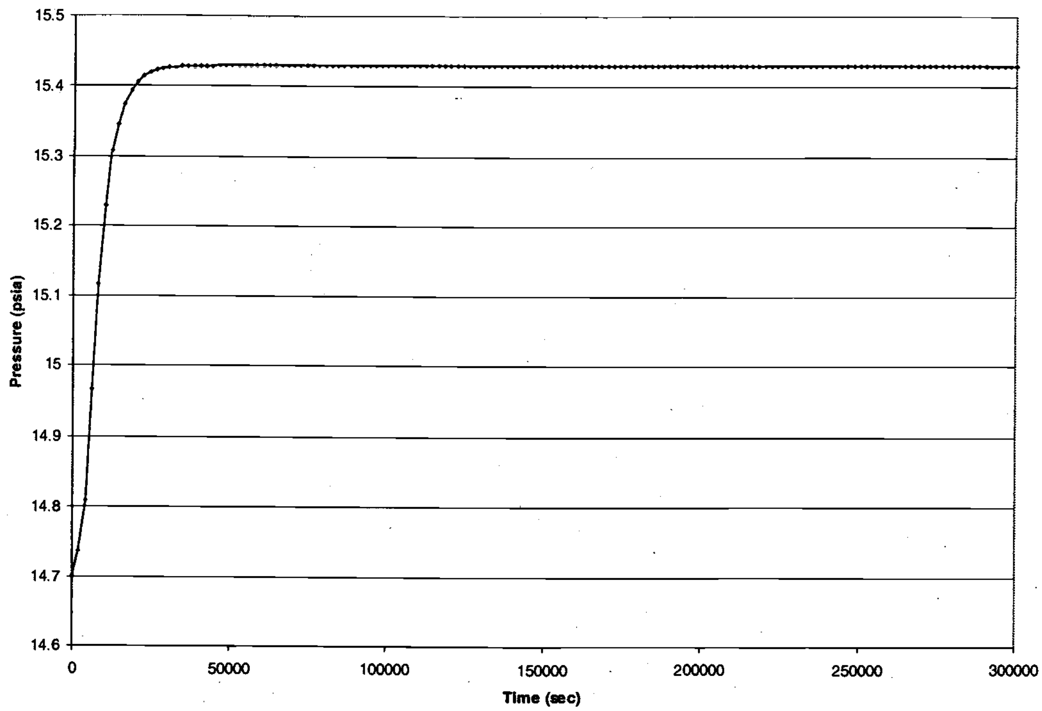

Figure 4.3: Full Scale Steady-State Pressure

The vapor and liquid temperature inside of containment are plotted in Figure 4.4. The steady-state values are 91.32 °F (32.96 °C) and 71.93 °F (22.18 °C), for the vapor and liquid respectively. The steady-state relative humidity of the containment atmosphere was 50.16% and is plotted in Figure 4.5.

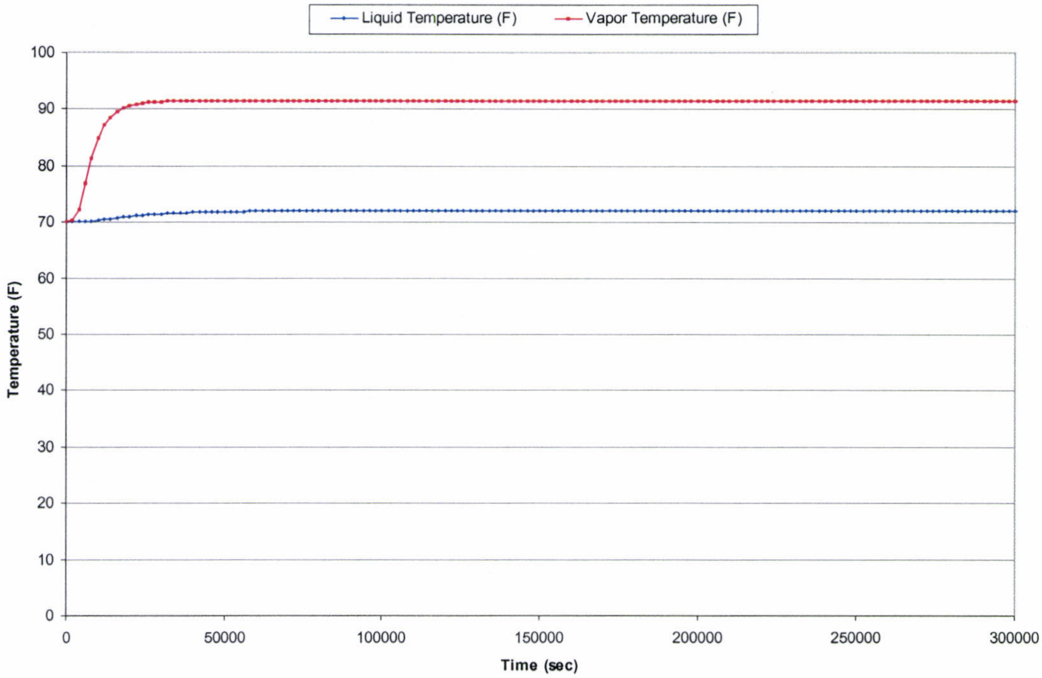

Figure 4.4: Full Scale Steady-State Containment Liquid and Vapor Temperatures

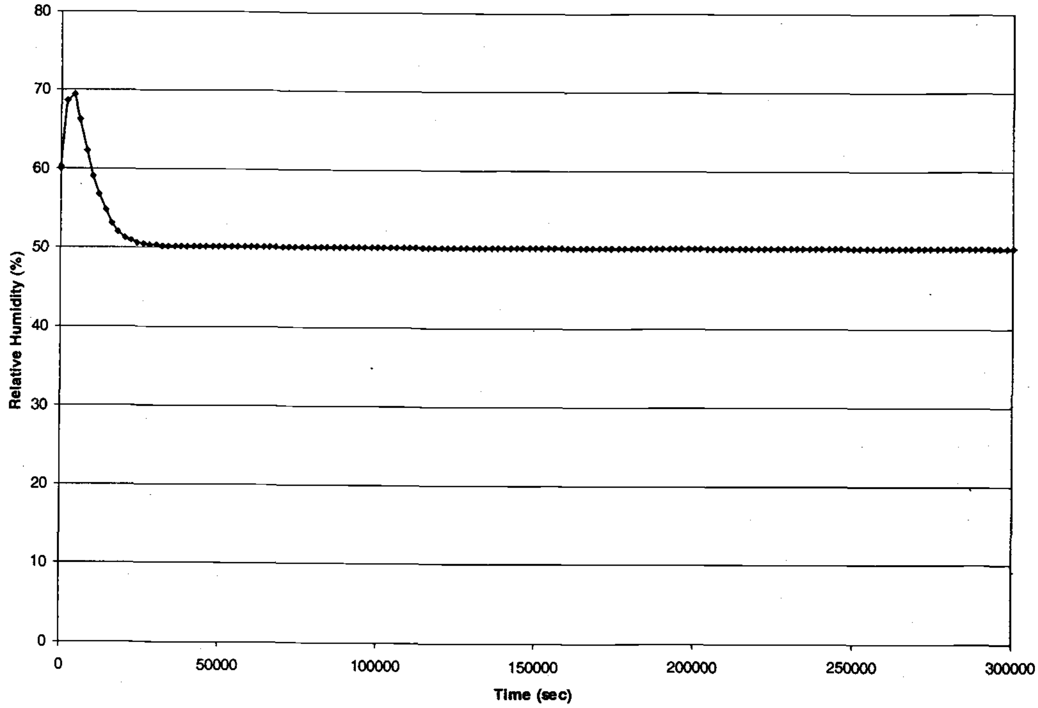

Figure 4.5: Full Scale Steady-State Relative Humidity

4.1.2 Transient Calculations

Transient calculations were performed on MASLWR to determine the containment response to accidents. To predict the phenomena associated with the use of the safety systems, a model was developed that was much more complicated than the steady-state model. The initial conditions for the model are the results of the steady-state calculation.

4.1.2.1 Model

The model developed for the transient simulations consists of three control volumes. The first control volume represents the RX/SG vessel. The second represents the ADS sparger, and the third is the containment vessel. Heat transfer between the control volumes and surroundings are modeled with conductors. The conductors represented here model the interaction of the containment with the containment cooling pool, and the RX/SG with the containment. The appropriate safety piping, valves and core power are also modeled.

4.1.2.2 Control Volumes

The transient model control volumes consist of regions subdivided using a linear orthogonal grid. Constructing the models this way enables a more detailed representation of the transport and mixing phenomena within the containment, sparger, and RX/SG.

4.1.2.2.1 Containment Volume

The containment volume has the same dimensions as in the steady-state case. The grid contains 19 cells in the vertical direction. In each vertical plane, the grid is 3X3, which gives a total of 171 cells with a volume of 0.78 m^3 each.

4.1.2.2.2 Reactor/Steam Generator Volume

The RX/SG volume was not modeled in the steady-state case except as a boundary condition on a conductor. Here the fluid volume of the RX/SG is modeled. The appropriate input dimensions required for GOTHIC are shown in Table 4.4.

Table 4.4: RX/SG Volume Input Dimensions

Parameter	Value
Height	13.27 m
Fluid Volume	49.75 m3
Hydraulic Diameter	1.81 m
Liquid Fraction	0.95

The volume was subdivided using a non-linear orthogonal grid. The reason is that a conductor connects the RX/SG vessel thermally to the containment. To do this, the conductor must span the same number of cells in both volumes. The grid lines must also match up in the vertical direction to maintain the appropriate gravity head for connected piping. The resulting grid has larger cells at the bottom where the sump and ADS lines are connected so the vertical grid lines match between the containment and RX/SG. The total number of cells is 171, the same as the containment with 19 cells in the vertical directions and 3X3 at each elevation. The cell volumes are 0.395 m^3 at the bottom, decreasing to 0.125 m^3 at the top.

4.1.2.2.3 Submerged ADS Sparger Volume

The sparger volume was also not included in the steady-state calculation because it did not participate thermally or with flow. During the transients this volume is where the submerged ADS vents. The sparger then distributes the submerged ADS flow through several holes in the top and bottom. The appropriate GOTHIC input for the sparger is presented in Table 4.5.

Table 4.5: Submerged ADS Sparger Volume Inputs

Dimension	Value
Height	0.2032 m
Fluid Volume	0.3416 m^3
Hydraulic Diameter	0.2032 m
Liquid Fraction	1.0

The sparger volume is subdivided using a linear orthogonal grid. There is a single cell in the vertical direction and 11 in the horizontal direction. The resulting 11 cells each have a volume of 0.031 m^3.

4.1.2.3 Conductors

The conductors in the transient models have the same thickness, materials, and noding as the steady-state model. The primary difference in the transient model is that there are different boundary conditions on some of the conductors. One other difference is that in a subdivided volume, the conductors span many cells to several sub conductors. The conductors need to span the appropriate bounding surfaces where walls or structures are located. This requires that the two different regions of conductors be broken up into two small conductors that span the two planes of the containment and RX/SG vessel.

4.1.2.3.1 Reactor/Steam Generator Vessel

The same conductor presented in the steady-state calculations represents the RX/SG vessel conductor in the transient cases. The only difference is in the boundary conditions. The boundary condition on the interior surface (A) is now a direct solution for heat transfer. All the same options as the steady-state direct solution are used except the condensation model used will be Uchida in one case and Gido/Koestel in the other.

The surface area of the two vapor section conductors is 34.59 m^2. The surface area of the two liquid section conductors is 33.44 m^2.

4.1.2.3.2 Containment Vessel

The containment vessel conductors are identical to those used in the steady-state calculation, including the boundary conditions. The only difference for the transient cases is that the conductors in the vapor and liquid regions are broken up into two conductors. In addition the condensation model will be Uchida in one case, and Gido/Koestel in the other.

The surface area of the two vapor section conductors is 72.73 m^2. The surface area of the two liquid section conductors is 48.38 m^2.

4.1.2.4 Flow Paths

In GOTHIC, pipes connecting different volumes are modeled as flow paths. The flow paths used in the MASLWR transient simulations represent the safety system piping. This includes the submerged ADS lines, steam vent lines, sump lines, and the holes in the sparger. Flow paths carry mass, momentum, and energy from one cell to another.

4.1.2.4.1 Steam Vent Lines

The steam vent lines come out of the top of the RX/SG vessel and vent into the containment. The appropriate input data required for GOTHIC is given in Table 4.6.

Table 4.6: Steam Vent Line Inputs

Parameter	Value
Pipe Flow Area	0.0081 m2
RX/SG Connection Height	13.55 m
Containment Exit Height	14.5 m
Hydraulic Diameter	0.1016 m
Relative Roughness	3.5E-4
Exit Loss Coefficient	2.78
Length	1 m

The relative roughness is a typical value for turbulent flow in a steel pipe. The exit loss coefficient is a value recommended by the GOTHIC user manual [#] for flows paths blowing down into large volumes. In addition to the physical input for the flow path different options need to be selected for momentum transport, and choked flow models. For the steam vent lines the momentum transport option is N&T (Normal and Transverse). This option includes the transport of the transverse and normal component of momentum within the cell where the flow path is connected. The choked flow model used is a table lookup. The tables are given in the GOTHIC technical manual [1].

The steam vent lines are connected to the top of the RX/SG vessel on opposite sides as shown in Figure 3.2. They then exit into the containment at an elevation of 14.5 m on opposite sides of the grid shown in Figure 4.6.

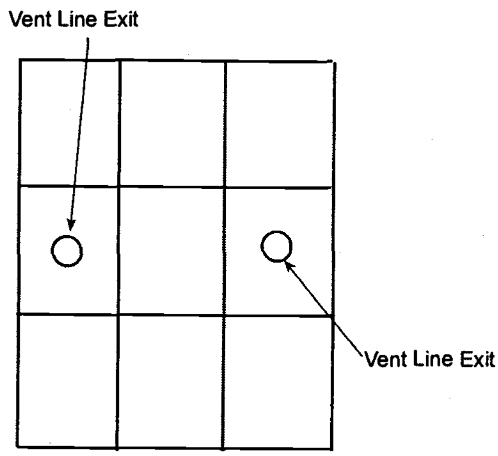

Figure 4.6: Vent Line Exit Locations

4.1.2.4.2 Submerged ADS Lines

The submerged ADS lines connect the RX/SG to the ADS sparger. These lines have the exact same flow area, relative roughness, and hydraulic diameter as the steam vent lines. They also use the same momentum transport and choked flow options. The only difference is the elevations, and exit loss coefficient. This data is given in Table 4.7. The exit loss coefficient for the submerged ADS lines is the typical value of a pipe exit since it is connected to such a small volume. The submerged ADS lines are connected to opposite sides of the RX/SG vessel at an elevation of 5.0 m as shown in Figure 3.2. The exit connects to the ADS sparger volume shown in Figure 4.7.

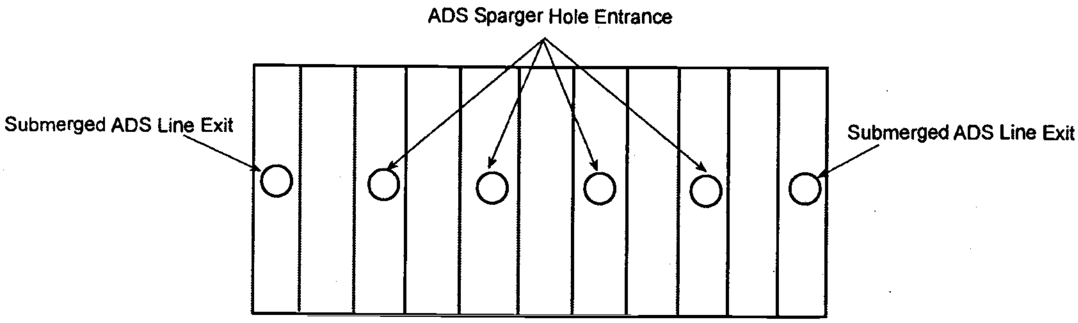

Figure 4.7: Flow Path Connections to ADS Sparger

Table 4.7: Submerged ADS Line Inputs

Parameter	Value
RX/SG Connection Height	5.0 m
ADS Sparger Connection Height	2.044 m
Exit Loss Coefficient	1.0
Length	2.96 m

4.1.2.4.3 ADS Sparger Holes

The connections that the ADS sparger volume makes with the containment are holes in a pipe in reality. GOTHIC does not have a model for holes, but the same effect can be achieved by the use of flow paths. In the full scale prototype there are 70, 1 inch diameter holes in the sparger. This is a rather large number of flow paths to model with GOTHIC. It would also increase the run time of the model dramatically. To simplify the model creation, and to shorten the run time, only 4 flows paths were used to model the entire flow area of the 70, 1 inch holes. The resulting data input into GOTHIC for these consolidated holes is given in Table 4.8.

Table 4.8: Sparger Hole Inputs

Parameter	Value
Sparger Connection Height	2.044 m
Containment Exit Height	2.044 m
Flow Area	0.00887 m^2
Hydraulic Diameter	0.1063 m
Exit Loss Coefficient	2.78
Relative Roughness	3.5E-4
Length	0.0254 m

The location of the flow path ends that represent the holes are distributed in the containment into four different cells at an elevation of 2.044 m shown in Figure 4.8.

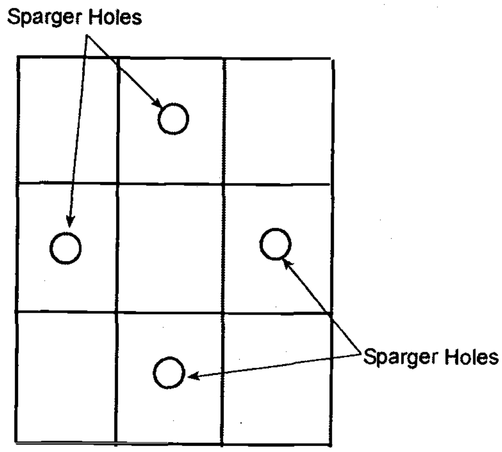

Figure 4.8: Sparger Hole Flow Path End Locations

4.1.2.5 Valves

The valves used in the GOTHIC transient model represent the 4 inch gate valves used for the steam vent system and submerged ADS system. Valves are also used to represent the 3 inch orifice in the steam vent lines, since GOTHIC does not include a component to model orifice plates.

4.1.2.5.1 Steam Vent Valves

The steam vent valves are 4 inch gate valves. To define a valve GOTHIC requires the valve flow area, loss coefficient curve, and the valve type. For all the valves used in the transient model the type is "Quick Open", this means that the travel time for the valve stem is zero. As a result the loss coefficient curve only needs two data points. The first is the loss when the valve is shut, which is an arbitrary number of the order 1E6. The second is the loss when the valve is completely open which has value of 0.136. The flow area for the valve is 0.0079 m^2. The valves require trips to open. The trips can be triggered on time or volume variables such as pressure, temperature, or level. The steam vent line open trip is triggered on time equal to 1 second, since the transient tests all begin with an inadvertent opening of a steam vent valve. For purposes of analysis once the valves open they are assumed to remain open throughout the transient.

4.1.2.5.2 Submerged ADS Valves

The submerged ADS valves are exactly the same as the steam vent valves, except for the trip used to actuate them. For these valves the open trip is on pressure. The set point is 500 kPa in containment with a 0.5 second delay. This trip was obtained from the MASLWR RELAP 5 safety system logic provided by Jim Fisher from INEEL. For purposes of analysis, once the valves open they are assumed to remain open throughout the transient.

4.1.2.5.3 Steam Vent Line Orifice

GOTHIC does not provide a component to model an orifice plate within a flow path. The steam vent line has a 3 inch orifice within the flow path. As a result this orifice was modeled using a valve. The inputs for this valve are a flow area of 0.00456 m^2, and a loss coefficient determined from Crane [19] of 2.25. The valve type is "Quick Open", and uses the same trip as the steam vent valves.

4.1.2.6 Heat Exchangers

To model the interaction of the core and the associated decay power with the system during a transient, a heater was used. The steam generator was not modeled, assuming that once an accident is initiated the feed water is secured and the steam generator no longer participates thermally.

To model the decay heat released after a reactor SCRAM, a heater was added to the transient model. This heater only supplies heat to the liquid phase within the RX/SG vessel. The inputs required for GOTHIC are a heat rate and heat rate forcing function. The heat rate is multiplied by the forcing function to obtain the heat supplied by the heater. The forcing function in this case represents the decay power curve derived from the Light Water Reactor Decay Heat Power Standard [21]. The calculated values are shown in Table 4.9.

Table 4.9: MASLWR Decay Power

Time After SCRAM	Power
1 second	9370.5 kW
10 seconds	7206 kW
100 seconds	4672.5 kW
1000 seconds	2829 kW
10000 seconds	1385.55 kW

The heater was located at an elevation of 2.0 meters, near the top the core in the center cell of the volume.

4.1.2.7 Initial Conditions

Initial conditions are necessary for each of the control volumes within the model. These include the pressure, liquid temperature, vapor temperature, liquid fraction, and relative humidity. The conductors also require initial conditions. The conductors in the transient case should begin with the temperature distribution of the steady-state results. GOTHIC only allows a constant temperature within the conductor at the beginning. To establish the correct temperature profile, a special step is taken when setting up the run options and will be explained in a later section.

4.1.2.7.1 Containment Initial Conditions

The initial conditions used for the transient case are the results of the steady-state calculations and are presented in Table 4.10.

Table 4.10: Transient Full Scale Containment Initial Conditions

Parameter	Value
Pressure	106.156 kPa
Vapor Temperature	32.3 °C
Liquid Temperature	22.4 °C
Relative Humidity	52.02%
Liquid Fraction	0.3155

4.1.2.7.2 Reactor/Steam Generator Initial Conditions

The initial conditions for the RX/SG volume were obtained from the steady-state RELAP 5 calculations performed by Jim Fisher. These values are given in Table 4.11.

Table 4.11: Transient Full Scale RX/SG Initial Conditions

Parameter	Value
Pressure	7.6 MPa
Vapor Temperature	291.85 °C
Liquid Temperature	255 °C
Relative Humidity	100%
Liquid Fraction	0.95

4.1.2.7.3 ADS Sparger Initial Conditions

The initial conditions for the ADS sparger volume are the same as the containment, except that the relative humidity is 100%, and the liquid fraction is equal to 1 since it is submerged in the pool within the containment.

4.1.2.8 Run Controls

The run parameters required for the transient model are different than those used in the steady-state calculation. Two time domains are used. The first establishes the conductor temperature profiles. The second is the actual simulation period. The input data for these time domains are shown in Table 4.12 and 4.13.

Table 4.12: Full Scale Transient Time Domain 1 Run Controls

Parameter	Value
Maximum Time Step (sec)	1
Minimum Time Step (sec)	1E-12
Transient Time (sec)	0.001
Conductor/Hydraulic Step Ratio	1E8
Solution Method	Semi-Implicit
Implicit Convergence Limit	0.0
Pressure Solution Method	Sparse
Pressure Convergence Limit	0.0
Differencing Scheme	Forward Upwind

Table 4.13: Full Scale Transient Time Domain 2 Run Controls

Parameter	Value
Maximum Time Step (sec)	1
Minimum Time Step (sec)	1E-8
Transient Time (sec)	5000
Conductor/Hydraulic Step Ratio	1
Solutions Method	Semi-Implicit
Implicit Convergence Limit	0.0
Pressure Solution Method	Sparse
Pressure Convergence Limit	0.0
Differencing Scheme	Forward Upwind
Graphics Interval (sec)	10

4.1.2.9 Transient Results

Four sets of simulations were completed for the full scale transient model. The simulations consisted of two accident scenarios. The first, referred to as Case 1, is an inadvertent steam vent valve opening with a sump system failure. The second, referred to as Case 2, is an inadvertent vent valve opening followed with a sump system failure, and a single submerged ADS failure. Both Cases were modeled with the Gido/Koestel and Uchida condensation models.

4.1.2.9.1 Case 1 Results

Case 1 was run on an Intel Pentium 4 1.4 GHz PC for a period of 3.5 days for each simulation. The results for the Gido/Koestel condensation model include a time integrated mass error of -0.314% and an energy error of -0.595%. The results for the Uchida condensation model include a time integrated mass error of -1.155% and an energy error of -1.747%. The error associated with both models occurred after the pressure between the containment and RX/SG vessel were equalized. The suspected cause of the errors is the code's difficulty in predicting low flows dominated by very small pressure differences and gravity. Every effort was made to reduce these errors, including refining and coarsing meshes, and changing numerical discretizations and solution techniques.

The time line of events for Case 1 is presented in Table 4.14.

Table 4.14: Case 1 Full Scale Event Time Line

Event	Uchida Time (sec)	Gido/Koestel Time (sec)
Inadvertent Steam Vent Valve Opening	1	1
Submerged ADS Triggered	59.5	105
Peak Containment Pressure Achieved	213	271
RX/SG Reflood (if occurred)	1467	NA
End of Transient	1500	1500

From the time line it appears that everything after the transient was initiated occurred sooner with the Uchida condensation model. The best explanation of this can be seen in the plot of wall heat transfer coefficients within the vapor region, Figure 4.10. This figure shows that the Uchida correlation reaches its upper bound of 1.578 kW/m^2-°C (278 BTU/hr-ft^2-°F), imposed by the correlation form used in GOTHIC, very rapidly. The Gido/Koestel model has no such limitations, and the resulting heat transfer coefficient is 32.93 kW/m^2-°C (5800 BTU/hr-ft^2-°F) an order of magnitude greater than the Uchida model. The higher heat transfer coefficient means more condensation and a reduced peak pressure (see Figure 4.9). The peak pressure for the Uchida simulation is 350 psia (2.413 MPa) compared with 290 psia (1.999 MPa) for the Gido/Koestel simulation.

The flow rates through the safety system lines are relatively close for the two condensation models, and are shown in Figure 4.11–4.16.

The Uchida simulation predicted RX/SG reflood, which is the return of liquid to the RX/SG vessel through the submerged ADS lines, at 1460 seconds. This is seen in Figure 4.15 and Figure 4.16. The Gido/Koestel simulation does not predict reflood during the transient time.

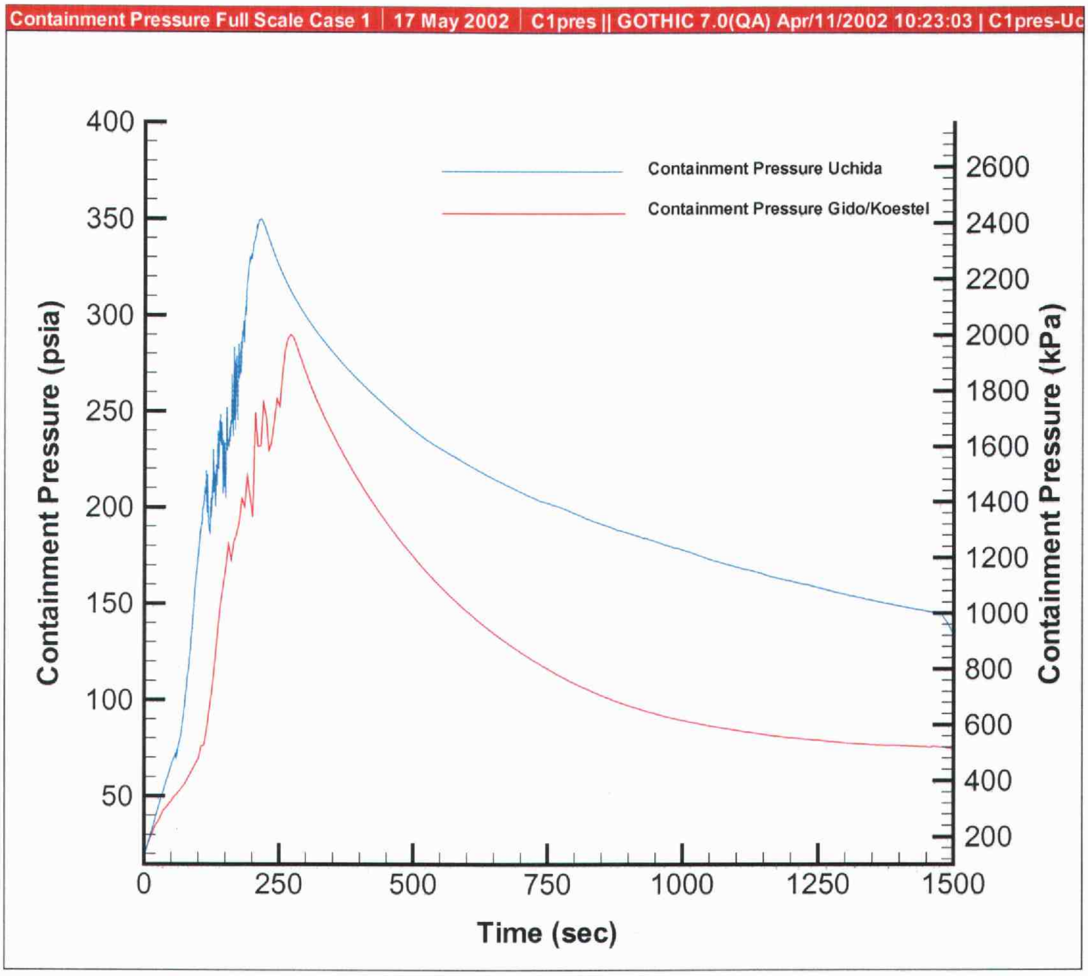

Figure 4.9: Case 1 Full Scale Containment Pressure

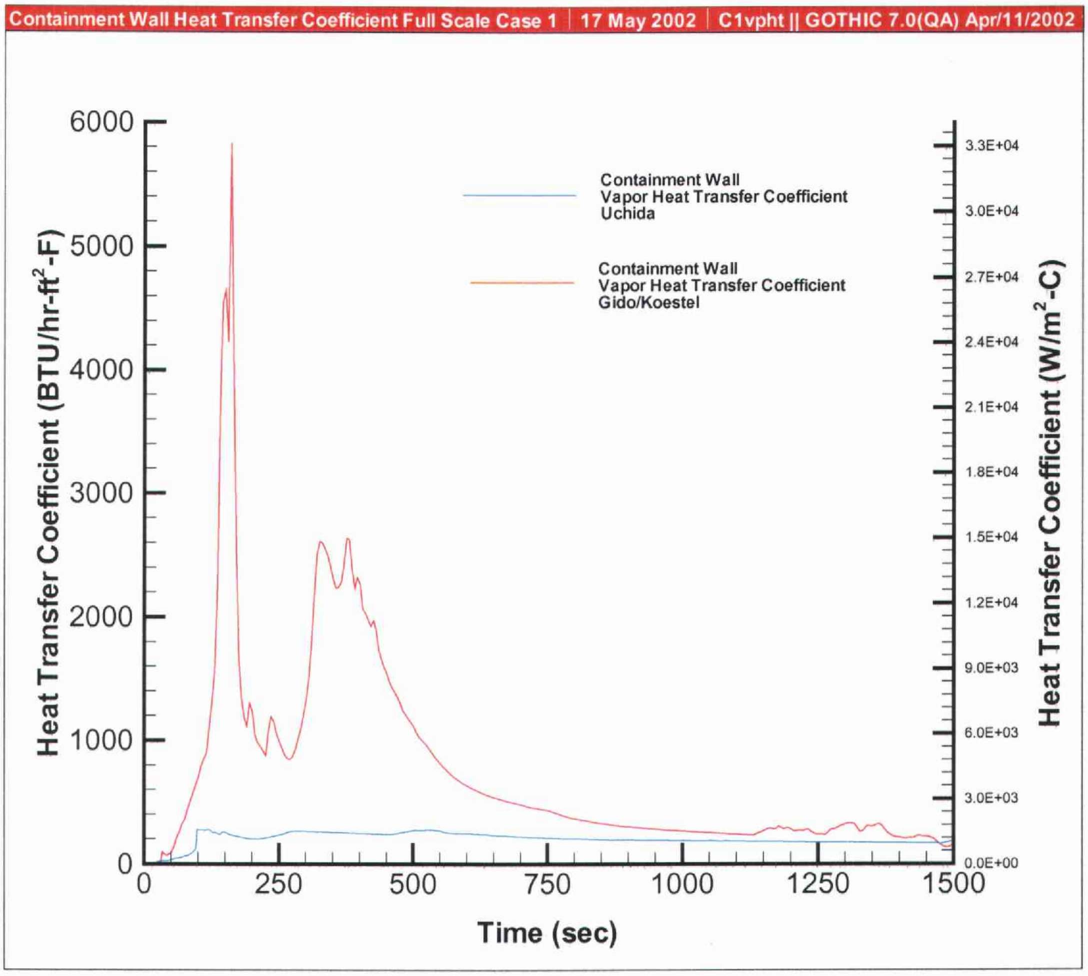

Figure 4.10: Case 1 Full Scale Wall Heat Transfer Coefficient

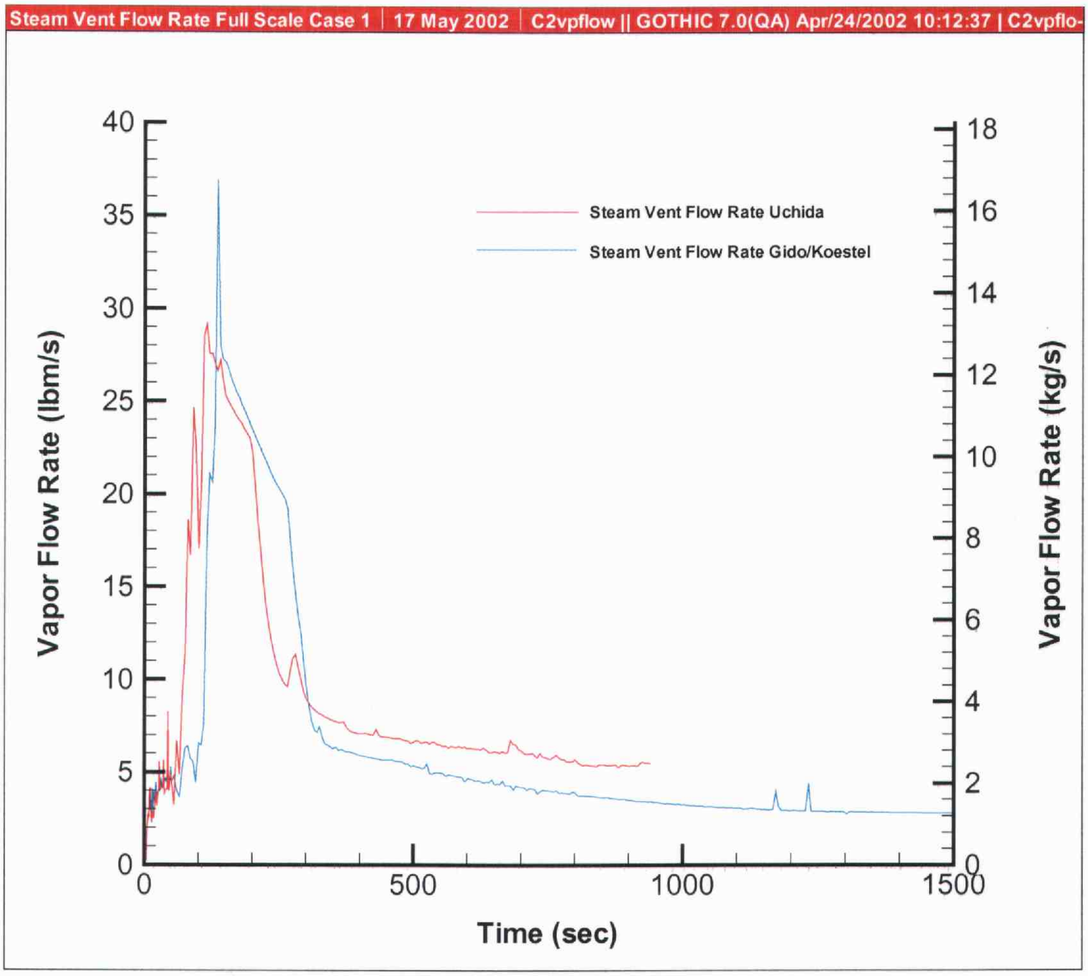

Figure 4.11: Case 1 Full Scale Steam Vent Vapor Flow Rate

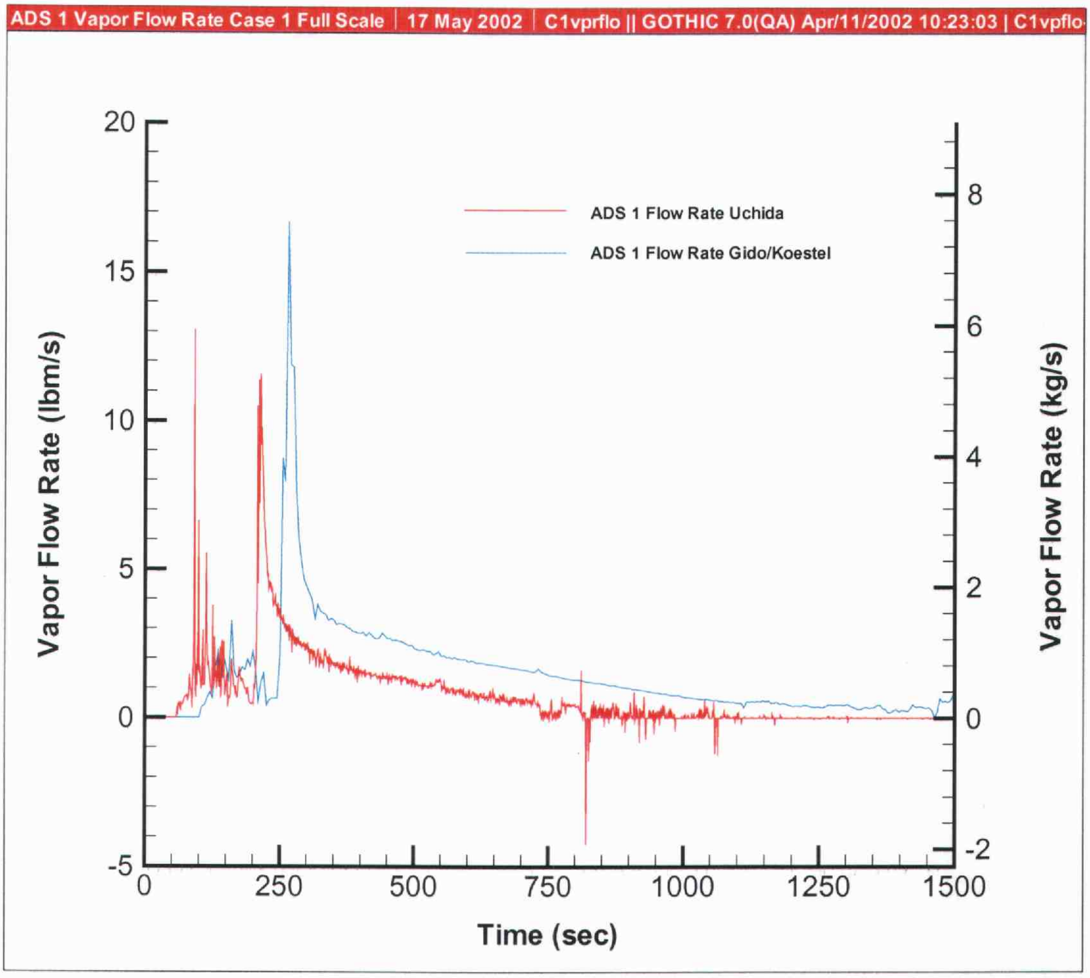

Figure 4.12: Case 1 Full Scale ADS 1 Vapor Flow Rate

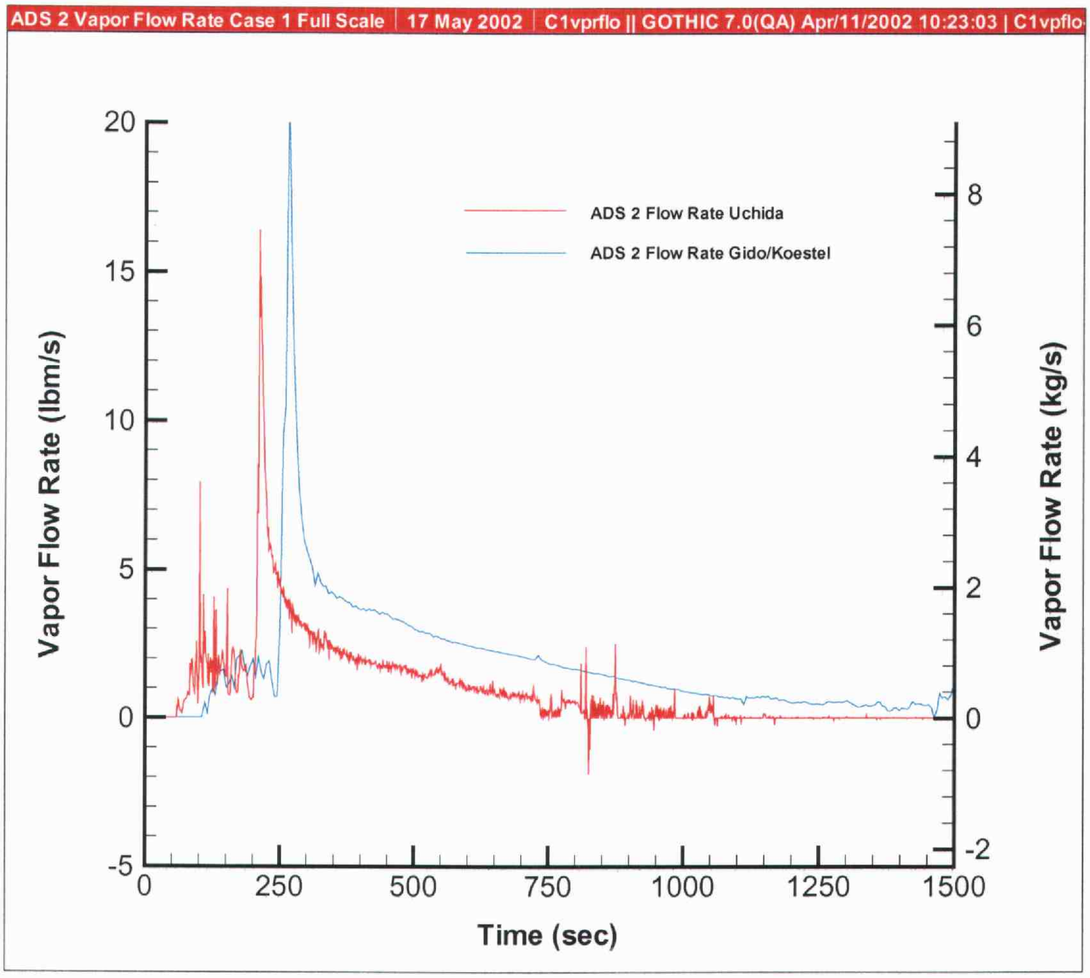

Figure 4.13: Case 1 Full Scale ADS 2 Vapor Flow Rate

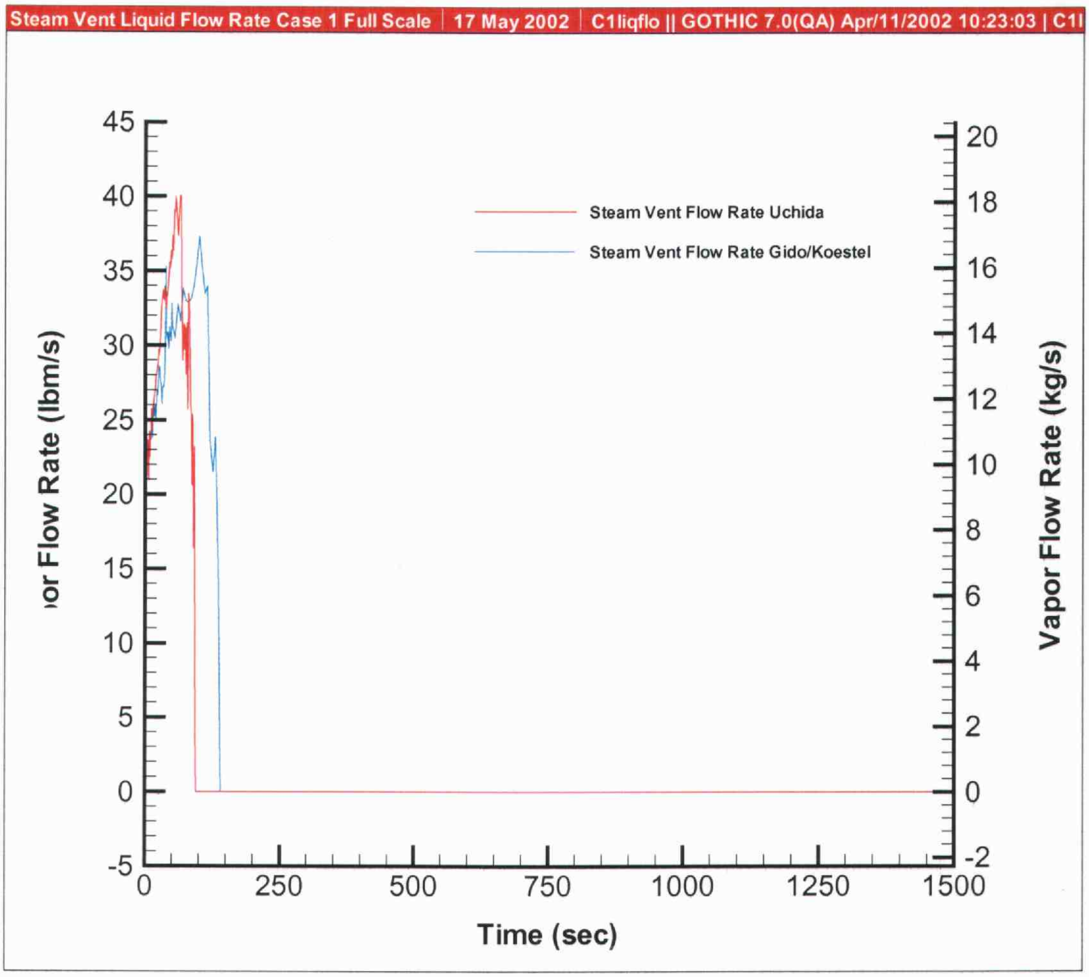

Figure 4.14: Case 1 Full Scale Steam Vent Line Liquid Flow Rate

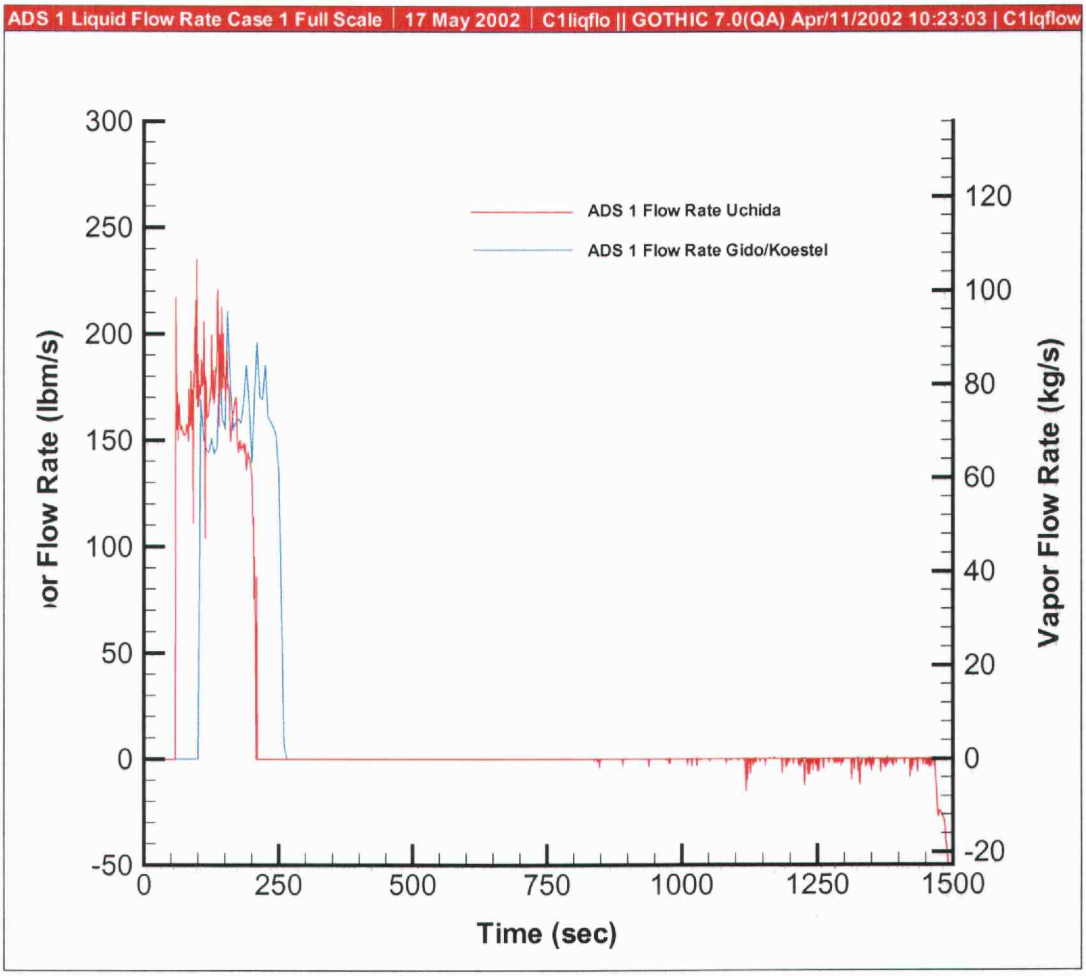

Figure 4.15: Case 1 Full Scale ADS 1 Liquid Flow Rate

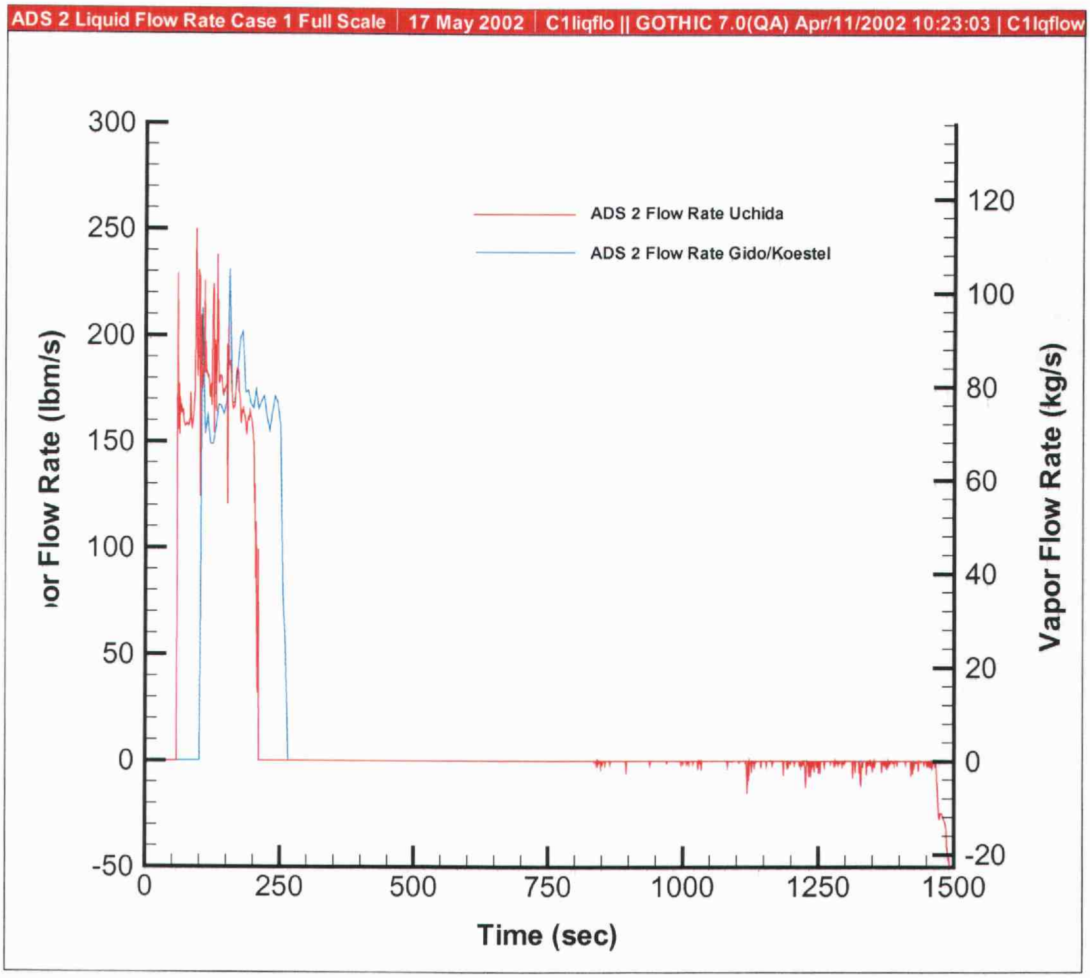

Figure 4.16: Case 1 Full Scale ADS 2 Liquid Flow Rate

4.1.2.9.2 Case 2 Results

Case 2 was run on an Intel Pentium 4 1.4 GHz PC for a period of 4 days. The results for the Gido/Koestel condensation model include a time integrated mass error of -0.359% and an energy error of -0.68%. The results for the Uchida condensation model include a time integrated mass error of -0.364% and an energy error of -0.617%.

The timeline of events for Case 2 is presented in Table 4.15.

Table 4.15: Case 2 Full Scale Event Time Line

Event	Uchida Time (sec)	Gido/Koestel Time (sec)
Inadvertent Steam Vent Valve Opening	1	1
Submerged ADS Triggered	60.3	110.5
Peak Containment Pressure Achieved	245	280
RX/SG Reflood (if occurred)	NA	NA
End of Transient	940	1000

From the timeline it appears that everything after the transient was initiated occurred sooner with the Uchida condensation model, similar to the Case 1 results. The cause of this is the calculated wall heat transfer coefficients within the vapor region. The heat transfer coefficient in Figure 4.18 shows that the Uchida correlation reaches its upper bound of 1.578 kW/m^2-°C (278 BTU/hr-ft^2-°F), imposed by the correlation form used in GOTHIC, very rapidly. The Gido/Koestel model has no maximum, and the resulting heat transfer coefficient is 22.79 kW/m^2-°C (4013 BTU/hr-ft^2-°F) an order of magnitude greater than that predicted by the Uchida model. The higher heat transfer coefficient means more condensation and an increased period of time until the submerged ADS actuation pressure is achieved. The increased condensation also results in a reduced peak pressure within the containment seen in Figure 4.17. The peak pressures are 408 psia (2.813 MPa) and 328 psia (2.261 MPa) for the Uchida and Gido/Koestel simulations respectively.

The flow rates through the safety system lines are not as close for the different condensation models as they were for Case 1. The exception is the steam vent flow rates shown in Figure 4.19, and Figure 4.21. The flow rates for this line are nearly the same for the two different condensation models. The only other safety system line with flow is the submerged ADS 2 line. In this line there are some discernable differences in both the vapor and liquid flow rates between the two different models shown in Figure 4.20 and Figure 4.22. The initial vapor flow rates from submerged ADS 2 are the same until the RX/SG level falls below 5.0 m, the outlet of the ADS line. At this point the Gido/Koestel simulation predicts a higher vapor flow rate through ADS 2 than the Uchida simulation, due to a higher pressure difference between the RX/SG vessel and the containment. The liquid flow rates show that the Gido/Koestel simulation predicts a much higher liquid flow rate than the Uchida simulation. This allows the RX/SG vessel to drain more rapidly explaining the higher pressure difference when the level drops below 5 m. This difference in flow rates is unexplained by the data. The same critical flow models were used and the flow paths and loss coefficients were identical. There is a slightly higher pressure difference between the RX/SG vessel and the containment (15 psia), but this does not explain a factor of two difference in flow rate.

During the simulation period for Case 2, there was no reflood observed. There might have been some observed for the Uchida simulation, but due to numerical simulation problems, the model could not be run for the desired amount of time.

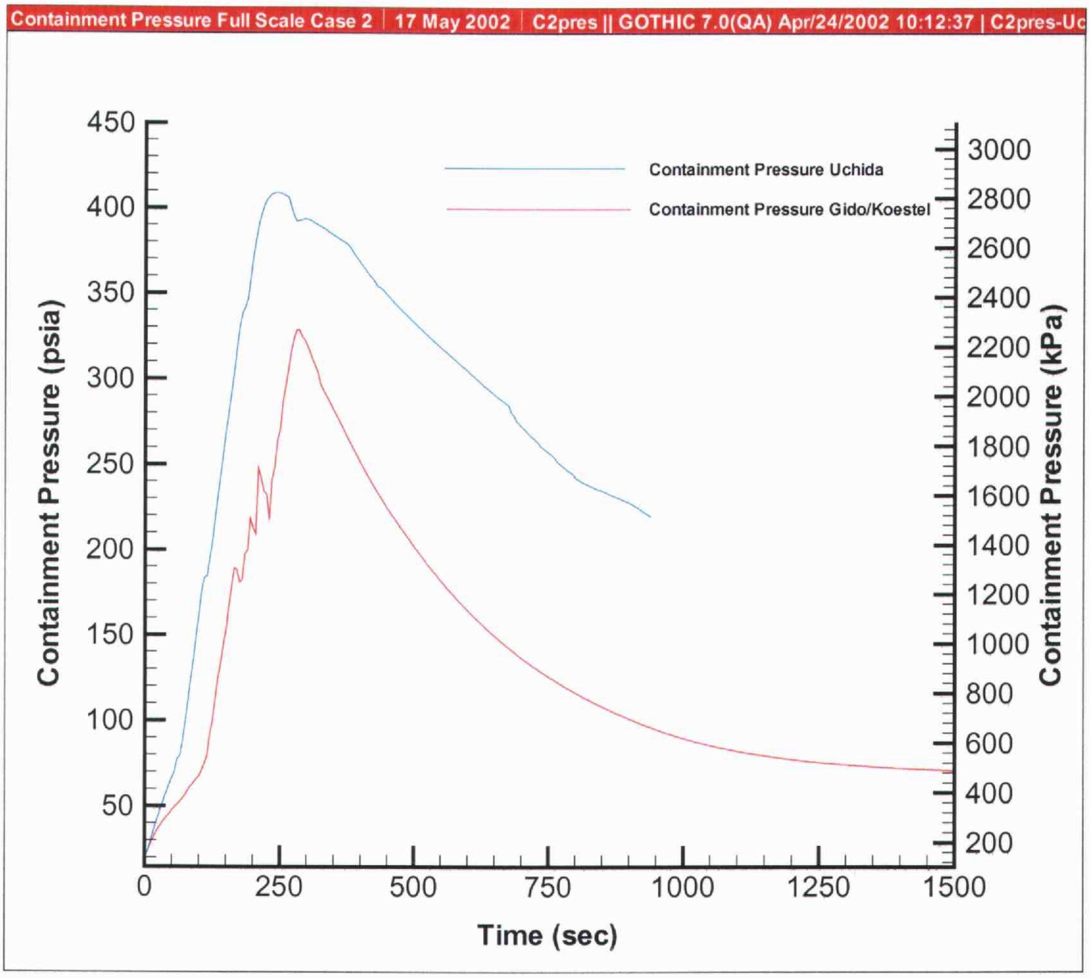

Figure 4.17: Case 2 Full Scale Containment Pressure

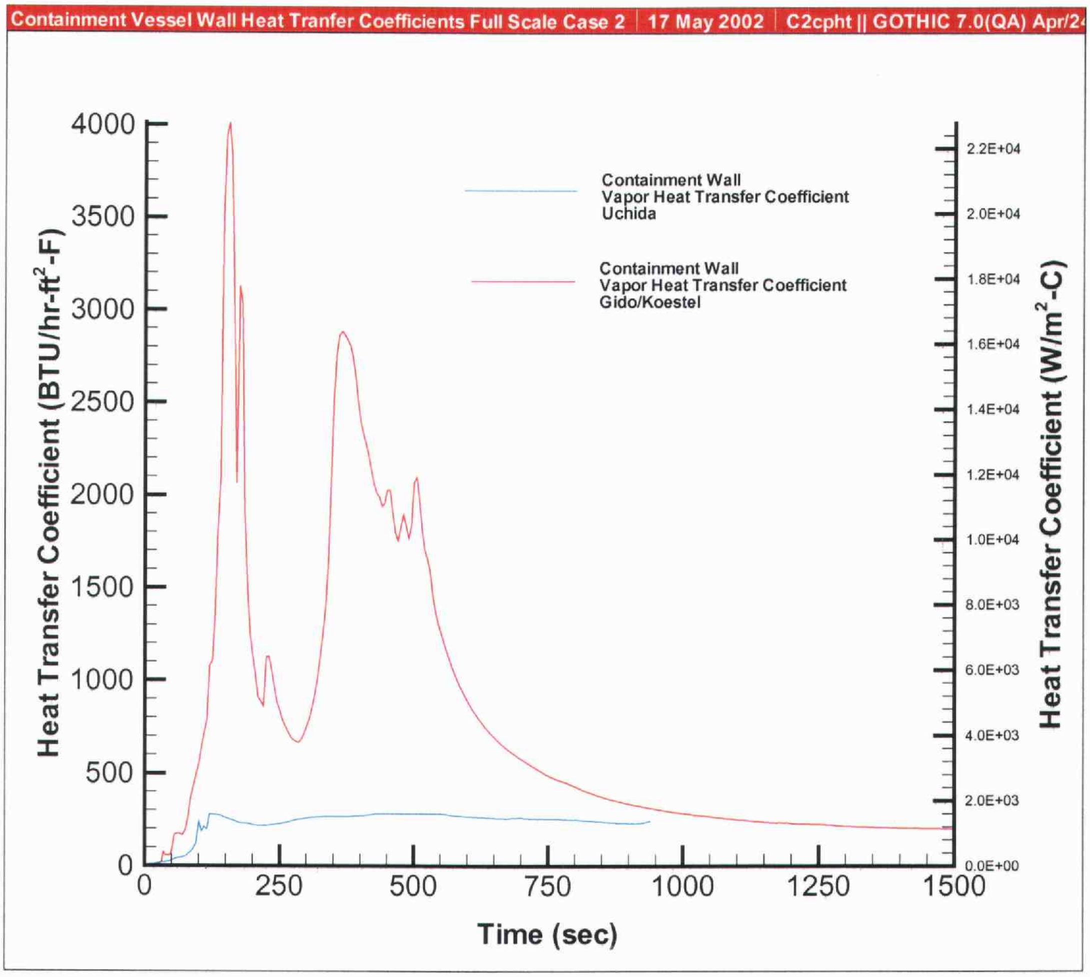

Figure 4.18: Case 2 Full Scale Containment Wall Heat Transfer Coefficient

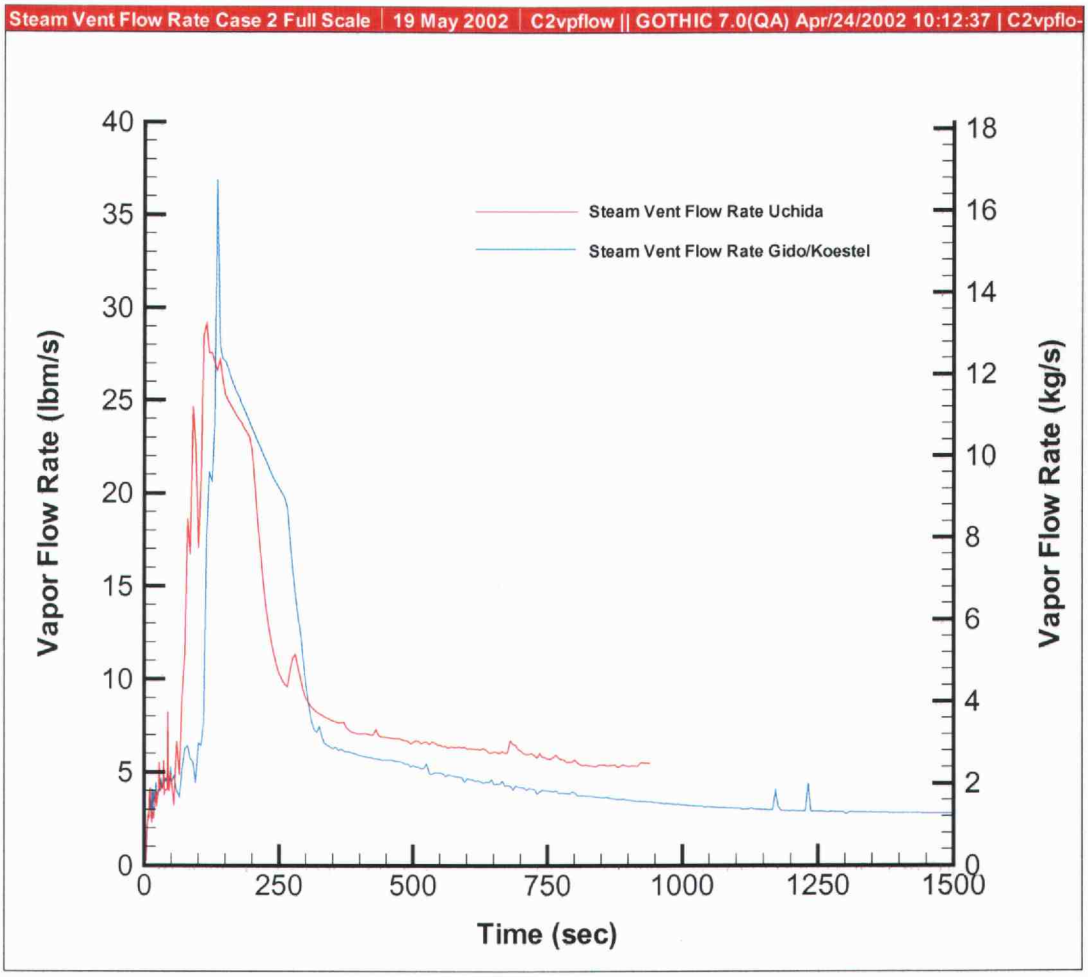

Figure 4.19: Case 2 Full Scale Steam Vent Vapor Flow Rate

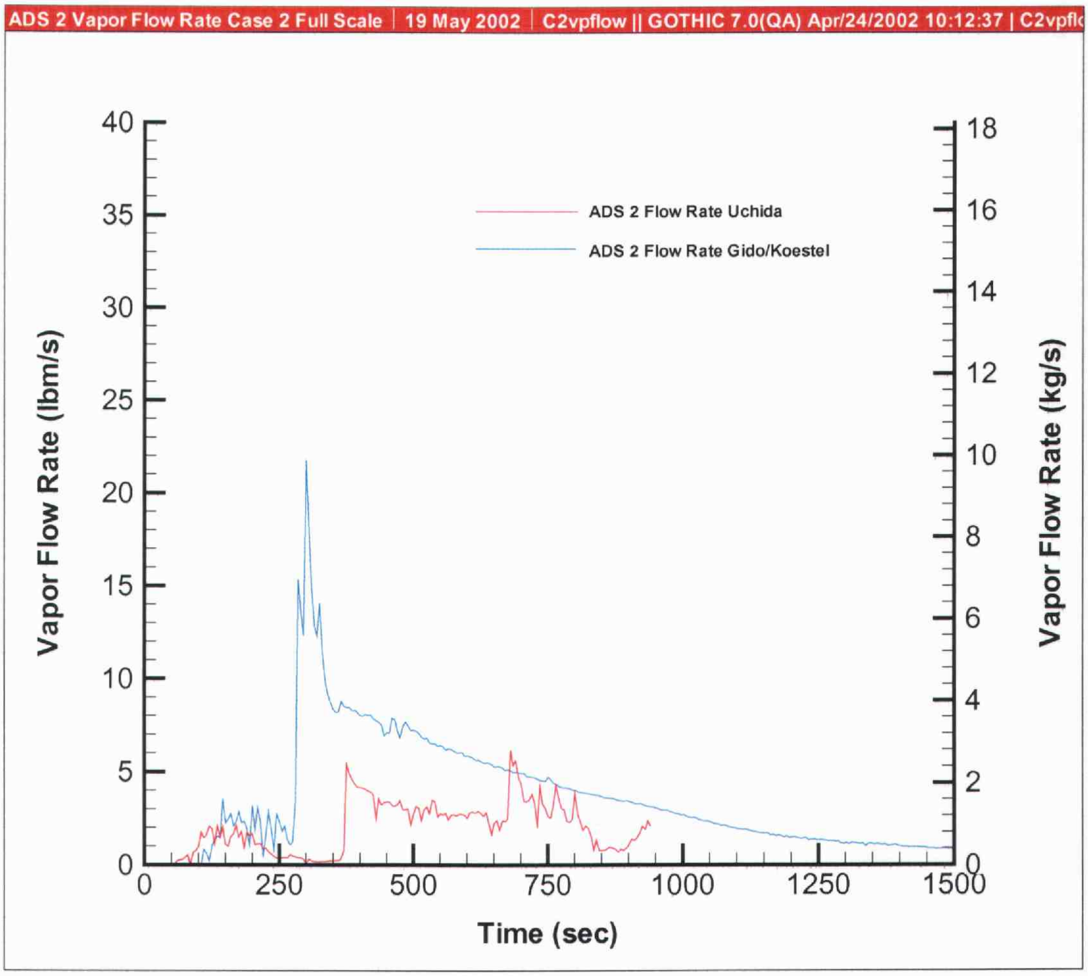

Figure 4.20: Case 2 Full Scale ADS 2 Vapor Flow Rate

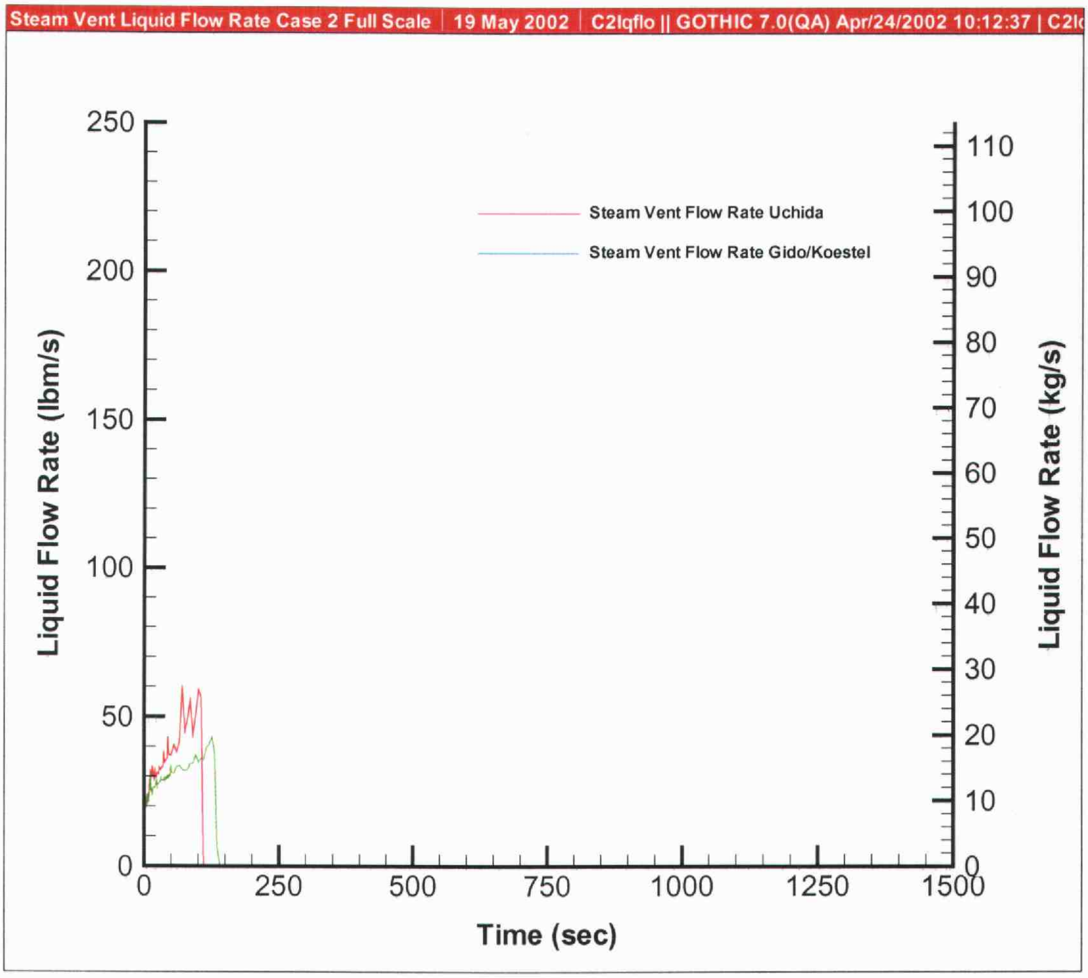

Figure 4.21: Case 2 Full Scale Steam Vent Liquid Flow Rate

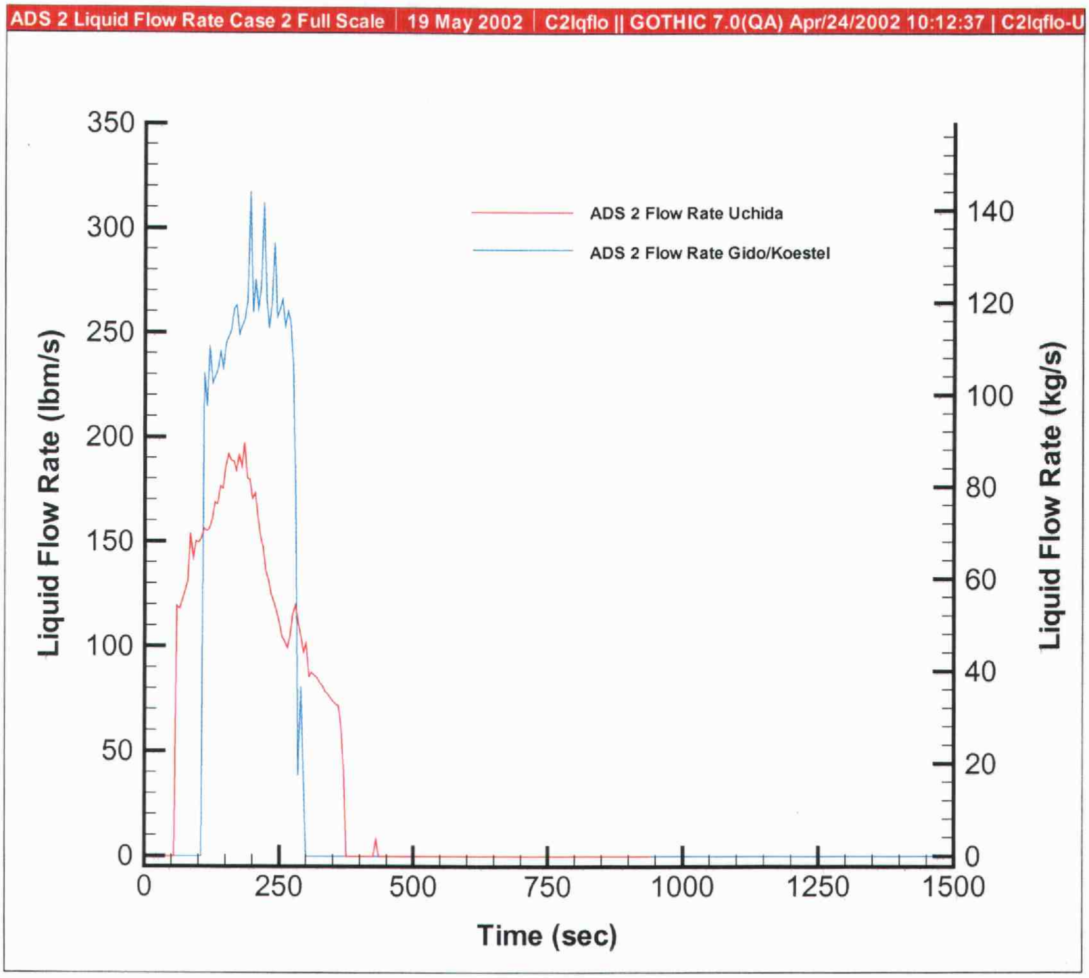

Figure 4.22: Case 2 Full Scale ADS 2 Liquid Flow Rate

4.2 OSU Test Facility

The scaled test facility dimensions were used to generate a model for simulations in GOTHIC. The initial conditions for the transients that were simulated came from the full scale steady-state calculations. The purpose of this analysis is to determine the peak pressures observed in the scaled containment as well as to compare with the full scale simulations to determine if the scaling was performed correctly.

4.2.1 Model

Only a single model was created for the test facility. This is a result of not being able to perform steady-state calculations since the RX/SG vessel is not within the containment. The appropriate initial conditions are assumed to be the same as the full scale prototype.

The model consists of three control volumes, just as in the full scale prototype. They are the RX/SG vessel, containment, and ADS sparger. Conductors were used to simulate the thermal interaction of the RX/SG, containment, and containment cooling pool. The appropriate piping, valves, and heaters were used to simulate all the necessary components for the model. Initial conditions were assigned along with appropriate run controls.

4.2.2 Control Volumes

For the test facility model three control volumes were required. These are the RX/SG vessel, containment, and ADS sparger. These volumes were subdivided using an orthogonal grid. The containment cooling pool is not modeled here since the time scales are relatively short. A constant temperature boundary condition is used in its place.

4.2.2.1 Reactor/Steam Generator Volume

The RX/SG volume inputs required by GOTHIC are given in Table 4.16.

Table 4.16: OSU Test Facility Containment Volume Input Dimensions

Parameter	Value
Height	4.51 m
Elevation	1.0 m
Fluid Volume	0.2612 m^3
Hydraulic Diameter	0.25 m

The RX/SG volume is subdivided using a linear orthogonal mesh. There are 27 cells in the vertical direction, and a 2X2 grid at each vertical plane. The resulting volume of each cell is 1.67E-3 m^3, with a total of 156 cells.

4.2.2.2 Containment Volume

The containment volume inputs required by GOTHIC are given in Table 4.17.

Table 4.17: OSU Test Facility Containment Volume Input Dimensions

Parameter	Value
Height	5.65 m
Elevation	0.8 m
Fluid Volume	0.5236 m^3
Hydraulic Diameter	2.18 m

The Containment volume is subdivided using a linear orthogonal mesh. There are 27 cells in the vertical direction, and a 3X3 grid of cells at each vertical plane. The resulting volume of each cell is 1.14E-3 m^3, with a total of 459 cells.

4.2.2.3 ADS Sparger Volume

The ADS sparger volume inputs required by GOTHIC are given in Table 4.18.

Table 4.18: OSU Test Facility ADS Sparger Volume Input Dimensions

Parameter	Value
Height	0.0224 m
Elevation	1.34 m
Fluid Volume	4.6E-4 m^3
Hydraulic Diameter	0.0224 m

The ADS sparger volume is subdivided using a linear orthogonal mesh. There is only 1 cell in the vertical direction, and a 3X3 grid in that plane. The resulting volume of each cell is 5.1E-5 m^3, with a total of 9 cells.

4.2.3 Conductors

Only the containment vessel conductor is used in this model. Since the RX/SG vessel does not sit within the containment, there is no thermal interaction except through the connected piping.

The containment conductor has the same material properties, thickness, noding, and boundary conditions as that used in the full scale model. The only difference here is the surface area, and number of conductors. In the test facility heat transfer will only be through a single plate, and only one conductor is used in the GOTHIC model. It is still broken up into the vapor and liquid sections, but only spans one wall, as in the actual test facility. The surface area of the vapor section is 0.5713 m^2, and the liquid section is 0.38 m^2.

4.2.4 Flow Paths

The flow paths used in this model represent the same safety systems as in the full scale model. This includes the steam vent lines, submerged ADS lines, and the ADS sparger holes.

4.2.4.1 Steam Vent Lines

The steam vent lines come out of the top of the RX/SG vessel and vent into the containment. The appropriate input data required for GOTHIC is given in Table 4.19.

Table 4.19: OSU Test Facility Steam Vent Line Input Dimensions

Parameter	Value
Pipe Flow Area	1.3E-4 m^2
RX/SG Connection Height	5.3 m
Containment Exit Height	5.3 m
Hydraulic Diameter	0.0127 m
Relative Roughness	3.5E-4
Exit Loss Coefficient	2.78
Length	0.5 m

The values of relative roughness, and loss coefficient are the same as the full scale facility because the materials and physics are the same. The same momentum transport option (N&T) is used along with the table lookup choked flow model. The vent lines connect to opposite sides of the top of the RX/SG vessel. They then exit into opposite sides of the containment at an elevation of 5.3 m. The location of the exits with respect to the grid is the same as shown in Figure 4.6.

4.2.4.2 Submerged ADS Lines

The submerged ADS lines connect the RX/SG to the ADS sparger. These lines have the exact same flow area, relative roughness, and hydraulic diameter as the steam vent lines. They also use the same momentum transport and choked flow options. The only differences are the elevations and exit loss coefficients. This data is given Table 4.20

Table 4.20: OSU Test Facility Submerged ADS Line Input Dimensions

Parameter	Value
RX/SG Connection Elevation	2.34 m
ADS Sparger Connection Elevation	1.34 m
Exit Loss Coefficient	1.0
Length	0.5 m

The submerged ADS lines connect to a tee with a single penetration of the RX/SG vessel at an elevation 2.43 m. They then connect to the ADS sparger as shown in Figure 4.23.

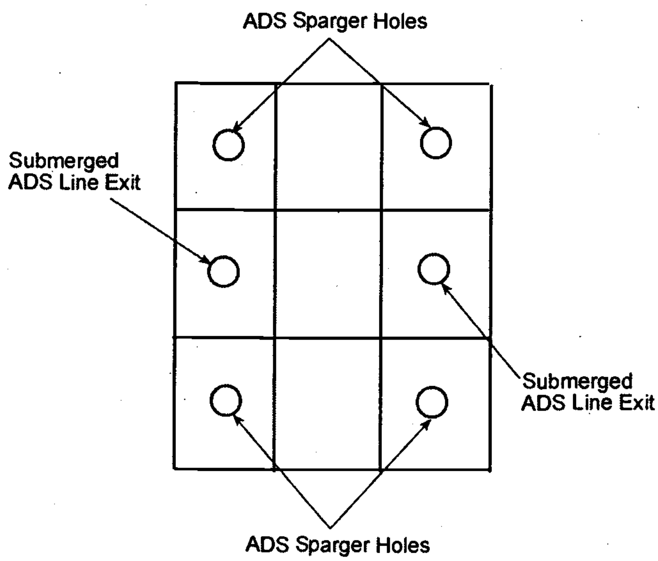

Figure 4.23: ADS Sparger Flow Path Connections

4.2.4.3 ADS Sparger Holes

The holes in the ADS sparger are too many to model in GOTHIC. As a result the total flow area has been preserved using only 4 flow paths. The appropriate GOTHIC input data for these flow paths is given in Table 4.21.

Table 4.21: OSU Test Facility ADS Sparger Hole Input Dimensions

Parameter	Value
Sparger Connection Elevation	1.34 m
Containment Exit Elevation	1.34 m
Flow Area	3.5E-5 m^2
Hydraulic Diameter	0.00127 m
Exit Loss Coefficient	2.78
Relative Roughness	3.5E-4
Length	0.0127 m

The placement of the flow path entrances for the ADS sparger holes is shown in Figure 4.23. The corresponding exit location in the containment is the same as in the full scale model, except for the elevation. The placement of the exits in the grid is shown in Figure 4.8.

4.2.5 Valves

The valves used in the GOTHIC model represent the 0.5 inch Schwagelock valves used for the steam vent system, and submerged ADS system. Valves are also used to represent the 0.094 inch orifice that is in the steam vent lines, since GOTHIC does not include a component to model orifice plates.

4.2.5.1 Steam Vent Valves

The steam vent valves are 0.5 inch Schwagelock valves. To define a valve GOTHIC requires the valve flow area, loss coefficient curve, and the valve type. For all the valves used in the model the type is "Quick Open" meaning that the travel time for the valve stem is zero. As a result the loss coefficient curve only needs two data points. The first is the loss when the valve is shut, which is an arbitrary number of the order 1E6. The second is the loss when the valve is completely open which has value of 38.8. The flow area for the valve is 1.3E-4 m^2. The valves require trips to open. The trips can be triggered on time or volume variables such as pressure, temperature, or level. The steam vent line open trip is triggered on time equal to 1 second, since the transient tests all begin with an inadvertent opening of a steam vent valve. For purposes of analysis once the valves open they are assumed to remain open throughout the transient.

4.2.5.2 Submerged ADS Valves

The submerged ADS valves are the same as the steam vent valves, except for the trip used to actuate them. For these valves, the open trip is on pressure. The set point is 500 kPa in containment with a 0.5 second delay. This trip was obtained from the MASLWR RELAP 5 safety system logic provided by Jim Fisher from INEEL. For purposes of analysis, once the valves open they are assumed to remain open throughout the transient.

4.2.5.3 Steam Vent Line Orifice

GOTHIC does not provide a component to model an orifice plate within a flow path. The steam vent line has a 0.094 inch orifice within the flow path. As a result this orifice is modeled using a valve. The valve flow area is 1.8E-5 m^2. A loss coefficient can be calculated, but is far too large due to the pipe-to-orifice diameter ratios. We assume that some type of flow nozzle will be built that has the correct flow area, but with a loss coefficient equal to that of the full scale 3 inch orifice (2.25). The valve type is "Quick Open", and uses the same trip as the steam vent valves.

4.2.6 Heat Exchangers

To model the interaction of the core and the associated decay power with the system during a transient a heater was used. The steam generator was not modeled assuming that once an accident is initiated the feed water is secured and the steam generator no longer participates thermally.

To model the decay heat released after a reactor SCRAM, a heater was added to the transient model. This heater only supplies heat to the liquid phase within the RX/SG vessel. The inputs required for GOTHIC are a heat rate and heat rate forcing function. The heat rate is multiplied by the forcing function to obtain the heat supplied by the heater. The forcing function in this case represents the decay power curve derived from the Light Water Reactor Decay Heat Power Standard [21]. The calculated values are shown in Table 4.22.

Table 4.22: OSU Test Facility Decay Power Curve

Time After SCRAM	Power
1 second	36.92 kW
10 seconds	28.39 kW
100 seconds	18.41 kW
1000 seconds	11.15 kW
10000 seconds	5.46 kW

The decay power heater is located at an elevation of 1.2 m, which is in the lower section of the core. It could not be placed in the center cell since it is a 2X2 grid, so it was placed on the opposite side of the submerged ADS lines.

4.2.7 Initial Conditions

The initial conditions for the OSU test facility model are identical to the full-scale transient model. [See Section 4.1.2.7.1]

4.2.8 Run Controls

The run controls for the OSU test facility model are identical to those used in the full scale transient model. [See Section 4.1.2.8]

4.2.9 Results

Four sets of simulations were completed for the OSU test facility model. The simulations were of the same two accident scenarios as in the full scale transient model. The first, Case 1, is an inadvertent steam vent valve opening with a sump system failure. The second, as Case 2, is an inadvertent vent valve opening with a sump system failure, and a single submerged ADS failure. Both cases were solved using both the Gido/Koestel and Uchida condensation models.

4.2.9.1 Case 1 Results

Case 1 was run on an Intel Pentium 4 1.4 GHz PC for a period of 3.5 days for each simulation. The results for the Gido/Koestel condensation model include a time integrated mass error of -5.1 % and an energy error of -7.041%. The results for the Uchida condensation model include a time integrated mass error of -7.175% and an energy error of -10.09%. The error associated with the both models remained below 1% until after the pressure between the containment and RX/SG vessel were equalized. The suspected cause of the errors is the code's difficulty in predicting low flows dominated by very small pressure differences and gravity. Every effort was made to reduce these errors, including refining and coarsing meshes, and using different numerical discretizations and solution techniques.

The timeline of events for Case 1 are given in Table 4.23.

Table 4.23: Case 1 OSU Test Facility Event Time Line

Event	Uchida Time (sec)	Gido/Koestel Time (sec)
Inadvertent Steam Vent Valve Opening	1	1
Submerged ADS Triggered	45	65
Peak Containment Pressure Achieved	185	230
RX/SG Reflood (if occurred)	NA	NA
End of Transient	1500	1500

From the timeline it appears that everything after the initiation of the transient occurred sooner with the Uchida Condensation model similar to the full scale results. The cause of this is the calculated wall heat transfer coefficients within the vapor region. The heat transfer coefficient plotted in Figure 4.25 show that the Uchida correlation reached its upper bound of 1.578 kW/m^2-°C (278 BTU/hr-ft^2-°F), imposed by the correlation form used in GOTHIC, very rapidly. The Gido/Koestel model has no such limitations, the resulting heat transfer coefficient is 16.16 kW/m^2-°C (2846 BTU/hr-ft^2-°F), an order of magnitude greater than the Uchida model. The higher heat transfer coefficient means more condensation and an increased period of time until the submerged ADS actuation pressure is achieved. The magnitude of Gido/Koestel heat transfer coefficient is smaller than in the full scale facility. This is attributed to the length of the conductor. In the correlation given in Equation 2.33 the heat transfer coefficient is a function of length. This will introduce a scaling distortion since we are not at full length scale. The peak pressures are 424 psia (2.923 MPa), and 389 psia (2.682 MPa) for the Uchida and Gido/Koestel simulations respectively [See Figure 4.24].

The flow rates through the safety system lines are relatively close for the two condensation models as seen in Figure 4.26 –4.31.

During the simulation neither the Uchida simulation nor the Gido/Koestel simulation predicted reflood.

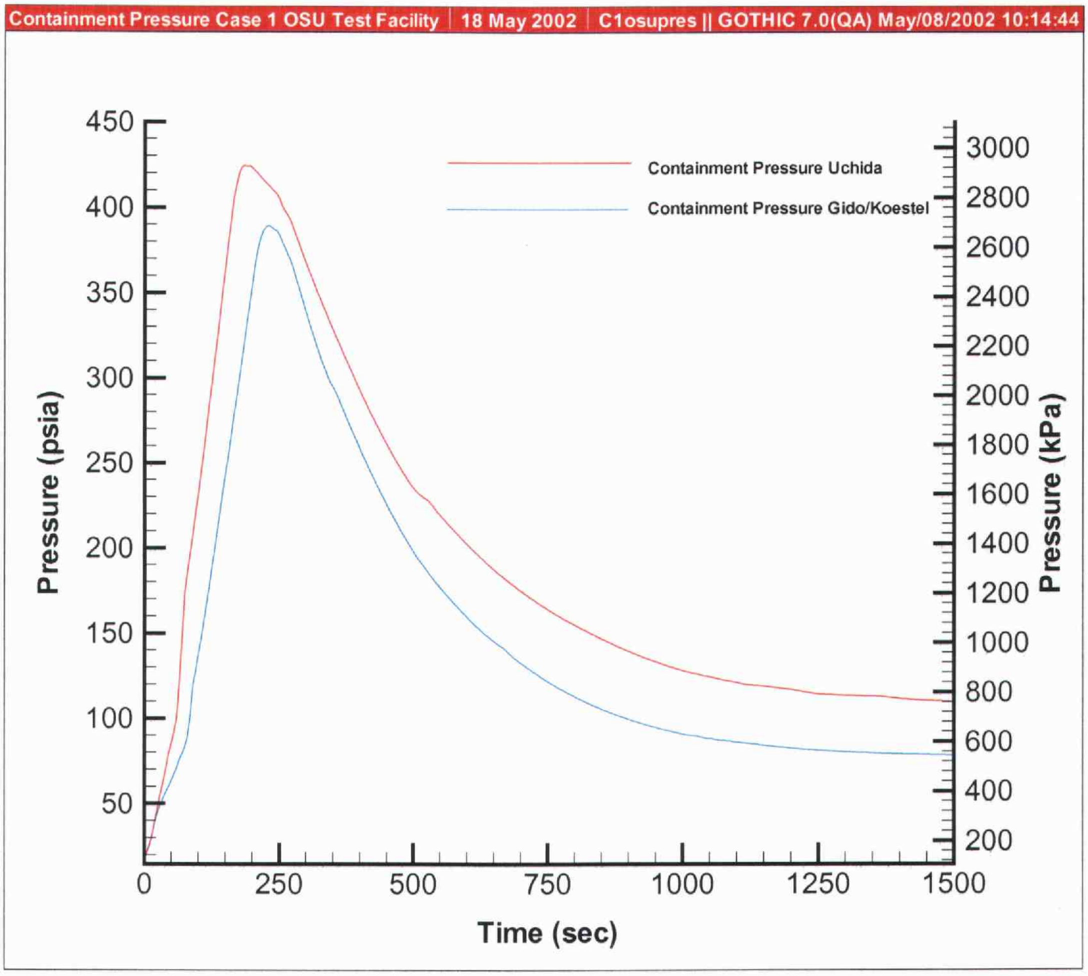

Figure 4.24: Case 1 OSU Test Facility Containment Pressure

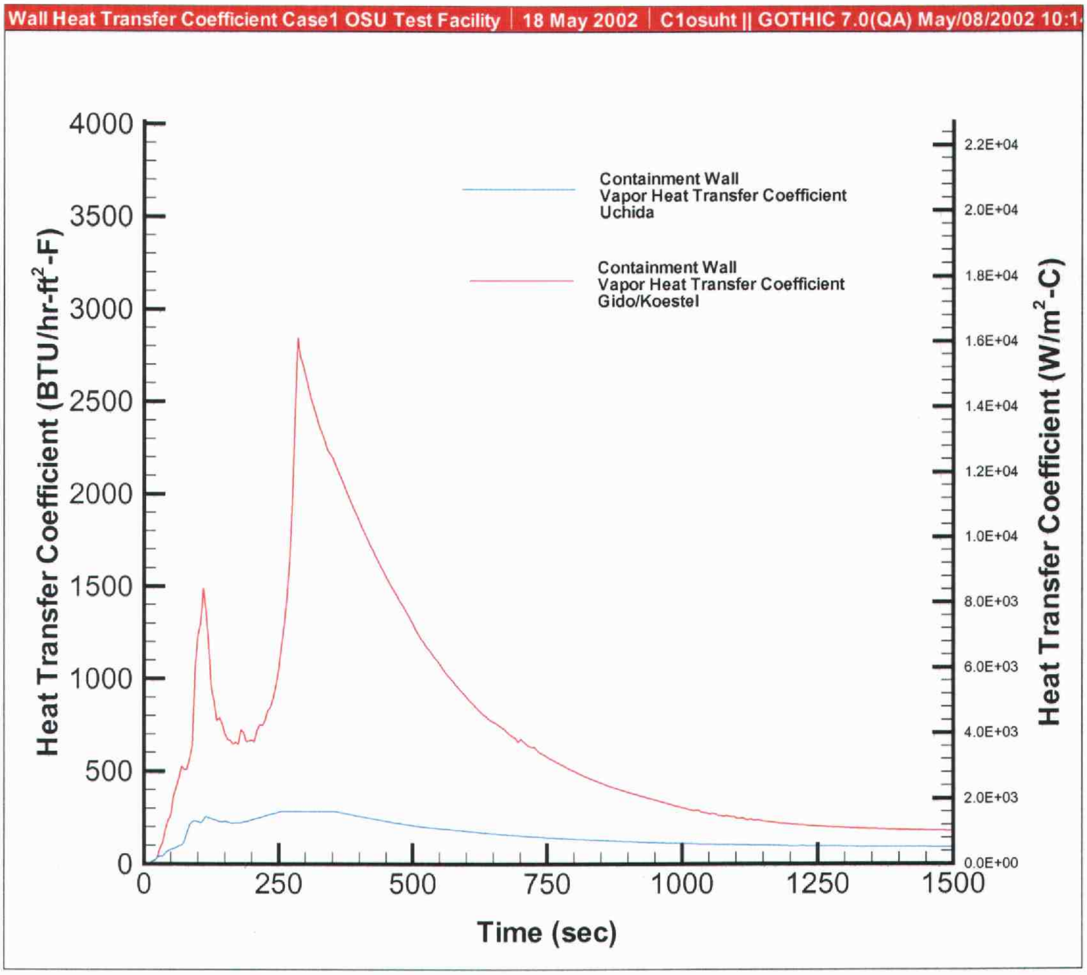

Figure 4.25: Case 1 OSU Test Facility Wall Heat Transfer Coefficients

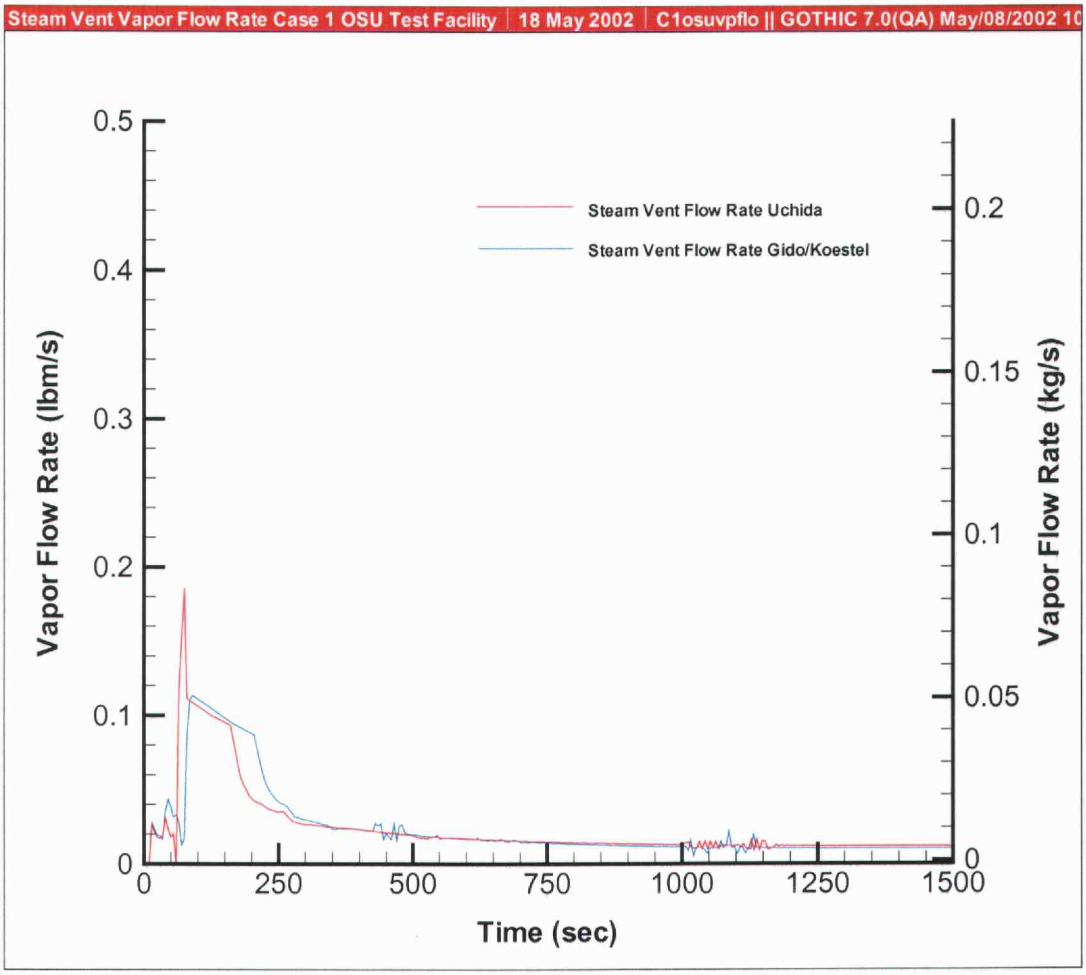

Figure 4.26: Case 1 OSU Test Facility Steam Vent Vapor Flow Rate

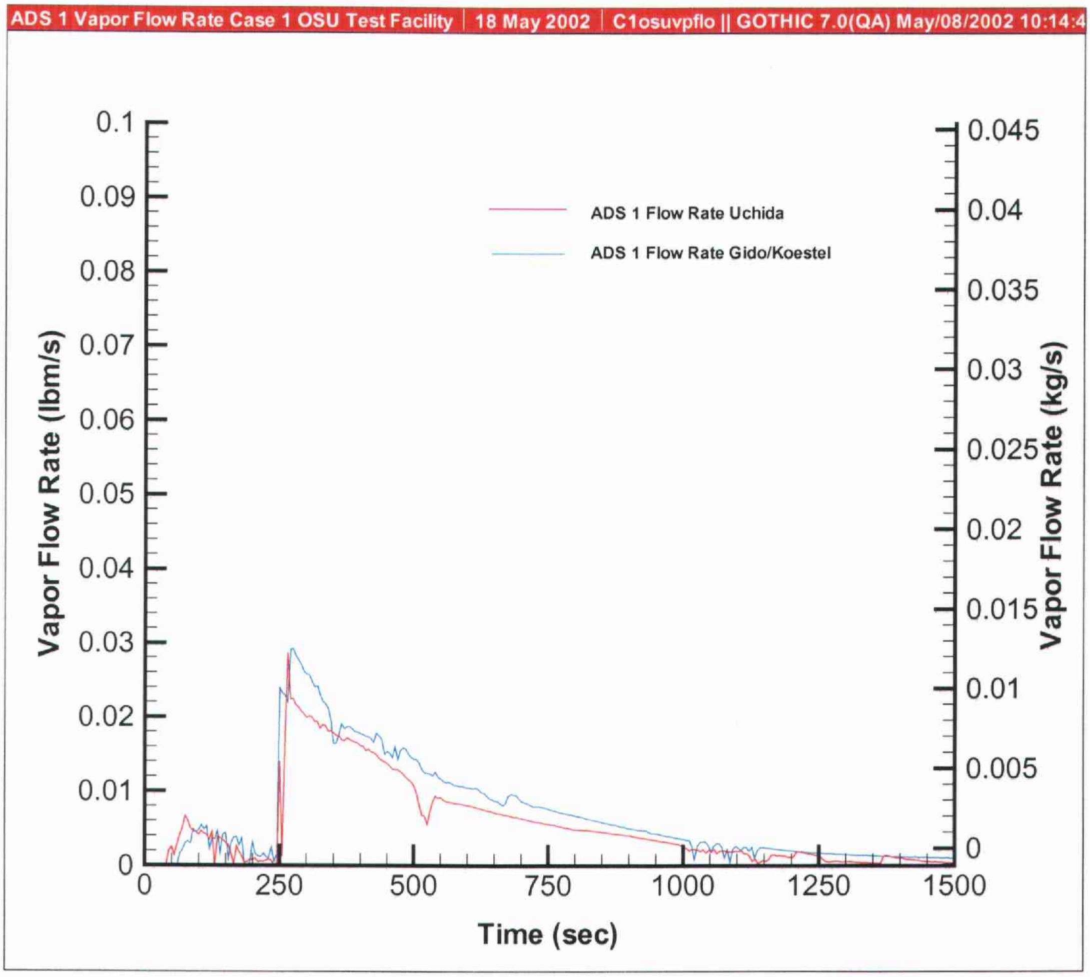

Figure 4.27: Case 1 OSU Test Facility Submerged ADS 1 Vapor Flow Rate

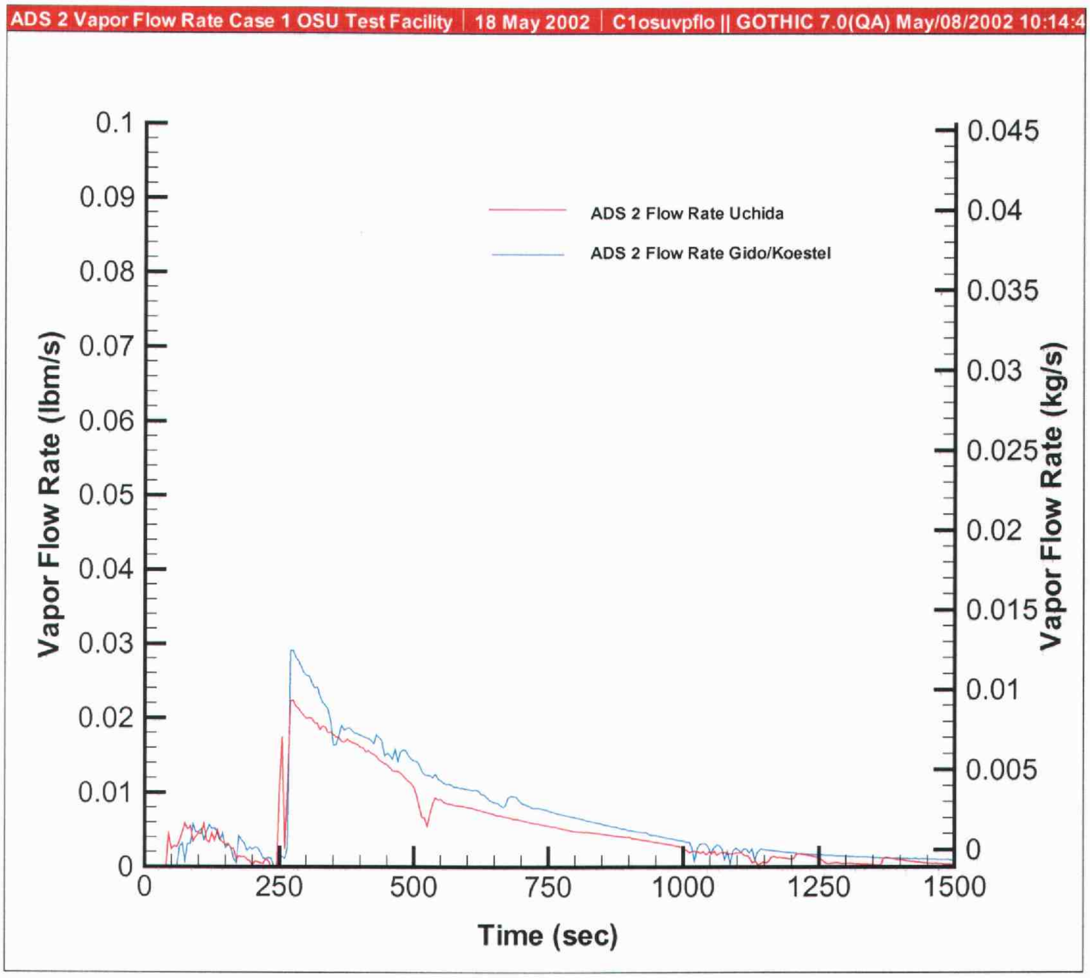

Figure 4.28: Case 1 OSU Test Facility Submerged ADS 2 Vapor Flow Rate

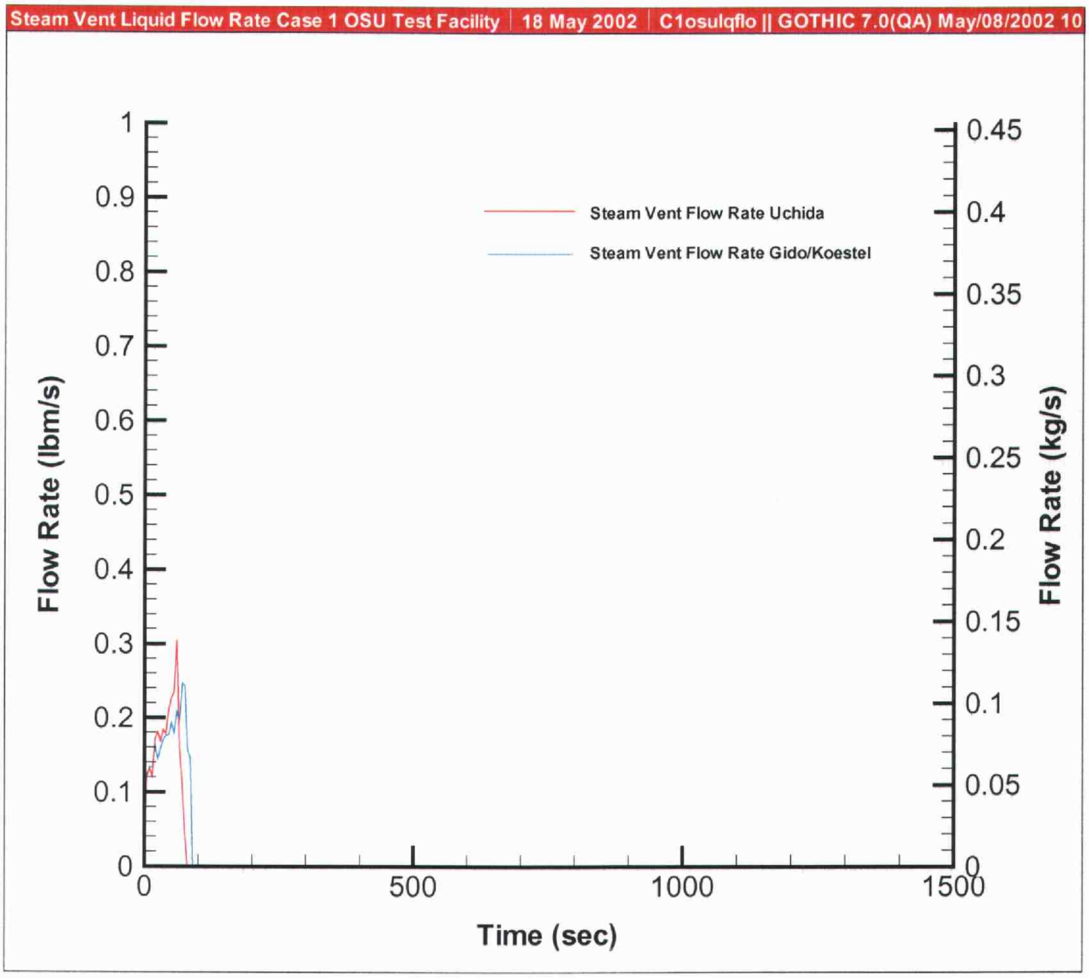

Figure 4.29: Case 1 OSU Test Facility Steam Vent Liquid Flow Rate

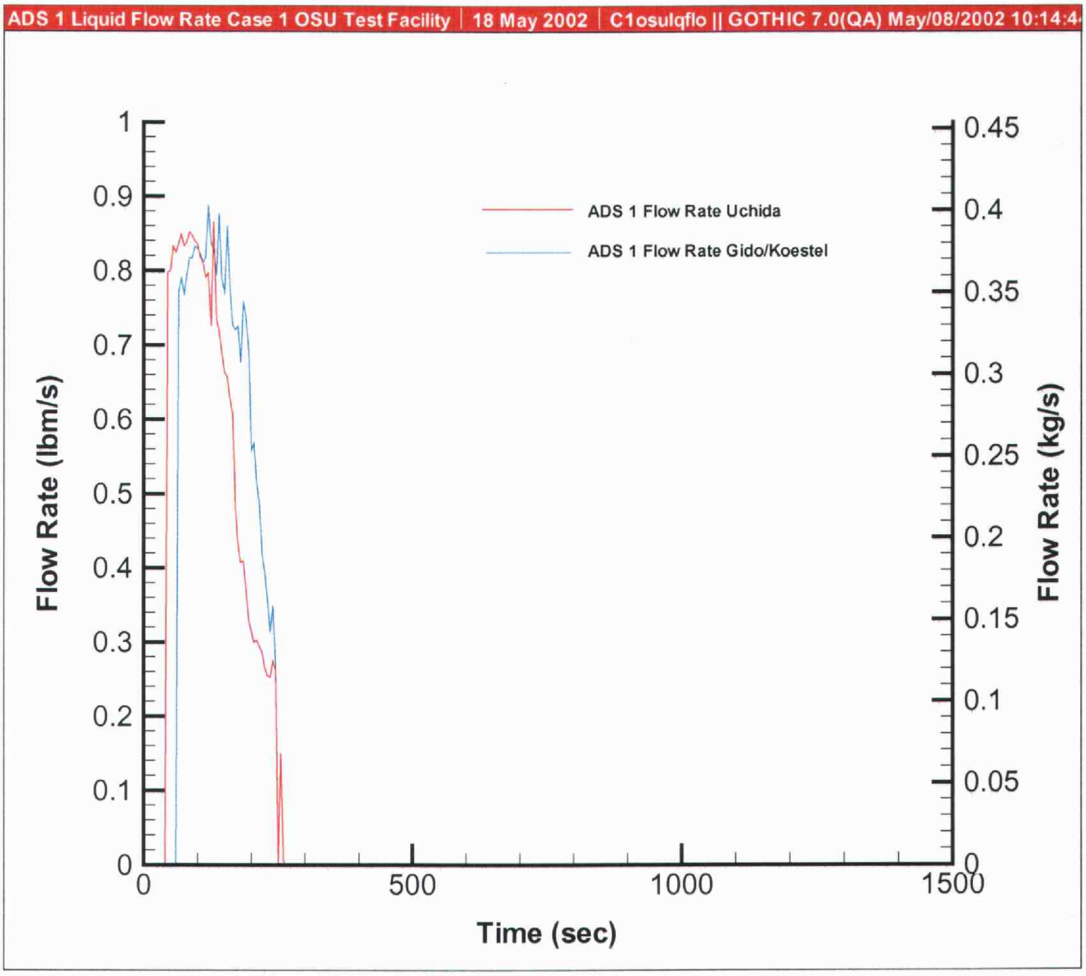

Figure 4.30: Case 1 OSU Test Facility Submerged ADS 1 Liquid Flow Rate

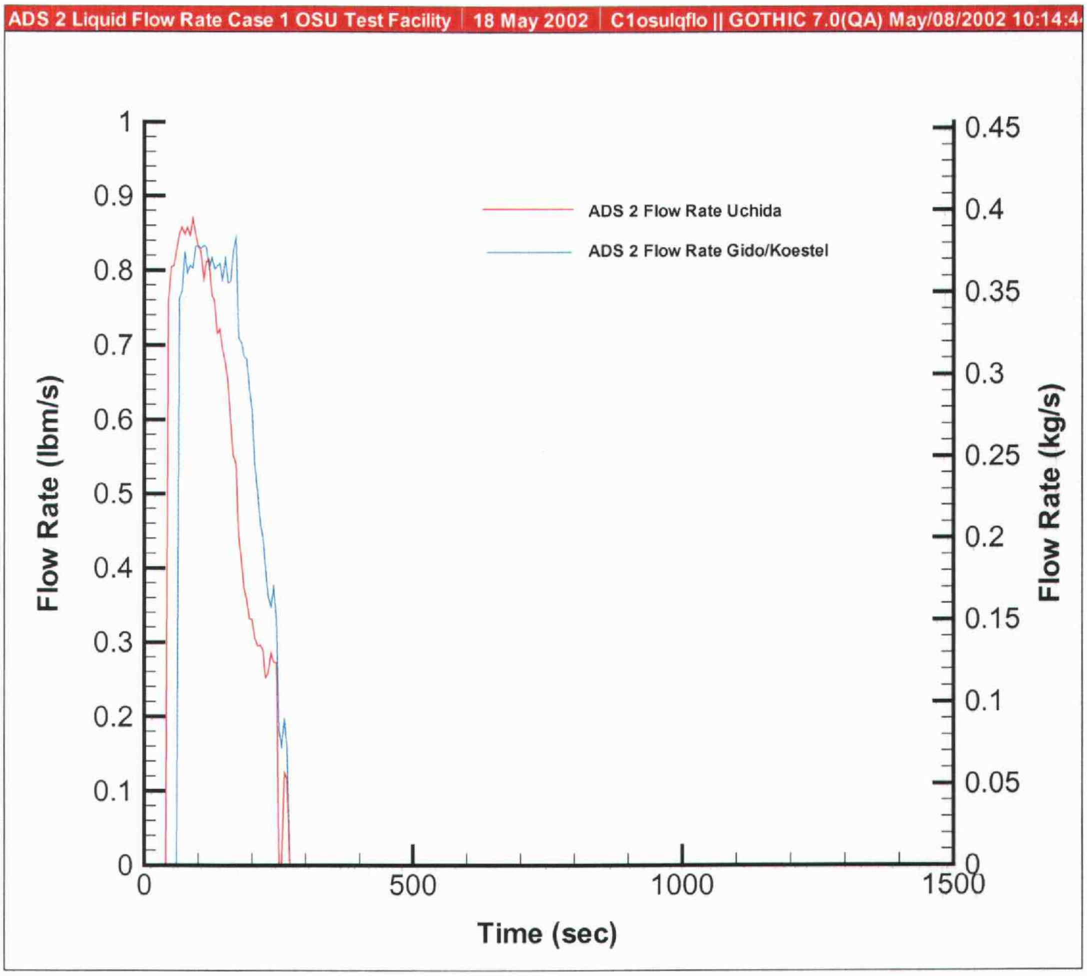

Figure 4.31: Case 1 OSU Test Facility Submerged ADS 2 Liquid Flow Rate

4.2.9.2 Case 2 Results

Case 2 was run on an Intel Pentium 4 1.4 GHz PC for a period of 3.5 days for each simulation. The results for the Gido/Koestel condensation model include a time integrated mass error of -0.40% and an energy error of -0.738%. The results for the Uchida condensation model include a time integrated mass error of -1.155% and an energy error of -1.747%. The error associated with the both models occurred after the pressure between the containment and RX/SG vessel equalized. The suspected cause of the errors is the code's difficulty in predicting low flows dominated by very small pressure differences and gravity. Every effort was made to reduce these errors, including refining and coarsing meshes, and using different numerical discretizations and solution techniques.

The timeline of events for Case 2 are given in Table 4.24.

Table 4.24: Case 2 OSU Test Facility Event Time Line

Event	Uchida Time (sec)	Gido/Koestel Time (sec)
Inadvertent Steam Vent Valve Opening	1	1
Submerged ADS Triggered	45	65
Peak Containment Pressure Achieved	225	280
RX/SG Reflood (if occurred)	NA	NA
End of Transient	325	582

From the timeline it appears that everything after the transient was initiated occurred sooner with the Uchida Condensation, model similar to the Case 1 results. The cause of this is the calculated wall heat transfer coefficients within the vapor region. The heat transfer coefficient plotted in Figure 4.33 show that the Uchida correlation reached its upper bound of 1.578 kW/m^2-°C (278 BTU/hr-ft^2-°F), imposed by the correlation form used in GOTHIC, very rapidly. The Gido/Koestel model has no such limitations, and the resulting heat transfer coefficient is 17.71 kW/m^2-°C (3118.7 BTU/hr-ft^2-°F), an order of magnitude greater than the Uchida model. The higher heat transfer coefficient means more condensation and an increased period of time until the submerged ADS actuation pressure is achieved. The increased condensation also results in a reduced peak pressure within the containment, as seen in Figure 4.32. The peak pressures are 427 psia (2.944 MPa), and 387 psia (2.668 MPa) for the Uchida and Gido/Koestel simulations, respectively.

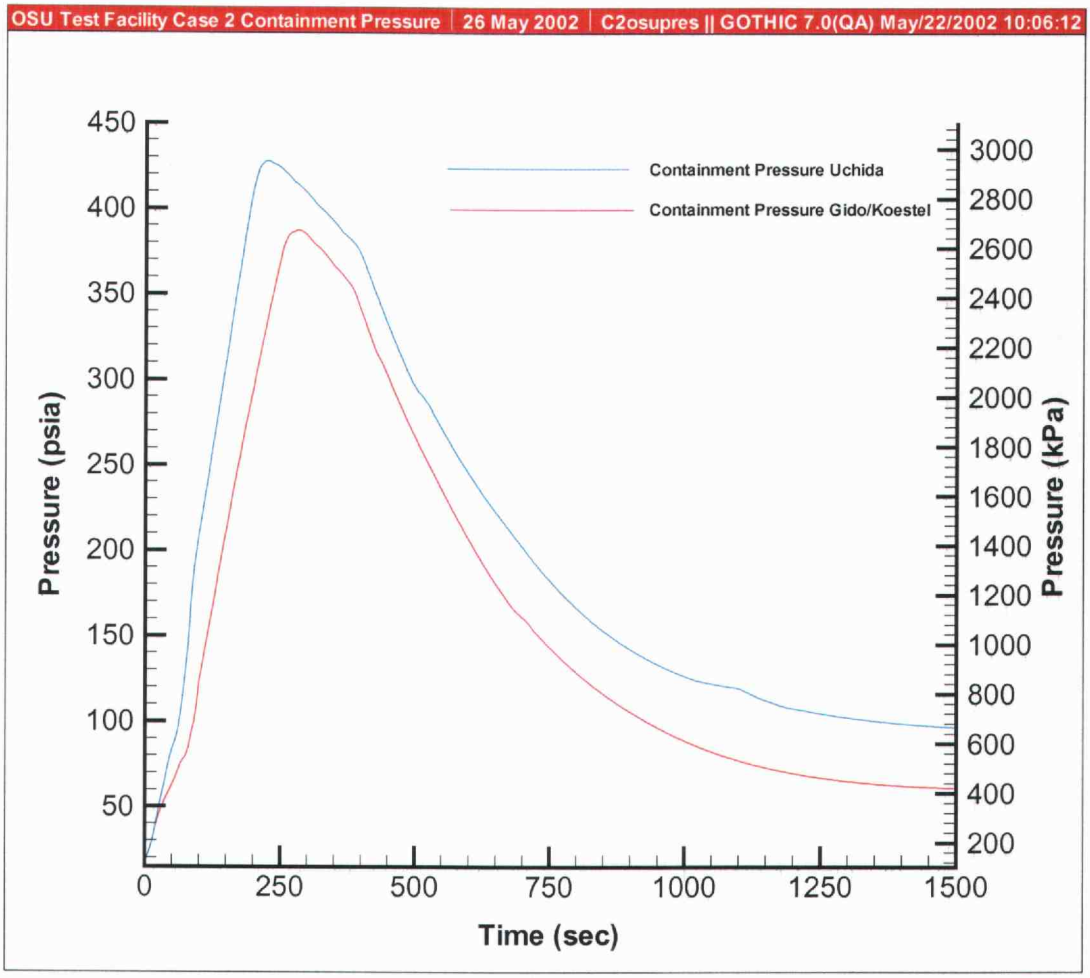

Figure 4.32: Case 2 OSU Test Facility Containment Pressure

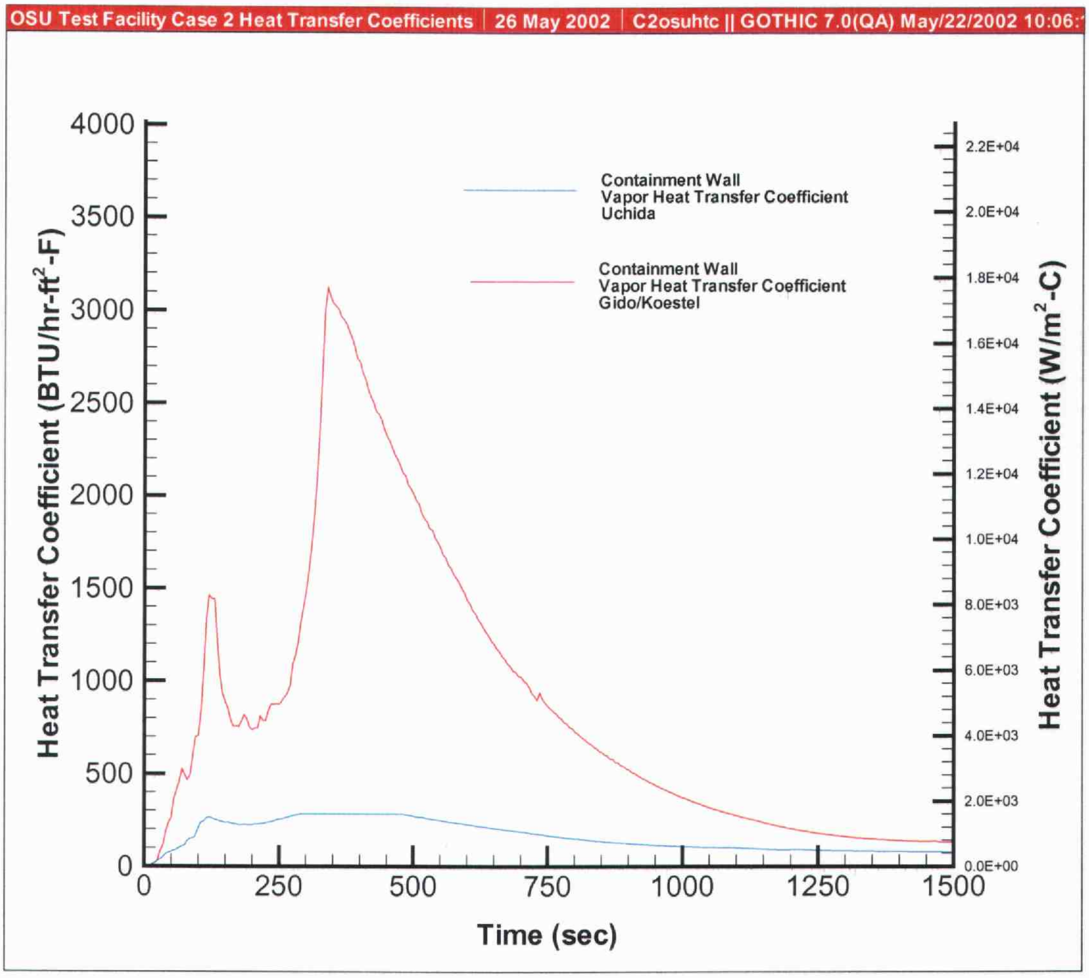

Figure 4.33: Case 2 OSU Test Facility Wall Heat Transfer Coefficients

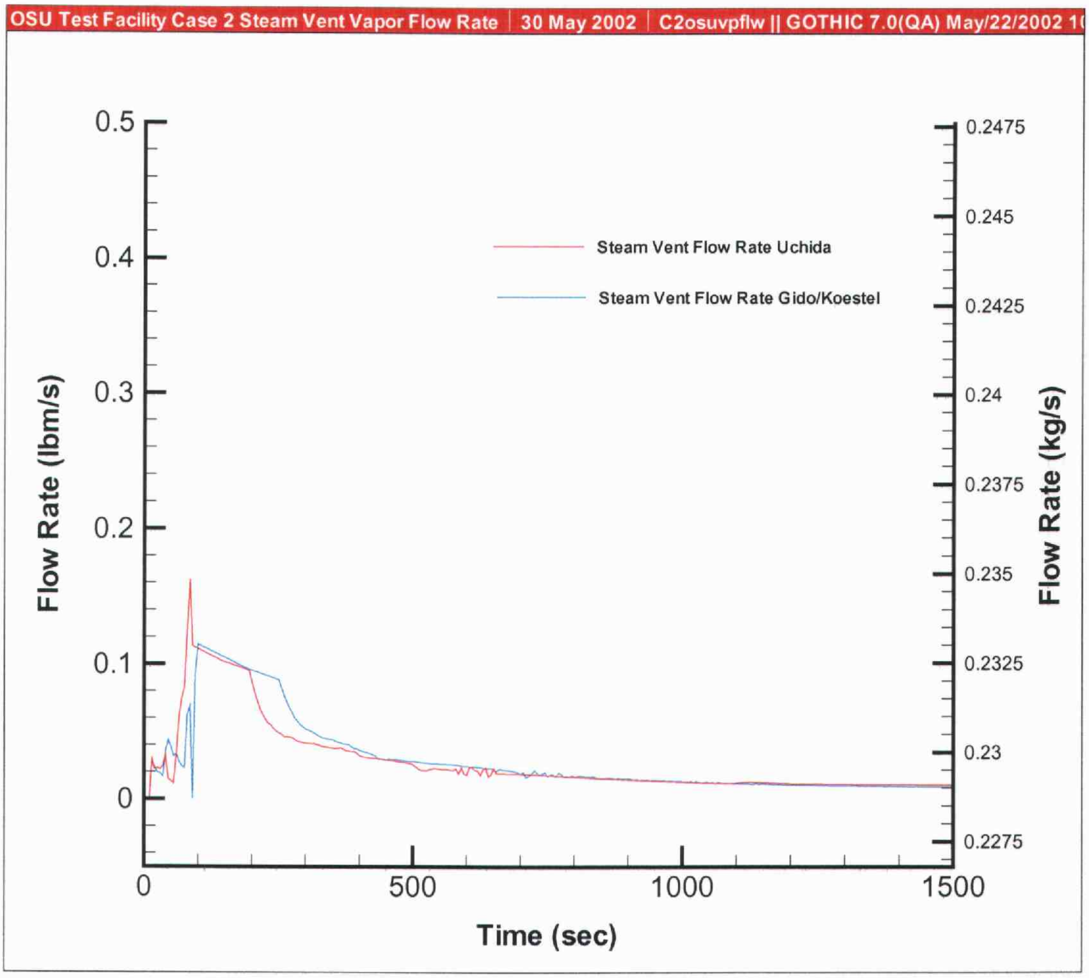

Figure 4.34: Case 2 OSU Test Facility Steam Vent Vapor Flow Rate

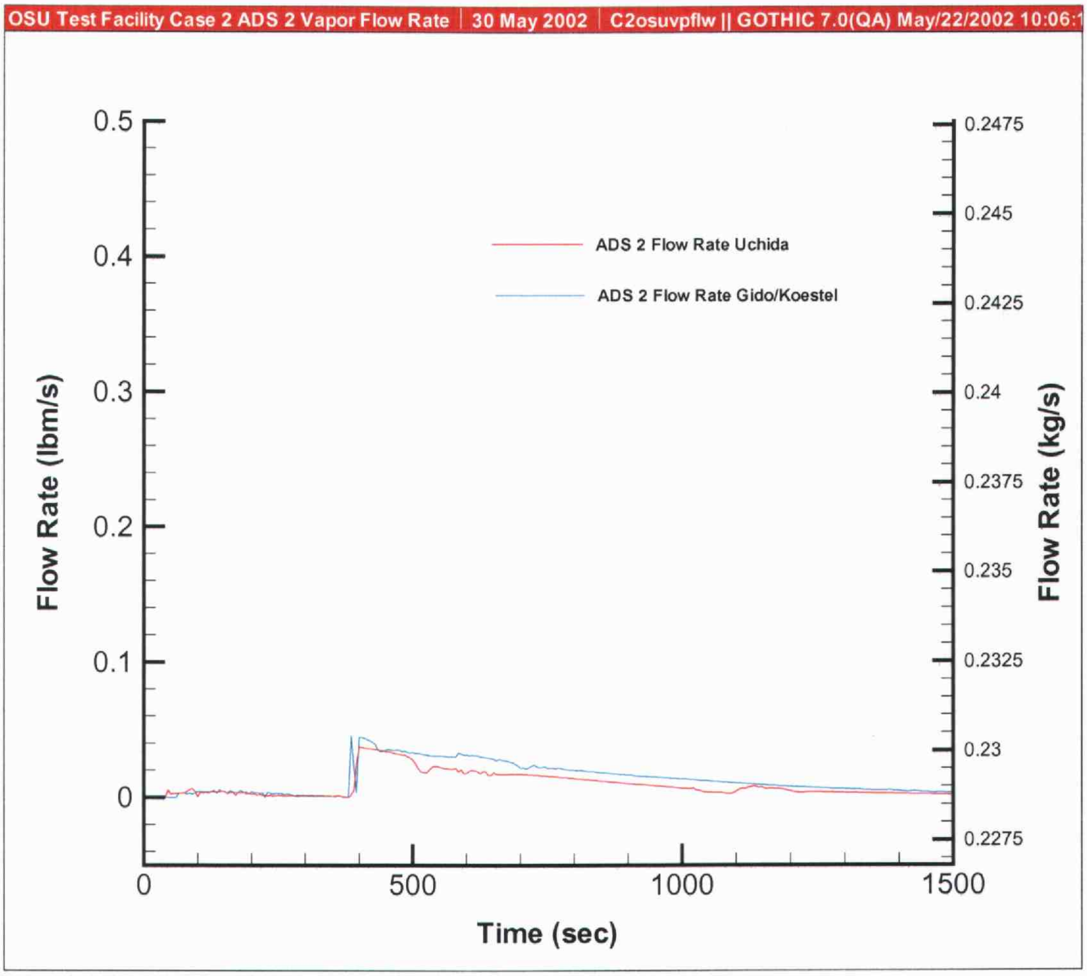

Figure 4.35: Case 2 OSU Test Facility Submerged ADS 2 Vapor Flow Rate

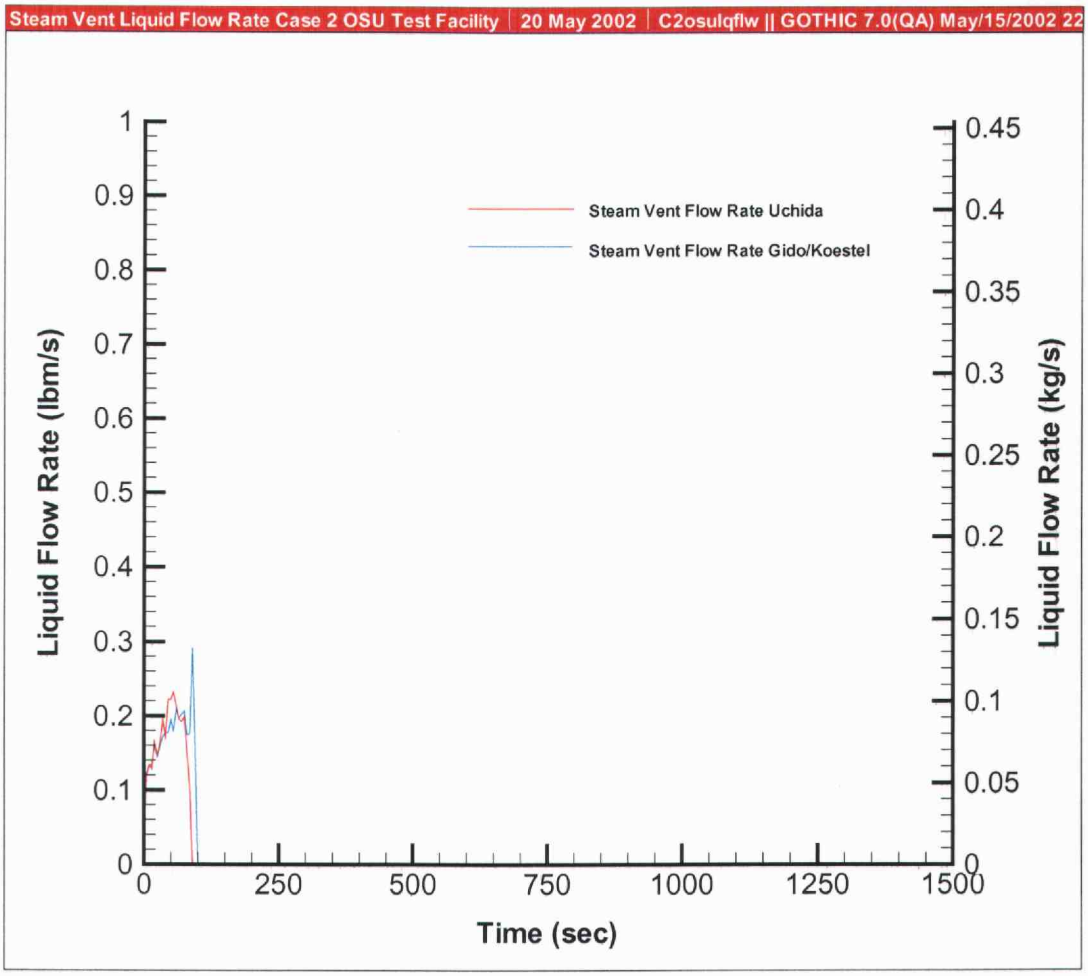

Figure 4.36: Case 2 OSU Test Facility Steam Vent Liquid Flow Rate

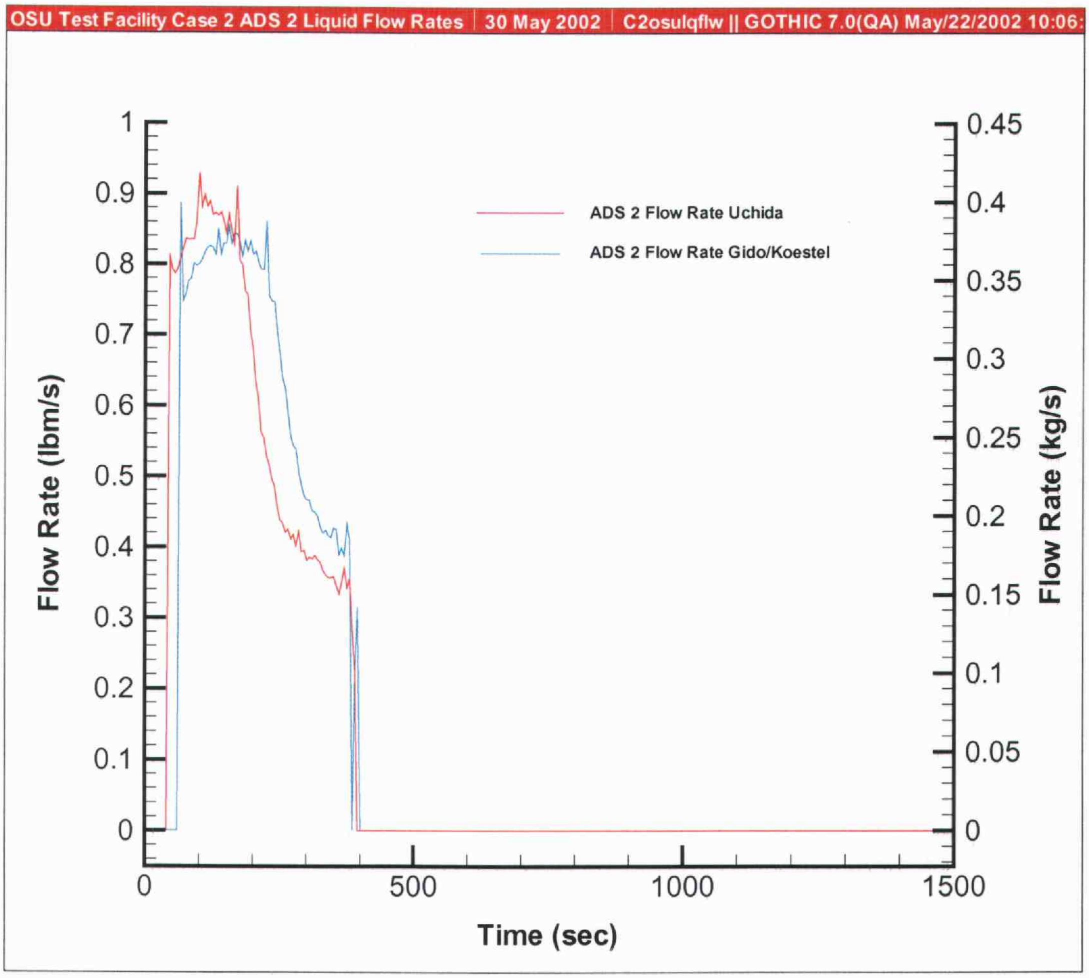

Figure 4.37: Case 2 OSU Test Facility Submerged ADS 2 Liquid Flow Rate

4.3 Calculation Comparisons

In this section the calculations from both the full scale prototype and test facility model will be compared. This should give some estimate of how well the pressurization rate, peak pressure, heat transfer, and flow rates are preserved between models. The comparison for the Uchida condensation model is shown in Table 4.25.

Table 4.25: Uchida Condensation Model Result Comparison

Uchida Condensation Model	Full Scale Case 1	OSU Test Facility Case 1	Full Scale Case 2	OSU Test Facility Case 2
Submerged ADS Triggered	59.5 sec	45 sec	60.3 sec	45 sec
Time to Peak Pressure	213 sec	185 sec	245 sec	225 sec
Containment Peak Pressure	350 psia 2.413 MPa	424 psia 2.923 MPa	408 psia 2.813 MPa	427 psia 2.944 MPa
Maximum HTC	278 BTU/hr-ft^2-°F 1.578 kW/m^2-°C	278 BTU/hr-ft^2-°F 1.578 kW/m^2-°C	278 BTU/hr-ft^2-°F 1.578 kW/m^2-°C	278 BTU/hr-ft^2-°F 1.578 kW/m^2-°C
Steam Vent Vapor Flow Rate Peak	29 lb_m/s 13.15 kg/s	0.17 lb_m/s 0.077 kg/s Scaling Adjusted 43.13 lb_m/s 19.56 kg/s	29 lb_m/s 13.15 kg/s	0.12 lb_m/s 0.054 kg/s Scaling Adjusted 30.44 lb_m/s 13.81 kg/s
Submerged ADS Vapor Flow Rate	16 lb_m/s 7.26 kg/s	0.023 lb_m/s 0.0104 kg/s Scaling Adjusted 5.84 lb_m/s 2.65 kg/s	7 lb_m/s 3.17 kg/s	0.03 lb_m/s 0.0136 kg/s Scaling Adjusted 7.62 lb_m/s 3.45 kg/s
Steam Vent Liquid Flow Rate Peak	40 lb_m/s 18.14 kg/s	0.27 lb_m/s 0.122 kg/s Scaling Adjusted 68.5 lb_m/s 31.07 kg/s	55 lb_m/s 24.95 kg/s	0.23 lb_m/s 0.104 kg/s Scaling Adjusted 58.4 lb_m/s 26.49 kg/s
Submerged ADS Liquid Flow Rate	220 lb_m/s 99.79 kg/s	0.86 lb_m/s 0.390 kg/s Scaling Adjusted 218.18 lb_m/s 98.97 kg/s	200 lb_m/s 90.72 kg/s	0.88 lb_m/s 0.399 kg/s Scaling Adjusted 223.26 lb_m/s 101.27 kg/s

The table shows the time scales are shifted for both cases, with the test facility model responding 15 seconds faster. There also is an increase in peak pressure for the test facility of 74 psia (0.5102 MPa) for Case 1.

In all the Uchida model simulations the heat transfer coefficients reached the upper bound for the correlation, so not much comparison can be made.

The comparison for the Gido/Koestel condensation model is shown in Table 4.26.

Table 4.26: Gido/Koestel Condensation Model Result Comparison

Gido/Koestel Condensation Model	Full Scale Case 1	OSU Test Facility Case 1	Full Scale Case 2	OSU Test Facility Case 2
Submerged ADS Triggered	105 sec	65 sec	105 sec	65 sec
Time to Peak Pressure	271 sec	230 sec	280 sec	280 sec
Containment Peak Pressure	290 psia 1.999 MPa	389 psia 2.682 MPa	328 psia 2.261 MPa	387 psia 2.668 MPa
Maximum HTC	5800 BTU/hr-ft^2-°F 32.93 kW/m^2-°C	2846 BTU/hr-ft^2-°F 16.16 kW/m^2-°C	4013 BTU/hr-ft^2-°F 22.79 kW/m^2-°C	3118.7 BTU/hr-ft^2-°F 17.71 kW/m^2-°C
Steam Vent Vapor Flow Rate Peak	36 lb_m/s 16.33 kg/s	0.115 lb_m/s 0.052 kg/s Scaling Adjusted 29.17 lb_m/s 13.23 kg/s	35 lb_m/s 15.88 kg/s	0.12 lb_m/s 0.054 kg/s Scaling Adjusted 30.44 lb_m/s 13.81 kg/s
Submerged ADS Vapor Flow Rate	20 lb_m/s 9.1 kg/s	0.3 lb_m/s 0.14 kg/s Scaling Adjusted 76.11 lb_m/s 34.52 kg/s	20 lb_m/s 9.1 kg/s	0.044 lb_m/s 0.0199 kg/s Scaling Adjusted 11.16 lb_m/s 5.06 kg/s
Steam Vent Liquid Flow Rate Peak	37 lb_m/s 16.78 kg/s	0.25 lb_m/s 0.1134 kg/s Scaling Adjusted 63.42 lb_m/s 28.77 kg/s	45 lb_m/s 20.41 kg/s	0.24 lb_m/s 0.109 kg/s Scaling Adjusted 60.89 lb_m/s 27.62 kg/s
Submerged ADS Liquid Flow Rate	215 lb_m/s 97.52 kg/s	0.84 lb_m/s 0.381 kg/s Scaling Adjusted 213.1 lb_m/s 96.66 kg/s	300 lb_m/s 136.1 kg/s	0.84 lb_m/s 0.381 kg/s Scaling Adjusted 213.12 lb_m/s 96.67 kg/s

This data shows a time shift similar to that in the Uchida comparison. In both cases the test facility responded 40 sec faster. Higher peak pressures were also observed in both Case 1 and Case 2 for the test facility model. For Case 1 the heat transfer coefficient in the test facility model is ½ that of the full scale prototype, resulting in the test facility model pressure 99 psia (0.683 MPa) greater than the full scale prototype. A possible explanation for this is that the Gido/Koestel condensation model takes into account the length of the conductor, which is not preserved in the test facility model. This may be a factor, but for Case 2 the values of the heat transfer coefficient are closer. In Case 2, the test facility model is only 59 psia (0.407 MPa) higher then the full scale prototype.

The comparison results show that the full scale prototype and OSU test facility model behave similarly in the transients analyzed. The OSU test facility model showed consistently more rapid response to the transients. The trend similarity and time shifts can be seen in comparison plots (Figure 4.38 and 4.39) of the submerged ADS and steam vent liquid flow rates for the Case 1 simulations.

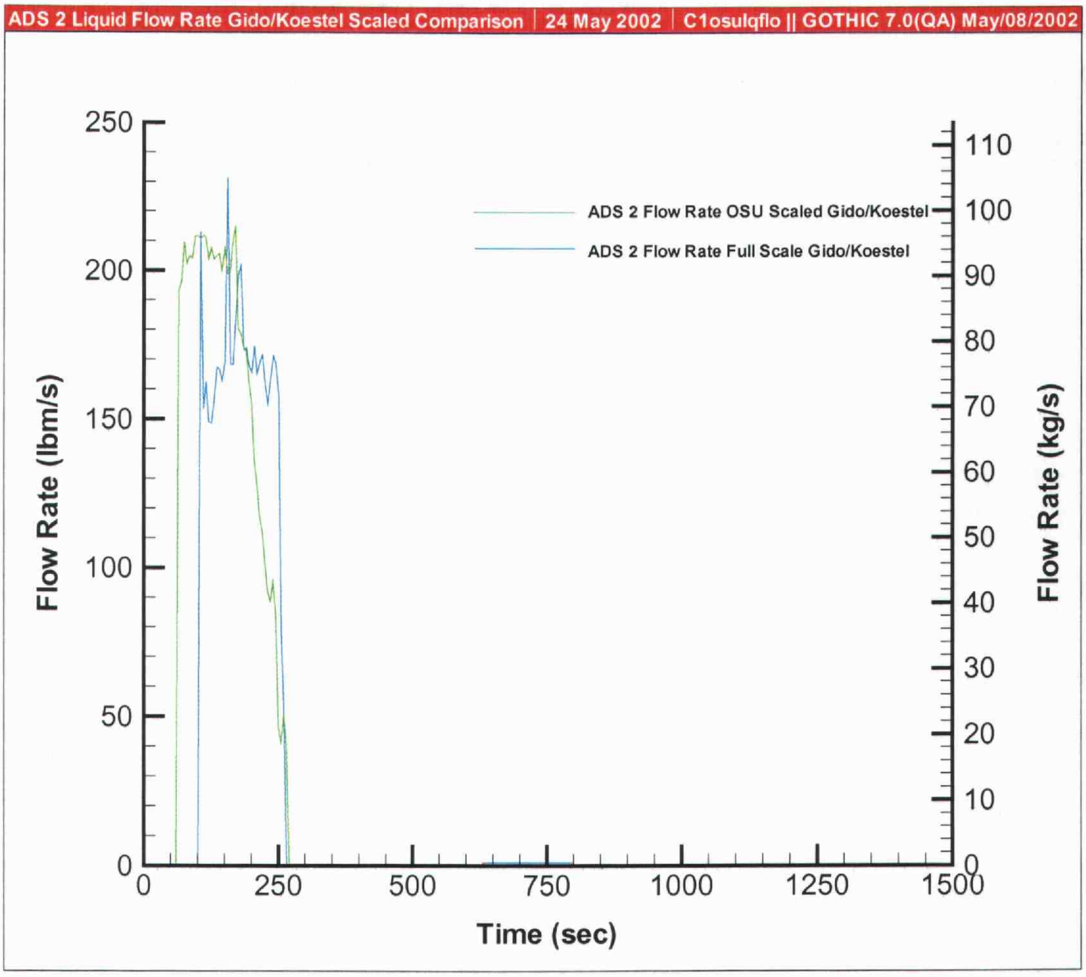

Figure 4.38: Case 1 Submerged ADS Liquid Flow Rate Comparison

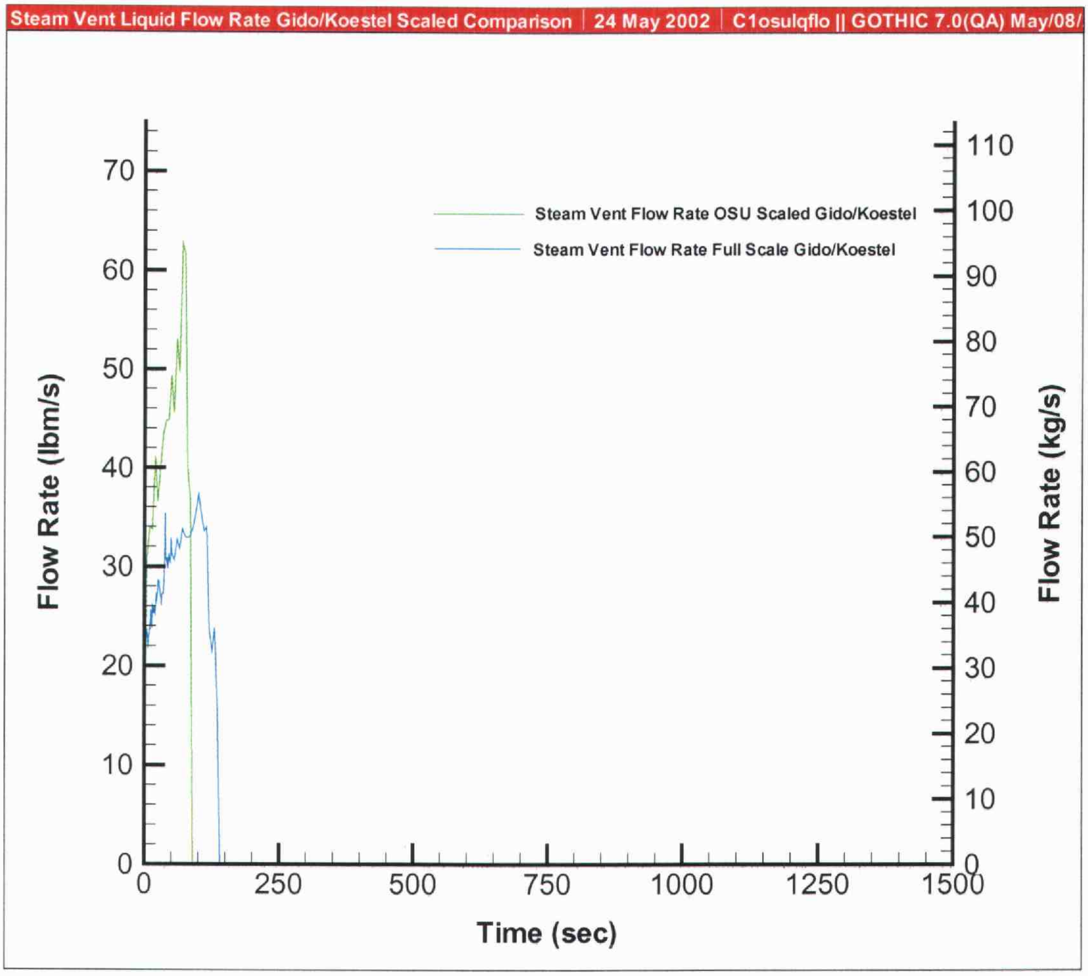

Figure 4.39: Case 1 Steam Vent Liquid Flow Rate Comparison

The comparison between the different condensation models was very interesting. The Uchida model consistently reached its upper bound of 278 BTU/hr-ft^2-^{o}F (1.578 kW/m^2-^{o}C) throughout a large part of the transient. While the Gido/Koestel model predicted heat transfer coefficients as high as 5800 BTU/hr-ft^2-^{o}F (32.93kW/m^2-^{o}C). When going from the full scale model to the test facility model, the difference in conductor length was observed in the Gido/Koestel heat transfer coefficients, suggesting that if this model is correct, then the length scale ratio of the conductor would need to be 1.

5 CONCLUSIONS

The MASLWR full scale prototype and OSU Test Facility were modeled in GOTHIC. A calculation was performed on the full scale model to establish steady-state operating parameters for the containment and to provide initial conditions for the transient analysis. Transient calculations were performed using these models for two different scenarios. The results of these simulations were presented and compared with one another. The key results of these comparisons related to the research objectives are presented here.

The bounding pressure for the MASLWR containment from the simulations calculated has been conservatively determined to be 427 psia. The OSU scaled containment shall be designed for a maximum pressure of 450 psia with a relief valve system as required by ASME code.

The Uchida condensation model consistently predicted lower condensation heat transfer coefficients, and consequently higher containment pressures than the Gido/Koestel Model. The Uchida model predicted condensation heat transfer coefficients that were an order of magnitude less than those predicted by the Gido/Koestel model. The Gido/Koestel model takes into account more of the physics of the problem and likely provides a more realistic estimate of the condensation heat transfer.

The comparison of the OSU test facility and full scale prototype MASLWR calculations revealed similar trends in thermal hydraulic behavior. The test facility containment pressures were consistently higher than the full scale predictions. This was due to the increased (i.e. greater than scaled) liquid mass flow rate through the steam vent and submerged ADS lines. The actual experiment will use an orifice to obtain the appropriate scaled liquid mass flow rates.

The work done here provided design guidance and pre-test predictions of the condensation heat transfer that should be seen in both facilities. It is important to remember that these calculations will need to be verified using the OSU experimental data.

6 FUTURE WORK

This thesis presented the predictions for the full scale prototype and OSU test facility containment thermal hydraulic behavior. Additional work will need to be performed to verify the predictions and will include the following:

- Obtain experimental test data using the OSU scaled MASLWR test facility to benchmark the GOTHIC computer code.
- Refine the current GOTHIC model for the OSU test facility as needed to best predict the OSU data.
- Assess the existing condensation heat transfer models using the OSU condensation heat transfer data.
- Develop a new condensation heat transfer model as needed.
- Add additional measurement instrumentation to the test facility, in particular mass fraction measurements near the containment wall.
- Perform additional parametric tests to measure condensation heat transfer in the test facility. Consider using different bulk fluids in the presence of a non-condensable gas.

REFERENCES

1. George T.L., Wiles L.E., Claybrook S.W., Wheeler C.L., McElroy J.D., "GOTHIC Containment Analysis Package Technical Manual," EPRI (2001).

2. Chan C.K., Lee C.K.B., "A Regime Map for Direct Contact Condensation," International Journal of Multiphase Flow 8 (1982), 11-20.

3. Bankoff S.G., "Some Condensation Studies Pertinent to LWR Safety," International Jouranl of Multiphase Flow 6 (1980), 61-67.

4. Kowalchuk, W., Sonin, A. A., "A Model for Condensation Oscillation in a Vertical Pipe Discharging Steam into Subcooled Water Pool," MIT, NUREG/CR-0221 (1978).

5. Sursock J.P., Duffey R.B., "Condensation of Steam Bubbles in a Subcooled Pool," Topic in Two-Phase Flow and Heat Transfer (1978), 135-142

6. Simpson H.C., Beggs G.C., Isikan O.M., "Collapse of Steam Bubbles in Subcooled Water,"

7. Nusselt W., "The Surface Condensation of Water Vapor (in German)," Z. Ver. Dt. Ing. 60 (1916), 541-546, 575-596.

8. Koh J.C.Y., "Laminar Film Condensation of Condensable Gases and Gaseous Mixture on a Flat Plate," Proc 4th USA Nat Cong Appl Mech 2 (1962), 1137-1336.

9. Rohsenow W.M., "Heat Transfer and the Temperature Distribution in Laminar Film Condensation," Trans ASME 78 (1956), 1645-1648.

10. Minkowycz W.J., Sparrow E.M., "Condensation Heat Transfer In the Presence of Noncondensables, Interfacial Resistance, Superheating, Variable Properties, and Diffusion," International Journal of Heat and Mass Transfer 9 (1966), 11125-1144.

11. Uchida H., Oyama A., Togo Y., "Evaluation of Post-Incident Cooling Systems of Light-Water Power Reactors", Proc. Int. Conf. Peaceful Uses of Atomic Energy 13 (1965), 93-103.

12. Gido R.G., Koestel A., "Containment Condensing Heat Transfer", NURETH-2, Santa Barbara CA (1983), 1111-1119.

13. Kanzleiter T., "Experimental Investigation of Pressure and Temperature Loads on a Containment After Loss-of-Coolant Accidents," Battelle-Institute e.v. Frankfult (1975).

14. Schmitt R.C., Bingham G.E., Norberg J.A., "Simulated Design Basis Accident Tests of the Carolinas Virginia Tube Reactor Containment Final Report," Idaho Nuclear Corporation report IN-1403 (1970).

15. Corradini M.L., "Turbulent Condensation on a Cold Wall in the Presence of a Noncondensable Gas," Nuclear Technology 64 (1984), 186-195.

16. Bird R.B. et al., *Transport Phenomena*, Wiley and Sons, Inc., New York (1960).

17. Perterson P.F., Schrock V.E., Kageyama T., "Diffusion Layer Theory for Turvulent Vapor Condensation with Noncondensable Gases," Transactions ASME 115 (1993), 998-1003.

18. Kataoka Y., Fukui T., Hatamiya S., Nakao T., Naitoh M., and Sumida I., "Experimental Study on Convection Heat Transfer Along a Vertical Flat Plate Between Different Temperature Pools," ANS Proceedings, National Heat Transfer Conference (1991) 5, 99-106.

19. Crane Co, "Technical Paper No. 410," Crane CO., Joliet IL (1988).

20. NEXANT Bechtel, Drawing SK-2500 Rev. 1, January, 10 2002.

21. ANSI/ANS-5.1-1979, " American National Standard for Decay Heat Power in Light Water Reactors", August 29, 1979.